

BEAM BUCKLING TESTS WITH VARIOUS BRACE STIFFNESSES

APPROVED:

Joseph A. Yura
D. Falzoni

BEAM BUCKLING TESTS WITH VARIOUS BRACE STIFFNESSES

BY

ROBERT WILLIAM GEDIES, B.S.C.E.

THESIS

Presented to the Faculty of the Graduate School of
The University of Texas at Austin
in Partial Fulfillment
of the Requirements
for the Degree of
MASTER OF SCIENCE IN ENGINEERING

THE UNIVERSITY OF TEXAS AT AUSTIN

December 1983

To my family and friends.

A C K N O W L E D G M E N T S

The author would like to express his deepest appreciation to Dr. Joseph A. Yura for his guidance, encouragement and patience during this research project. Special thanks are also given to Dr. Dimos Polyzois for his suggestions.

The support of all the technical personnel at the Phil M. Ferguson Structural Engineering Laboratory of The University of Texas at Austin is acknowledged.

The funds used in this project were provided by the American Iron and Steel Institute.

R.W.G.
October 1983

A B S T R A C T

The goal of this study was to provide experimental data on the lateral-torsional buckling of braced beams. Of particular interest was the magnitude of the brace forces, the brace stiffness necessary to develop a particular critical moment and the effect of forced initial imperfections on these parameters. To accomplish this goal, twenty tests were performed using a wide flange beam which was loaded in the elastic range with uniform moment and braced at the midspan of the compression flange. The brace stiffness and magnitude of the forced initial imperfections were varied.

Brace forces less than 0.2 percent of the compression region force were observed for the beams buckling into the second mode. A finite brace stiffness was adequate to force the beam to buckle into the second mode and the test results were found to be in agreement with analytical methods of predicting this brace stiffness. The required stiffness for a distributed brace applied along the compression flange was determined using the results from the finite element program BASP [7].

T A B L E O F C O N T E N T S

Chapter		Page
I	INTRODUCTION	1
	1.1 Bracing	1
	1.2 Bracing of Ideal Columns	2
	1.3 Columns with Imperfections	7
	1.4 Beam vs. Column Behavior	11
	1.5 Objectives of the Research Program	11
II	BRACING OF BEAMS	15
	2.1 Ideal Brace Stiffness for Compression Flange	15
	2.2 Previous Approaches for Beam Bracing	21
	2.3 Forces in Beam Bracing	24
III	TEST PROGRAM	28
	3.1 Description of Experiments	28
	3.2 Test Setup	30
	3.3 Brace Spring	37
	3.4 Forced Initial Imperfections	42
	3.5 Load and Deflection Measurement	47
IV	TEST PROCEDURE AND RESULTS	50
	4.1 Test Procedure	50
	4.2 Determination of Midspan Moment	52
	4.3 Test Results	52
V	ANALYSIS OF TEST RESULTS	66
	5.1 Calculation of Bifurcation Moment	66
	5.2 Techniques for Determining Critical Moments	67
	5.3 Critical Moments from Tests	72
	5.4 Moment vs. Brace Stiffness	79
VI	EXAMPLE PROBLEMS	85
	6.1 Beam Braced at Midspan	85
	6.2 Distributed Brace along Compression Flange	89
VII	CONCLUSIONS	94

T A B L E O F C O N T E N T S (continued)

Chapter	Page
APPENDIX A: BRACED IMPERFECT COLUMN	97
APPENDIX B: SUMMARY OF PLOTTING METHOD RESULTS	103
APPENDIX C: DESCRIPTION OF BASP PROGRAM	114
NOTATION	117
REFERENCES	119

L I S T O F T A B L E S

Table		Page
4.1	Brace Forces	55
5.1	Plotting Method Results	76
B.1	Southwell (ILS = 1) Plotting Method Results	104
B.2	Lundquist (ILS = 2) Plotting Method Results	107
B.3	Meck (ILS = 2) Plotting Method Results	111

L I S T O F F I G U R E S

Figure		Page
1.1	Behavior of braced ideal column	3
1.2	Hinge assumed at brace point	6
1.3	Displacements of unbraced imperfect column	8
1.4	Displacement of braced imperfect columns	8
1.5	Column having elastic limit	11
2.1	Wide flange beam loaded by uniform moment	16
2.2	Center of rotation of buckled shape	20
2.3	Braced beam with uniform moment	20
2.4	Critical moment vs. brace stiffness for brace at the compression flange	23
2.5	Compression flange of beam as column	23
2.6	Model having initial imperfections	25
3.1	Section properties	29
3.2	Loading and support of test specimen	31
3.3	Buckled shape of compression flange	31
3.4	Test frame schematic	33
3.5	Beam deflecting under load	33
3.6	End loads	35
3.7	Bracket arrangement at load point	35
3.8	Load cell and roller bearing at support location	36
3.9	Out-of-plane supports	36

L I S T O F F I G U R E S (continued)

Figure		Page
3.10	Schematic of brace spring	38
3.11	Brace spring details	39
3.12	Brace spring mounted on sliding tee plate in frame	41
3.13	Brace spring connected to brace bar	43
3.14	Vertical track for brace bar support which accommodates vertical motion	43
3.15	Verification of brace spring stiffness during testing	44
3.16	Restraint angle for forced imperfections	45
3.17	Forced initial imperfections	45
3.18	Inclinometer	48
3.19	Optron--optical tracking device	48
4.1	Load vs. inplane deflection	53
4.2	Buckling deflections for beam with no midspan brace ...	58
4.3	Comparison of Tests 15 and 16	60
4.4	Brace point deflection for various brace stiffnesses	62
4.5	Quarterpoint deflections for beam with various brace stiffnesses	63
4.6	Moment vs. quarterpoint lateral deflection for Test 30 taken to failure	64
5.1	Southwell plot	69
5.2	Lundquist plot	69

L I S T O F F I G U R E S (continued)

Figure		Page
5.3	Meck plots for beam buckling	71
5.4	Southwell and Lundquist plots for Test 11	73
5.5	Meck plot for Test 11-- u/M vs. θ	74
5.6	Meck plot for Test 11-- θ/M vs. u	75
5.7	Moment vs. deflection plot	80
5.8	Critical moment vs. brace stiffness-- Meck plots (initial load stage = 1)	81
6.1	Beam braced at midspan at the compression flange	86
6.2	Continuously braced column--first mode shape.....	90
6.3	Continuously braced column--second mode shape	91
6.4	Beam with continuous brace at compression flange	92
A.1	Deflections of braced imperfect column	97
A.2	Deflections of imperfect column with various brace stiffnesses	102
B.1	Critical moment vs. brace stiffness from Southwell plots	106
B.2	Critical moment vs. brace stiffness from Lundquist plots	110
B.3	Critical moment vs. brace stiffness from Meck plots at centroid	113
C.1	Model of W12 x 16	116

CHAPTER I

INTRODUCTION

1.1 Bracing

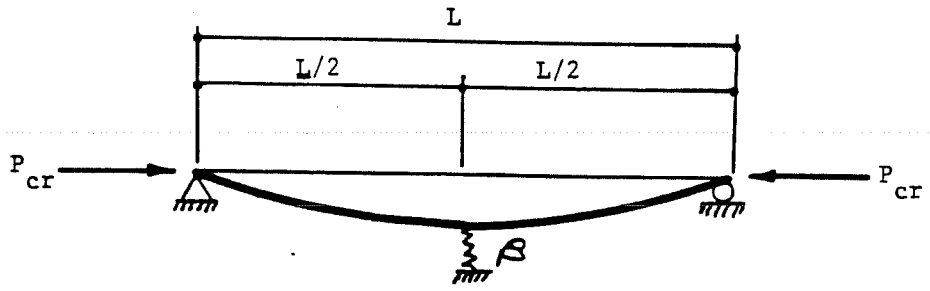
Bracing is used to prevent the displacement of a compression element in a direction other than that of the compression force. The compression element may be a column which is compressed by applied axial loads or the compression flange of a beam which is loaded by applied transverse loads. Buckling of these elements can occur when equilibrium can exist at a deflected position at which the member axis does not coincide with the line of action of the compression force. The P-delta moment developed at this deflected position is resisted by additional bending of the element cross-section. Increasing the bending resistance of the section would increase the load at which buckling may occur; however, this may not be as economical as using a few well-placed braces depending on the cost of connections and the cross-section material saved.

Bracing of beams may be provided by another part of the primary load carrying system, such as a slab, or a secondary bracing member such as bridging. The provision of bracing for a gravity loaded member has been, historically, an engineering judgment. The empirical approach based on years of experience can be augmented by analytical procedures. For example, the SSRC Guide to Stability Design Criteria for Metal Structures [1], herein referred to as the "SSRC Guide,"

suggests that a brace should be designed to resist 2 percent of the force in the compression member. This approach does not explicitly guarantee that the stiffness of the brace is sufficient also. The stiffness and strength requirements for column braces have been researched and are reviewed in the next section. The bracing of beams, however, has received less attention than columns and is the subject of this research project.

1.2 Bracing of Ideal Columns

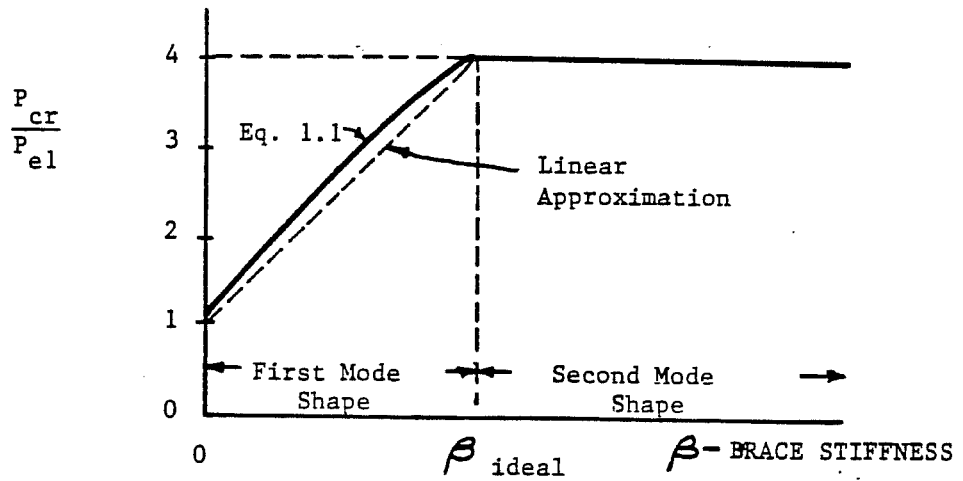
A member is defined as being ideal if it is perfectly straight and has a homogeneous and isotropic material. As an increasing compression force is applied to a coincident centroid and shear center longitudinal axis, there will be no lateral deflection or bending until the column is loaded to its bifurcation load. At this point, there are two possible equilibrium positions: the column can either remain perfectly straight or it can deflect an indefinite distance. This behavior is typical of ideal columns loaded in compression regardless of the type and location of braces and supports as long as the system is initially stable. The critical load is that at which bifurcation of equilibrium occurs. In the case of a column with an elastic brace at midspan, as shown in Fig. 1.1(a), the axial load, P , is sufficient to cause the column to buckle into the first mode shape. The relationship between the critical load, P_{cr} and the brace stiffness, β , was developed by Mutton and Trahair [2], in terms of the length of the column, L , and the Euler load for this length, P_{e1} , as follows:



(a) first mode



(b) second mode



(c) load vs. brace stiffness

Fig. 1.1 Behavior of braced ideal column

$$\beta = \frac{(4 P_{cr}/L)}{1 - \left(\tan \frac{\pi}{2} \sqrt{P_{cr}/P_{e1}} / \frac{\pi}{2} \sqrt{P_{cr}/P_{e1}} \right)} \quad \text{for } 0 \leq P_{cr} \leq 4P_{e1} \quad (1.1)$$

When the brace stiffness is equal to zero, which is the case if there is no brace, Eq. (1.1) is satisfied only when $P_{cr}/P_{e1} = 1$, and the critical load is the Euler load, $P_{e1} = \pi^2 EI/L^2$. As the brace stiffness is increased, a higher load is required to cause the member to buckle. The stiffness, which is sufficient to cause buckling into the second mode shape, as shown in Fig. 1.1(b), is defined as the ideal brace stiffness, β_{ideal} , which is given by Refs. 2 and 5 as

$$\beta_{ideal} = \frac{16\pi^2 EI}{L^3} \quad (1.2)$$

The relationship between critical load and the brace stiffness is shown in Fig. 1.1(c). For brace stiffnesses between zero and β_{ideal} , the P_{cr} - β relationship is nearly linear and departs from this, at most, 3 percent conservatively. When the brace stiffness is greater than β_{ideal} , there is no further increase in the critical load since buckling of the column takes place between the brace and the ends.

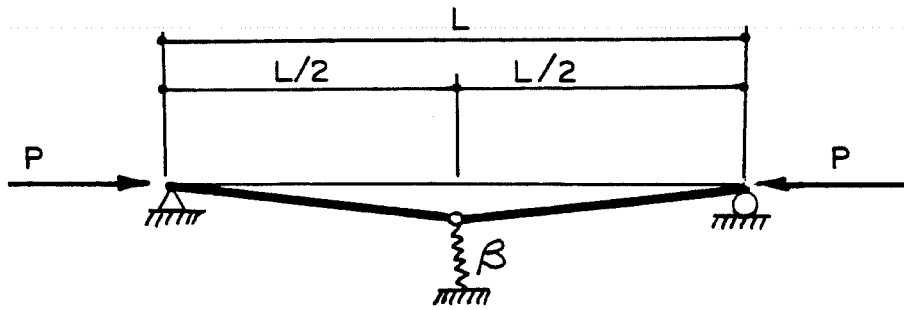
Winter [6] approximated the behavior of a braced ideal column by assuming a hinge at the brace point, as shown in Fig. 1.2(a). A hinge, assumed at the brace point, is appropriate when an inflection point is expected at this location as in the case of the second mode shape. The

required brace stiffness to support a particular load can be found from statics and is given by

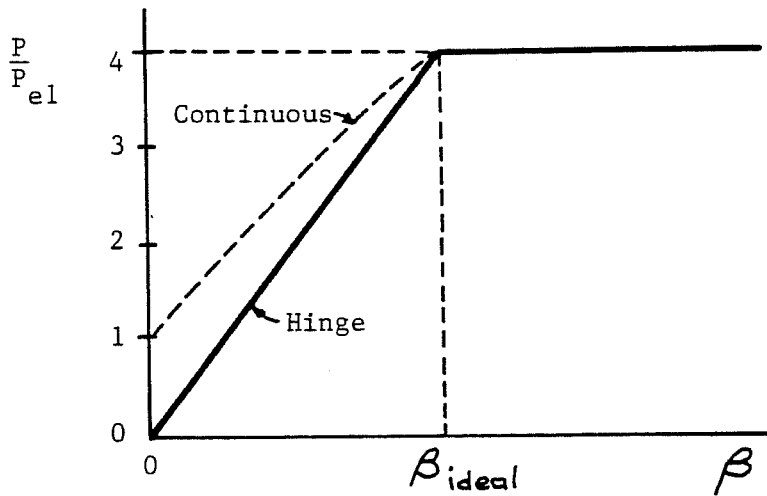
$$\beta = \frac{4P}{L} \quad (1.3)$$

The relationship between critical load and the brace stiffness is shown in Fig. 1.2(b) as a solid line. If the brace stiffness is zero, the system is unstable in the unloaded condition. As the brace stiffness is increased, the critical load increases linearly until the stiffness is large enough to cause buckling into the second mode shape. Substituting the second mode critical load, $4\pi^2EI/L^2$, into Eq. (1.3), the ideal brace stiffness is determined to be equal to that given in Eq. (1.2). If the brace stiffness is increased above the ideal value, the critical load will not change since buckling takes place between the brace and the ends. Winter's model can also be used to approximate the behavior of a continuous column when the brace stiffness approaches the ideal stiffness. The relationship between the load and the stiffness for the continuous case is shown as a dotted line, in Fig. 1.2(b).

In the analysis of ideal compression members, the critical load corresponding to a particular brace stiffness can be calculated but the magnitude of the brace force cannot be determined. The lateral deflections at the bifurcation point are indefinite which precludes the multiplication of brace deflection times the brace stiffness to get the brace force. The brace force, however, can be calculated when the compression member is assumed to be non-ideal or imperfect.



(a) hinge at brace point



(b) load vs. brace stiffness

Fig. 1.2 Hinge assumed at brace point.

1.3 Columns with Imperfections

Geometric imperfections will affect the behavior of a real column [3]. Immediately upon loading, a P-delta moment will be present on the column cross-section since the neutral axis for bending will not be coincident with the line of action of the compression force. The larger the initial imperfection, the larger the P-delta moment. To develop a resisting moment equal to the P-delta moment, the column must deflect further. Representing the initial imperfection shape which is a half sine wave with a magnitude equal to Δ_0 at midspan, the load-deflection relationship for an unbraced column is given by Winter [6] as

$$\Delta_A = \frac{P\Delta_0}{P_{e1}(1-P/P_{e1})} \quad 0 \leq P \leq P_{e1} \quad (1.4)$$

where Δ_A is the additional deflection, P_{e1} is the Euler load, and P is the axial load. Equation (1.4), plotted in Fig. 1.3, represents a hyperbola with a horizontal asymptote at $P = P_{e1}$. The column must deflect laterally a distance of 20 times Δ_0 to carry a load of 95 percent of P_{e1} . The Euler or bifurcation load is achieved at an equilibrium position which corresponds to an infinite lateral displacement. If the initial shape consists of component shapes of higher buckling modes, the load vs. deflection plot will deviate significantly from the hyperbolic function, given by Eq. (1.4) and shown in Fig. 1.3, at low load levels but will be well represented by this function as the load approaches P_{e1} . The case of an unbraced column having an arbitrary

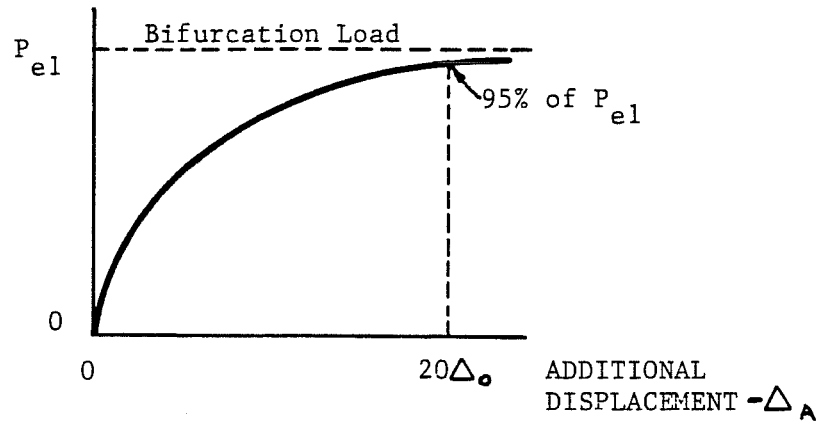


Fig. 1.3 Displacements of unbraced imperfect column.

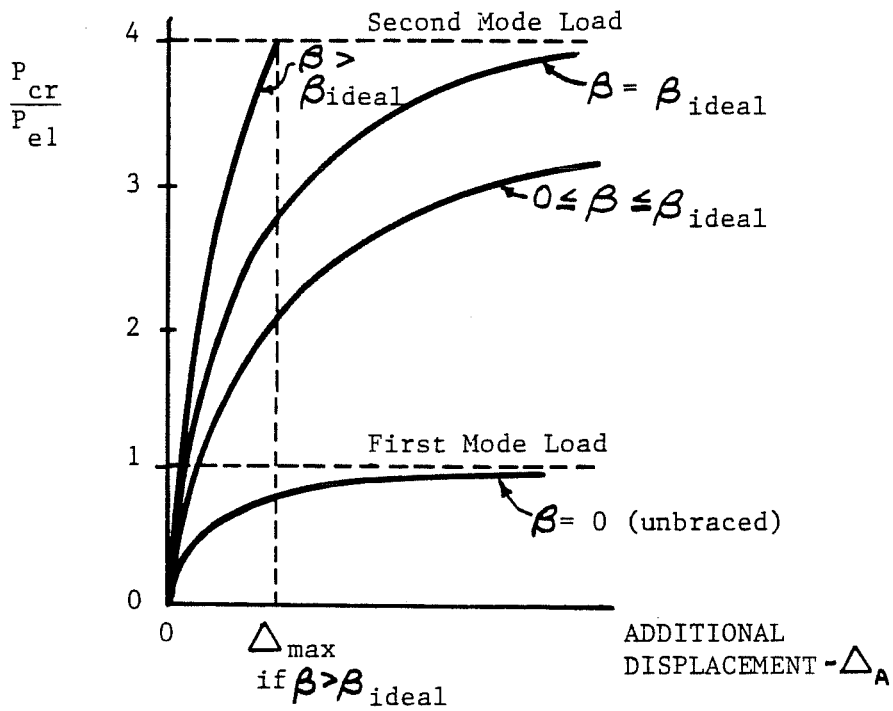


Fig. 1.4 Displacements of braced imperfect columns.

initial shape is presented in Appendix A where a relationship between load and deflection is developed.

For braced imperfect columns, the bifurcation load for an ideal member is the maximum or critical load for an imperfect member. This load is attained only after some or all of the span has deflected laterally an infinite distance. The load-deflection plots for a pinned end column having various brace stiffnesses are shown in Fig. 1.4. When the brace stiffness, β , equals zero, the critical load is the Euler load for the entire length. The relationship between critical load and brace stiffness is linear up to the ideal brace stiffness, as shown in Fig. 1.1(c). The load vs. deflection curves in Fig. 1.4 become more hyperbolic in character as the load approaches the critical load for a given brace stiffness. The behavior at low load levels is very dependent on the initial imperfection shape having components which correspond to higher buckling modes. The differential equation solution for the braced case is also developed in Appendix A. The lateral deflection of the brace point becomes infinite when the column load approaches its critical value if the brace stiffnesses is smaller than the ideal brace stiffness. If the brace stiffness is greater than the ideal stiffness, the column will be forced to buckle into the second mode shape. This phenomenon is shown in Fig. 1.4, where the brace deflection is limited to a finite displacement, Δ_{\max} , while the spans between the brace and the ends deflect an infinite distance. It is desirable to design a brace with a brace stiffness greater than the ideal stiffness in order to limit the brace deflection and, consequently, the brace force. The

magnitude of this limiting deflection is dependent on the initial shape and would be maximum when this shape has component shapes which have positive midspan amplitudes for the first and higher order mode shapes which are symmetric about the brace point.

In the foregoing discussion it was assumed that the material remains linearly elastic until failure by lateral buckling takes place. For members with material having an elastic limit, the superposition of axial stress and the lateral bending stress will always exceed the yield stress before the member can attain its bifurcation load, since the column must deflect laterally an infinite distance to carry its critical load. Figure 1.5 shows the load vs. deflection behavior of a column with a material having an elastic limit. Depending on the magnitude of the initial imperfections, the usable capacity of the member may be significantly below that predicted by the bifurcation load. Once the material yields, the lateral bending stiffness starts to decrease. Failure will be sudden if the member is loaded by gravity load or other non-removable load. If a design procedure presumes that a member can carry a load equal to its bifurcation load, any discrepancy due to the imperfections or non-linear material behavior must be covered by the safety factor used. The bifurcation load is still an important concept because the actual load vs. deflection curves can be approximately described in terms of this load and the magnitude of the initial imperfections as is done in Eq. (1.4).

When testing actual compression members, the assumptions used in an elastic range buckling analysis will become invalid when the specimen

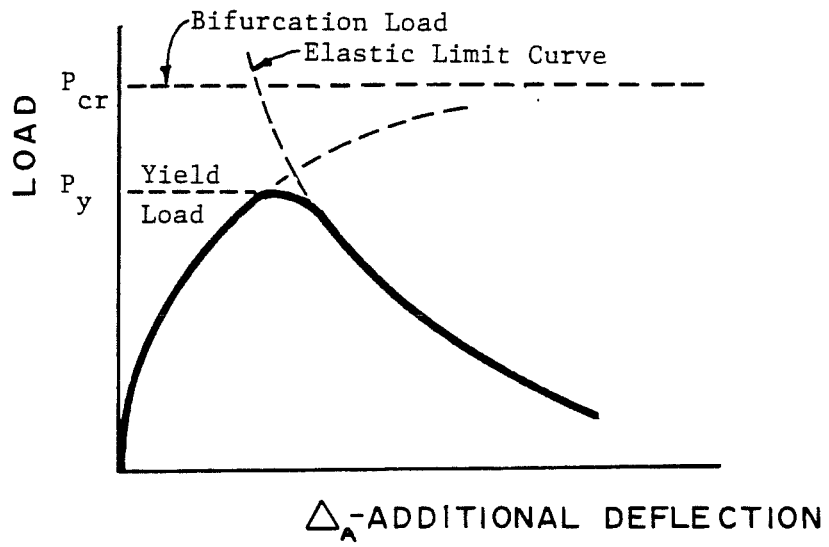


Fig. 1.5 Column having elastic limit.

starts to yield. Critical loads predicted by an elastic analysis will never be attained. The critical load can be obtained by extrapolation from the load vs. deflection data if these data points are taken at high load levels where the cross-section is still elastic and the data has the hyperbolic character of Eq. (1.4). It is important to load the specimen as close to the critical buckling load as possible to ensure that the predominant deflection mode has an amplitude which is much larger than all other possible mode shapes. This, however, may not be possible with stocky cross-sections which will yield at loads which are a much lower than the elastic buckling load. The most common method for determining the experimental elastic buckling loads is the use of the Southwell plot [4]. If the test data is strongly hyperbolic throughout the entire range of deflection, the critical load and the magnitude of the initial imperfection can be calculated by this method. These parameters can then be used with Eq. (1.4) to describe the load vs. deflection behavior. The Southwell plot and other plotting methods such as the Lundquist [8] and Meck [9] plots can be applied to the buckling deflections of beams. These methods will be discussed in detail in Chapter V.

1.4 Beam vs. Column Behavior

Mutton and Trahair [2] show that the buckling of an ideal, or perfectly straight, braced beam is similar to a braced column. Specifically, they demonstrated that beams braced at midspan will buckle into the second mode shape when the stiffness of this brace is a finite value like the ideal brace stiffness for columns. The foregoing discussion on

braced column behavior will be used as a basis for describing the behavior of the compression flange of flexural members. The differential equation solution for a braced beam is much more complex than that of the braced column since it involves the solution of two simultaneous equations for the lateral deflection and twist. The load-deflection behavior of an imperfect beam has been documented by Zuk [5]. The form of the derived solutions is difficult to interpret and implement. As a result of the complexity of the solutions, braced imperfect beams have received less attention analytically and experimentally than columns.

1.5 Objectives of the Research Program

A testing program was undertaken to study experimentally the lateral-torsional buckling of braced beams. The program involved the testing of a steel wide-flange beam under uniform moment. An elastic brace was attached to the compression flange at the midspan of the test beam. The stiffness of the brace was varied to observe how this parameter affected the lateral-torsional buckling behavior of the specimen. Several forms of initial imperfections were also considered. The objective of the experimental program was to measure the brace forces and to study the effects of brace stiffness and initial imperfections on the lateral-torsional buckling behavior.

A review of pertinent analytical methods in the area of braced beams is given in Chapter II followed by a detailed description of the testing program in Chapter III. The test results are presented in Chapter IV and compared to the analytical predictions in Chapter V.

Several example problems are given in Chapter VI. Finally, conclusions are drawn regarding the bracing requirements for flexural members.

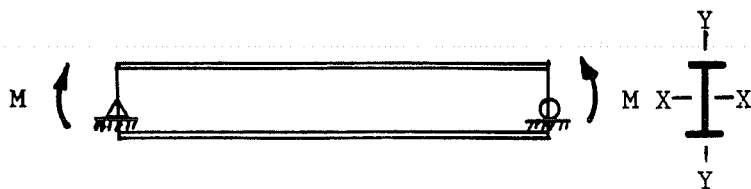
C H A P T E R I I

BRACING OF BEAMS

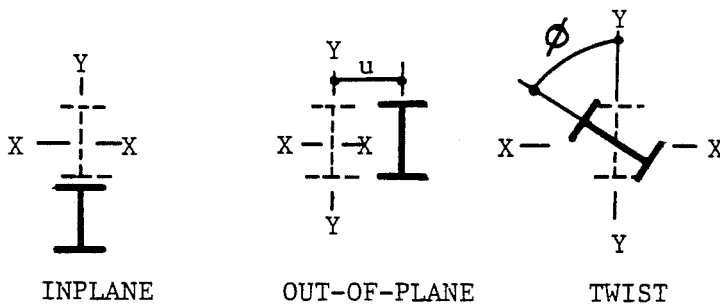
The ideal brace stiffness required to force a column to buckle into the second mode shape has been discussed in Chapter I. The ideal brace stiffness required to force a beam, loaded by uniform moment and braced at the compression flange at midspan, to buckle into the second mode shape is given in this chapter. This stiffness is derived from the solutions to differential equations of braced beams which are developed by Mutton and Trahair [2]. Similarities between the solutions for braced beams and columns suggest a model based on column behavior [6]. Ideal beam theory and this column behavior model are reviewed and the evaluation of proper bracing for the compression flange of a beam is detailed in this chapter.

2.1 Ideal Brace Stiffness for Compression Flange

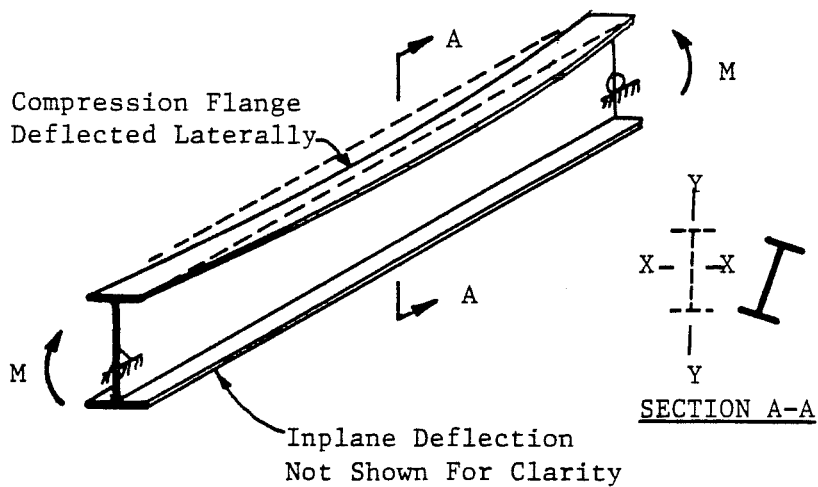
A simply-supported wide-flange beam, loaded by uniform moment and laterally braced at the compression flange at midspan, is shown in Fig. 2.1(a). Three types of displacement, as shown in Fig. 2.1(b), are possible at any cross-section: translation parallel to the Y-Y axis, which is defined as inplane deflection resulting from the loads and moments which are applied in the plane of the web; translation parallel to the X-X axis, which is defined as lateral or out-of-plane deflection, u , and twist, ϕ , the rotation of the beam about its longitudinal axis.



(a) inplane loading



(b) modes of beam deflection



(c) lateral-torsional buckling

Fig. 2.1 Wide flange beam loaded by uniform moment.

When the beam is loaded by inplane forces, there will be inplane moments along the span of the beam. If the compression flange is not sufficiently supported against lateral deflection, the cross-section can bend laterally and twist, as shown in Fig. 2.1(c). This behavior is characterized as lateral-torsional buckling.

Three simultaneous differential equations can be written to describe the lateral-torsional buckling of a beam. The influence of the inplane deflections is usually neglected which leaves the following two simultaneous equations for lateral deflection and twist:

$$EI_y \frac{d^2 u}{dz^2} - M\phi = 0 \quad (2.1)$$

$$GJ \frac{d\phi}{dz} - EC_w \frac{d^3 \phi}{dz^3} + M \frac{du}{dz} = 0$$

where z is the position along the longitudinal axis; M is the moment along this axis; E and G are the elastic and shear modulus, respectively; I_y is the weak axis moment of inertia; J is the St. Venant torsional constant; and C_w is the warping constant. From the SSRC Guide [1], the solution to these equations for the critical moment is

$$M_{cr} = \frac{\pi(EI_y GJ)^{1/2}}{(aL)} \left(1 + \frac{\pi^2 EC_w}{(aL)^2 GJ} \right)^{1/2} \quad (2.2)$$

where aL is the length between inflection points of the beam. The first mode critical moment is calculated using $a = 1.0$ if there is no brace along the span. The second mode critical moment can be calculated using $a = 0.5$ if a brace is placed at midspan which has sufficient stiffness to force the beam to buckle into the second mode shape. This solution is adequate only if the lateral deflection and force at the brace point is zero. However, if the brace stiffness is not sufficient to enforce the second mode, there will be a force in the brace and extra terms must be included in the equilibrium relations, Eq. (2.1), as is done in Ref. 2.

Before reviewing the results from Ref. 2 for a braced beam loaded by uniform moment, Eq. (2.2) will be rewritten in another form. The terms which represent the weak axis flexural buckling load, P_{cr} , are collected as

$$P_{cr} = \frac{\pi^2 EI_y}{(aL)^2} \quad (2.3)$$

The center of rotation (2,5), b_o , of the buckled cross-section, as shown in Fig. 2.2, is defined as

$$b_o = \frac{d}{2} \left(1 + \left(\frac{aL}{\gamma} \right)^2 \right)^{1/2} \quad (2.4)$$

where $\gamma = \left(\frac{\pi^2 EC_w}{GJ} \right)^{1/2}$

The center of rotation, b_o , will always be below the tension flange but will move upwards toward it if γ increases or aL decreases. For most economy sections with $aL/d = 10.0$, b_o ranges from $1.2 (d/2)$ to $1.4 (d/2)$. The equation for the critical moment, Eq. (2.2), now reduces to the multiplication of a force times the distance from the shear center to the center of rotation,

$$M_{cr} = P_{cr} b_o \quad (2.5)$$

A brace with stiffness, β , located at the compression flange at midspan of a beam under uniform moment as shown in Fig. 2.3 will increase the critical moment of the beam, M_{cr} , above that of the unbraced case. An expression for the relationship between M_{cr} and brace stiffness in this case is derived by Mutton and Trahair [2] and given here in a different form as:

$$\beta = \frac{4P_{cr}/L / (1 + b/b_o)}{(1 - \tan \left(\frac{\pi}{2} \sqrt{\frac{P_{cr}}{P_{e1}}} \right) / \left(\frac{\pi}{2} \sqrt{\frac{P_{cr}}{P_{e1}}} \right))} \quad (2.6)$$

where P_{cr} is calculated from Eq. (2.3) using values for a between 1.0 and 0.5, P_{e1} is the first mode critical load using $a = 1.0$, and b is the height of the brace attachment as shown in Fig. 2.2. The critical moment for this brace stiffness is derived from Eqs. (2.4) and (2.5) and is shown graphically in Fig. 2.4. If the brace is attached at a

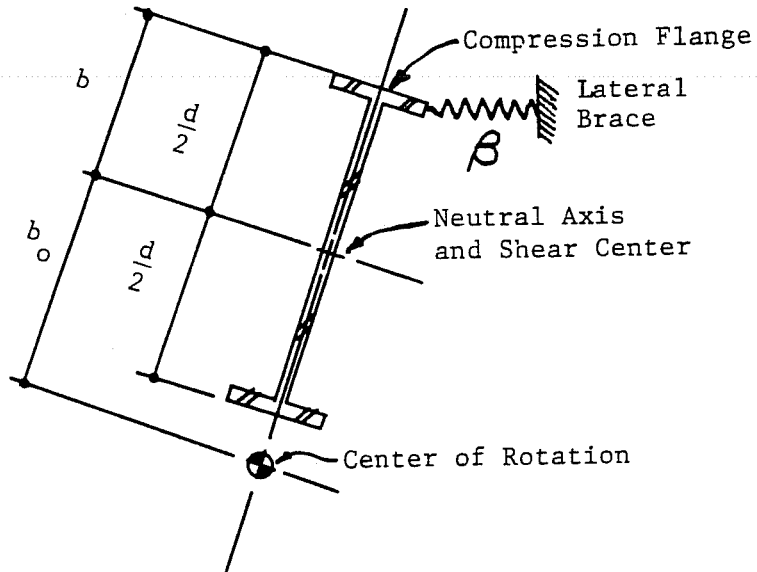


Fig. 2.2 Center of rotation of buckled shape.

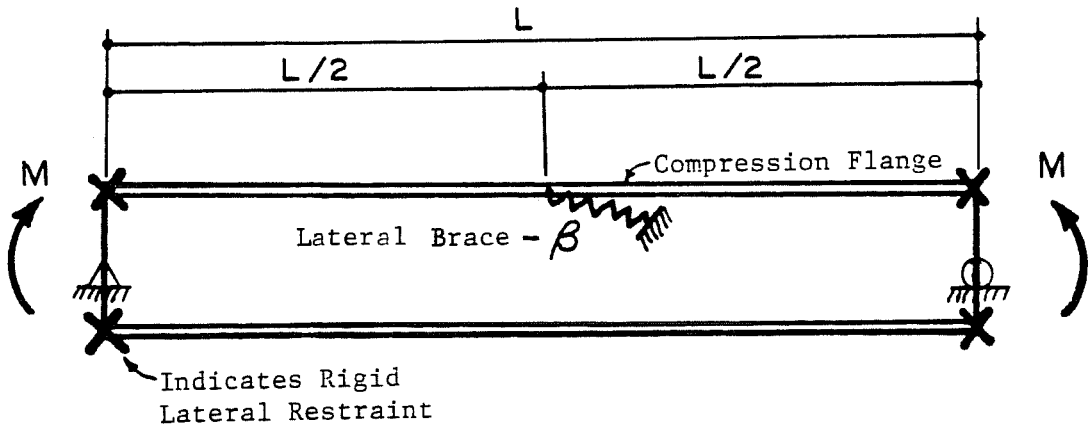


Fig. 2.3 Braced beam with uniform moment.

location below the top flange, the translational brace stiffness may have to be augmented by a rotational brace stiffness to enable this moment to be achieved. These requirements are discussed in Ref. 2, and are not within the scope of this study.

The ideal brace stiffness for a beam braced at the compression flange, based on a = 0.5, is

$$\beta_{\text{ideal}} = \frac{16\pi^2 EI_y / L^3}{(1 + b/b_o)} = \frac{4P_{\text{cr}} / L}{(1 + b/b_o)} \quad (2.7)$$

From this equation, it is seen that the ideal brace stiffness for a beam braced at the compression flange is smaller than that obtained for a column by Eq. (1.2) by the factor (1 + b/b_o). The magnitude of this factor is greater than 1.0 but not more than 2.0, when the brace is at the compression flange, and is between 1.70 and 1.85 for most economy sections with aL/d = 10.0. The similarity between the solutions for braced columns and beams is useful in establishing the validity of an approximate model of braced beam behavior based on column behavior.

2.2 Previous Approaches for Beam Bracing

The 2 percent "rule of thumb" used for the bracing of columns was extended by the SSRC Guide [1] to the bracing of the compression region of beams. The strength of a lateral brace is said to be sufficient if it is at least 2 percent of the force in this region. If so designed, Zuk [5] contends that the stiffness might also be adequate. Other

models, however, are available [5, 6] which can be used to evaluate the stiffness and strength requirements more precisely.

The "beam flange as a column" analogy is presented by Winter in Ref. 6. In this model, the compression region of a beam, such as that shown in Fig. 2.3, is isolated and treated as a column as shown in Fig. 2.5. The flange of this region provides the lateral bending resistance since the web contributes little to the weak axis moment of inertia. The techniques discussed in Chapter I for the bracing of columns can be used to calculate the ideal stiffness. The question in the actual use of this approach is, however, what force P in Eq. (1.3) should be applied to the compression region or "column". Winter [6] uses the total compression force above the neutral axis of the beam. Another supposition might be to divide the moment by the depth of the beam to get the force. The similarities between Eq. (1.1) for braced columns and Eq. (2.6) for braced beams indicate that the proper force, P , to use in Eq. (1.3) is $P_{cr}/(1 + b/b_0)$. Using this value, the brace stiffness for a beam is seen to be that of a column divided by the quantity $(1 + b/b_0)$ which can be characterized as a correction factor which accounts for the enhanced effectiveness of a brace when it is above the shear center toward the compression flange. When evaluating the ideal stiffness for beams, the correction factor may be conservatively assumed equal to 1.0 which results in overestimating the required stiffness by a factor of not more than two. However, the calculation of b_0 is necessary to get M_{cr} , as in Eq. (2.5), so there is no extra calculation effort required to calculate $(1 + b/b_0)$. A better understanding of the evaluation of M_{cr} for braced

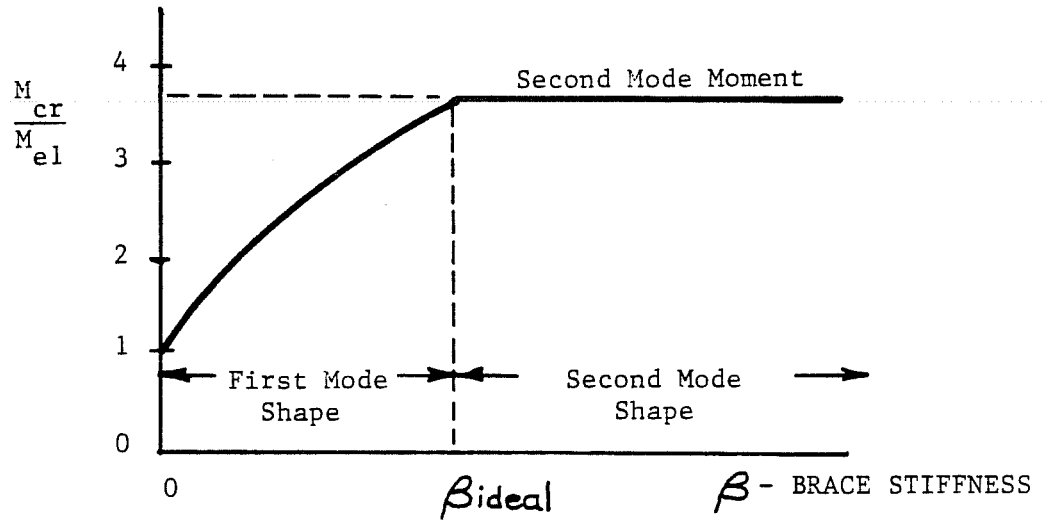


Fig. 2.4 Critical moment vs. brace stiffness for brace at the compression flange.

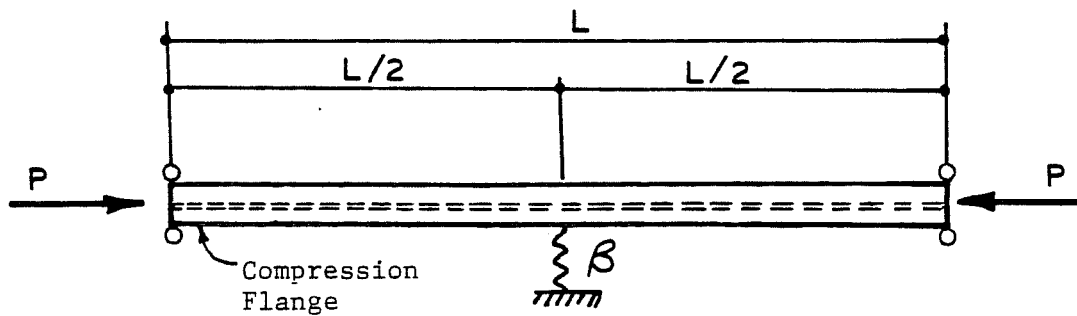


Fig. 2.5 Compression flange of beam as column.

beams results from the use of Eq. (2.5) rather than the conventional form in Eq. (2.2).

2.3 Forces in Beam Bracing

Brace forces can be computed if initial imperfections are included in a model. Zuk [5] obtained approximate solutions to the differential equations for an imperfect beam but the results have not been reduced to a form which can permit the behavior to be clearly defined. The initial imperfections may be composed of both lateral displacement and an initial twist components. Each of these may be composed of several component mode shapes. The study of braced columns indicates that the first mode component of the initial shape will have the greatest influence on the deflections of the brace point. It may be assumed that the compression flange of a beam will behave similarly. Winter [6] models a beam flange, braced with one or more elastic restraints, as a series of links connected by hinges at the restraint locations. Concentrating on the most simple case of one restraint at midspan, the flange is assumed to buckle into the second mode and a hinge is placed at midspan, as shown in Fig. 2.6. A first mode initial imperfection shape is simulated by displacing the hinge, laterally, a distance, Δ_0 , at the brace point. This representation is reasonable when the load is near the second mode load, P_{e2} , which is calculated using $\alpha = 0.5$ in Eq. (2.3). At this load the brace will deflect an additional distance, Δ_A , to maintain equilibrium. The moment equilibrium relation is

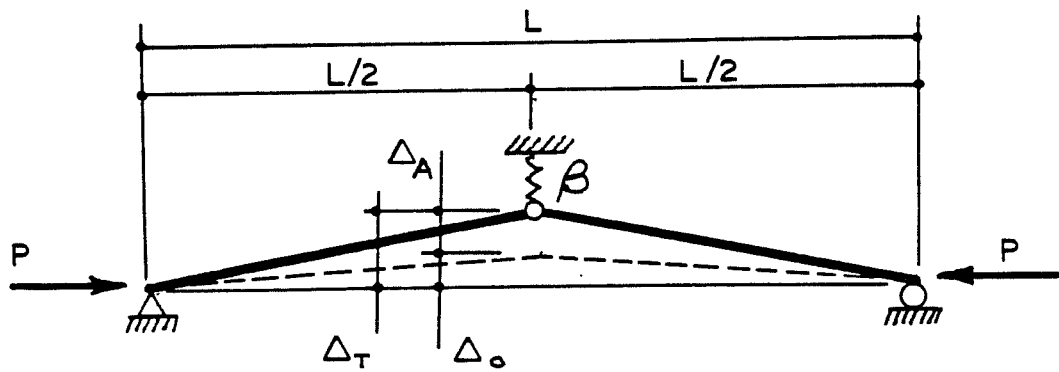


Fig. 2.6 Model having initial imperfections.

$$P_{e2} (\Delta_A + \Delta_o) = \frac{\beta L}{4} \Delta_A \quad (2.8)$$

Rearranging this equation and recognizing that $\beta_{ideal} = 4 P_{e2}/L$ from Eq. (1.2), the additional deflection required at the brace point is

$$\Delta_A = \Delta_o / \left(\frac{\beta}{\beta_{ideal}} - 1 \right) \quad (2.9)$$

When the brace stiffness is equal to the ideal stiffness, the deflection at the brace is infinite. The brace deflection can be limited to a finite magnitude by utilizing a brace with a stiffness greater than the ideal value. For example, the limiting deflection will be equal to the magnitude of the initial imperfection if the brace is twice as stiff as the ideal stiffness. The required strength of the brace is given by

$$F_{brace} = \beta \Delta_A = 4 \frac{P_{e2}}{L} (\Delta_o + \Delta_A) \quad (2.10)$$

A brace stiffness greater than the ideal brace stiffness is needed to limit the force in the brace. As the brace stiffness increases toward an infinite value, the additional deflection becomes zero. The brace force will not be less than

$$F_{rigid\ brace} = 4 \frac{P_{e2}}{L} \Delta_o \quad (2.11)$$

When using this column model for a beam braced at the top flange at midspan, it is appropriate to divide the brace stiffness and force by the quantity, $(1 + b/b_0)$. If the validity of this model for beams was established, say, through a testing program, then more complex bracing conditions, such as a continuous elastic restraint, could be analyzed in a similar manner as is done by Winter [6].

In the next chapter, a testing program is described in which a steel beam is loaded by uniform moment and braced at the compression flange at midspan. The objectives of this testing program are to study the effects of brace stiffness and initial imperfections on the lateral-torsional buckling behavior and brace forces.

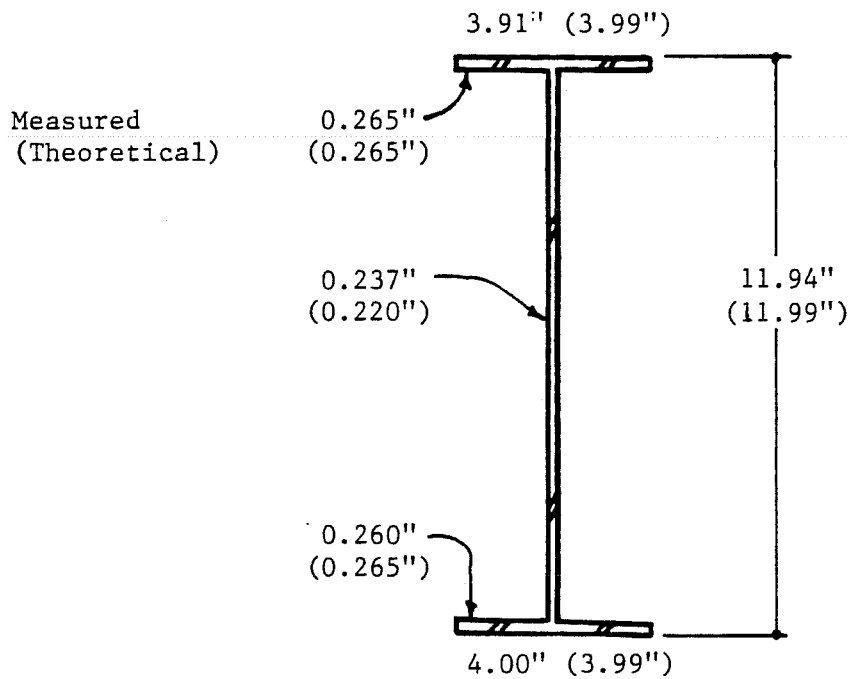
CHAPTER III

TEST PROGRAM

Thirty tests were performed on a single specimen to obtain data on bracing requirements for steel wide-flange beams. The first ten tests were considered pilot tests to evaluate the performance of the experimental setup. The last twenty tests, Tests 11 through 30, are reported here. Of these twenty tests, nineteen, or Tests 11 through 29, were conducted in the elastic range and the last test, Test 30, was tested to failure.

3.1 Description of the Experiments

The goal of this study is to provide experimental data on the lateral-torsional buckling of braced beams. Of particular interest was the force in the brace, the magnitude of the brace stiffness necessary to develop a particular critical moment, and the effect of initial imperfections on these parameters. To accomplish this goal, a simply supported wide-flange beam was braced at midspan at the compression flange and loaded with uniform moment. A single W12x16 specimen with ASTM A572-Grade 50 material was used for the 20 tests reported here. The W12x16 shape is relatively slender and is representative of typical beams used in building construction. The section properties were measured and are tabulated along with the published theoretical values in Fig. 3.1. The static yield stress obtained by ASTM tension coupon tests was 55 ksi and the elastic modulus was assumed to be 29,000 ksi.



SUMMARY AND COMPARISON TO THEORETICAL VALUES

<u>Property</u>	<u>Actual</u>	<u>Theoretical</u>	<u>% Difference</u>
A (in. ²)	4.78	4.71	+1.5
I _x (in. ⁴)	100.20	103.00	-2.7
S _x (in. ³)	16.80	17.10	-1.8
I _y (in. ⁴)	2.71	2.82	-3.9
S _y (in. ³)	1.35	1.41	-4.3

840

Fig. 3.1 Section properties.

The two important variables of this study were the brace stiffness and the magnitude of the initial imperfections. Theoretically, the ideal brace stiffness was expected to be sufficient to cause the beam to buckle into the second mode shape. Therefore, stiffnesses above and below the theoretical ideal stiffness were used so that its value could be bracketed experimentally. Initial imperfections were expected to influence the force in the brace. Forced imperfections or misalignments were imposed on the test specimen since these occur in actual structures and the need for many specimens each having its own unforced or natural imperfection was avoided. Magnitudes of forced imperfections equal to $1/2000$ and $1/1000$ of the test span were used. Tests with no forced imperfections were also performed so the effect of the natural or geometric imperfections could be observed.

3.2 Test Setup

The test setup was designed to approximate the behavior of the ideal model shown in Fig. 2.3. The end moments must be applied by practical means, however, the points of loading usually produce restraints that inhibit buckling deflections. To attenuate the effect of these restraints, the load and support points were located as far as possible from the region of the beam where the buckling originates. The loads, pts. A, and the supports, pts. B, were symmetrically placed at the ends of the specimen, as shown in Fig. 3.2. The beam was simply-supported in the plane of the loads, which were located 5 ft from the supports and produced a uniform moment region between the supports. Rigid out-of-plane supports, denoted by the X's in Fig. 3.2, were placed

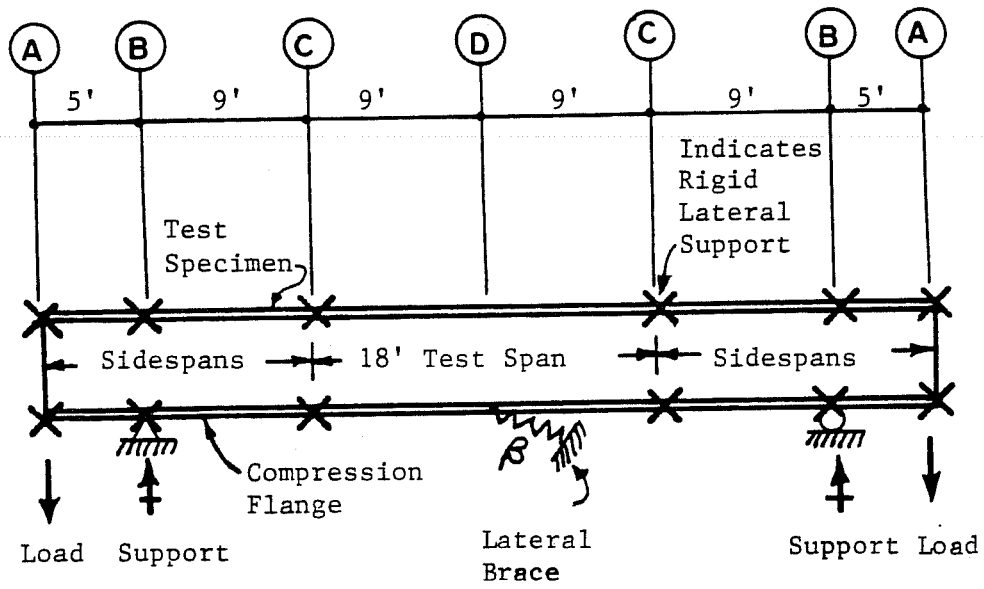


Fig. 3.2 Loading and support of test specimen.

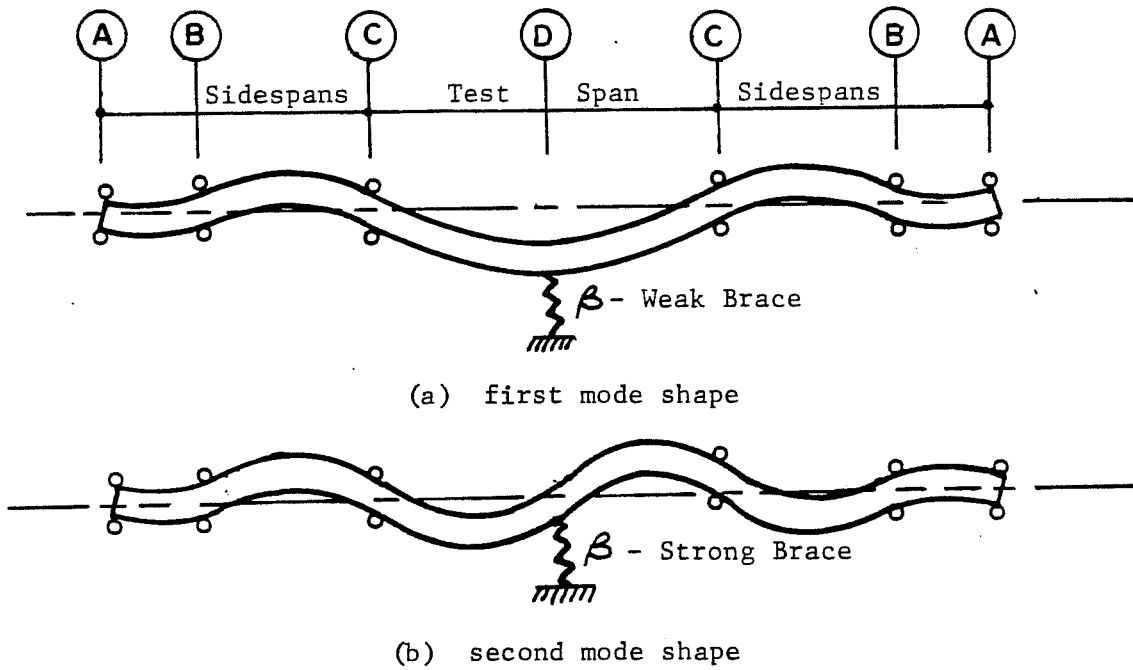


Fig. 3.3 Buckled shape of compression flange.

at the load and support points to prevent lateral translation of the specimen. An elastic brace was placed at the midspan of the specimen, pt. D, at the bottom flange which was in compression. At pts. C, out-of-plane restraints were placed to further isolate the center section of the beam from the inplane loading and supports. Buckling deflections were observed in the 18 ft center region of the beam defined as the test span. The adjacent 9 ft panel and the 5 ft panel are defined as the side spans.

The test span differed from the ideal beam model due to the continuity of the beam with the adjacent sidespans. To illustrate this difference, a flexible brace is placed at the midspan of the test span, as shown in Fig. 3.3(a). Significant weak axis bending or warping restraint is expected when the compression flange of the beam buckles into the first mode shape since the unbraced length of the test span is twice that of the sidespans. When the brace at the midspan is stiff, as shown in Fig. 3.3(b), the flange will buckle into the second mode. The test span and adjacent sidespans are close to buckling simultaneously since their unbraced lengths are approximately the same. Therefore, for this choice of dimensions, the warping restraint at pt. C in Fig. 3.2 is maximized when the beam buckles into the first mode shape and minimized when the beam buckles into the second mode shape.

Figure 3.4 shows the test specimen in the test frame. The frame was composed of two parallel W27's that were connected, intermittently, by cross-members. The frame was clamped to tie-down beams that were anchored to a reaction slab. Figure 3.5 shows the test frame and the

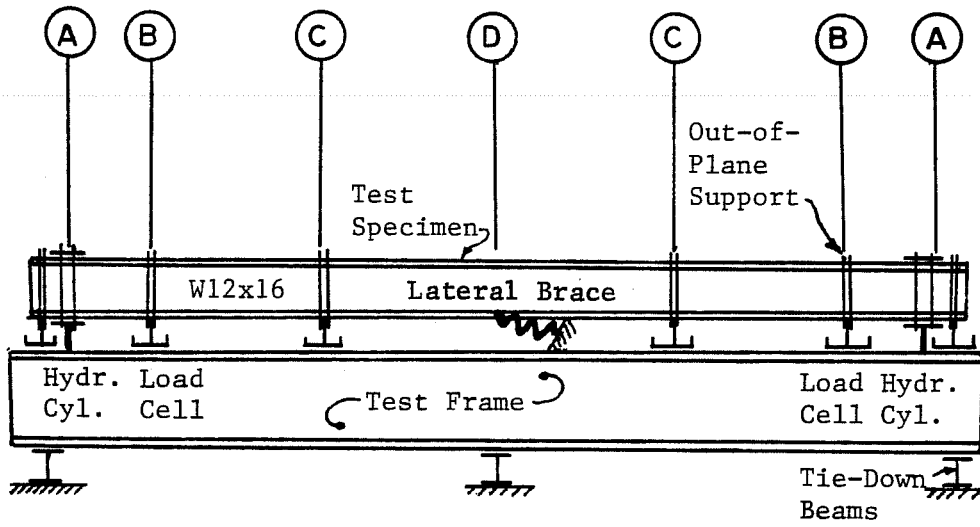


Fig. 3.4 Test frame schematic.

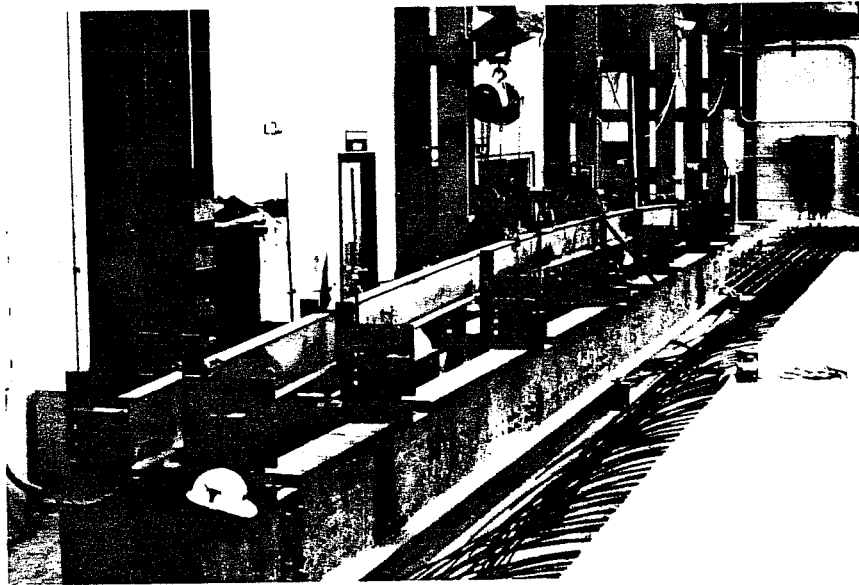


Fig. 3.5 Beam deflecting under load.

specimen during testing. The inplane loads were applied by 20-ton hydraulic cylinders acting in tension at pts. A as shown in Fig. 3.6. The rams were connected to a transfer beam spanning between the frame girders at the base of the frame where a clevice and pin were used to provide a pinned end in the plane of the frame. The tension from the ram was applied to the specimen through the bracket arrangement shown in Fig. 3.7. Two threaded rods on each side of the specimen passed through three plates which served to keep the specimen in proper alignment, to prevent crippling of the specimen, and to provide adjustment at the pinned connection to the cylinder rod end of the ram. The hydraulic pressure to the rams at each end of the test frame was supplied by a hand pump and common pressure and return hydraulic hoses. The hydraulic system had no significant leakage and was able to hold loads at any given level of pressure.

Roller bearings, shown in Fig. 3.8, were used to provide pinned supports at pts. B. These bearings were able to accommodate the inplane rotation of the specimen and were unable to transmit any moment or horizontal shear. Web crippling was prevented by a bearing plate between the flange and the rollers. The rollers were supported by a compression load cell and a transfer beam spanning between the frame girders.

Slotted plates, as shown in Fig. 3.9, were used to prevent out-of-plane translation of the specimen at pts. A, B, and C, shown in Fig. 3.2. Extension plates were bolted to the inside surface of these plates

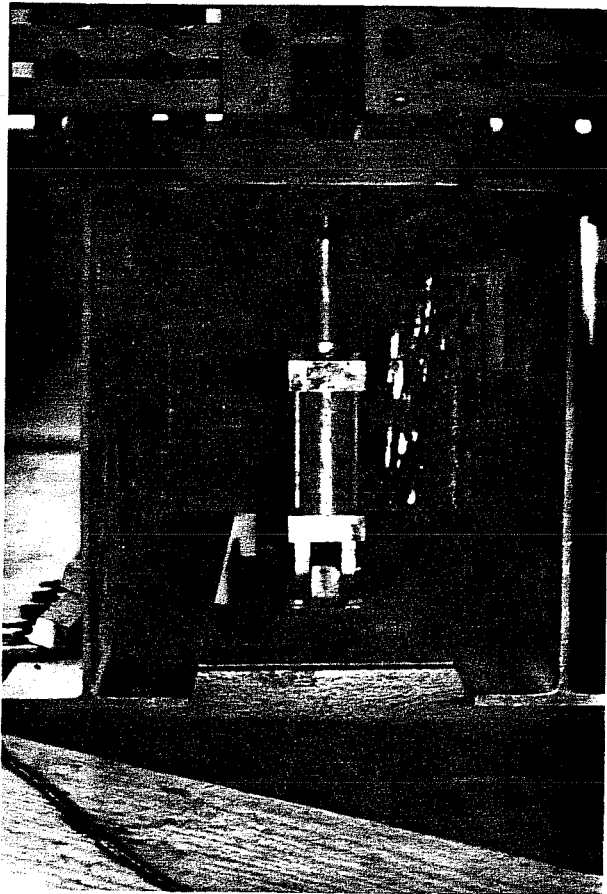
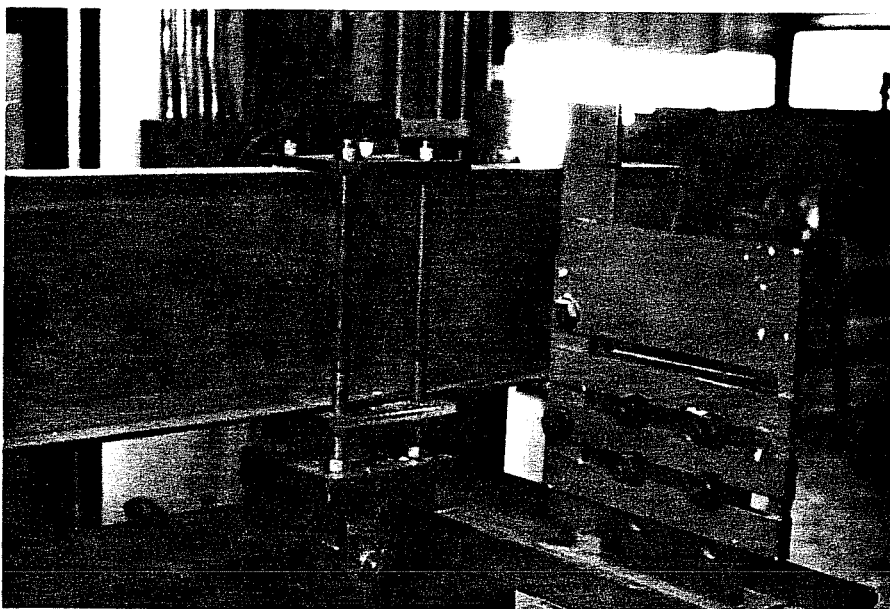


Fig. 3.6 End loads.

Fig. 3.7 Bracket arrangement at load point.



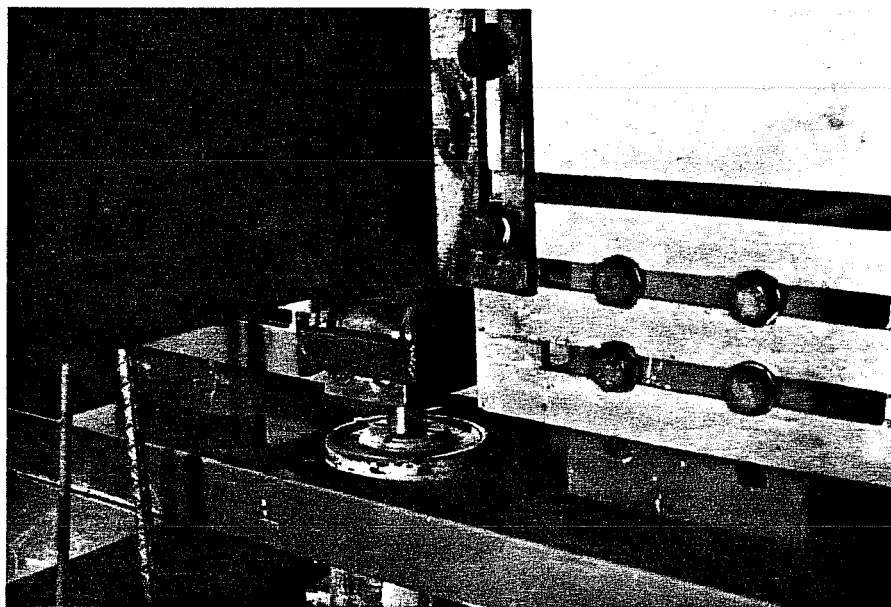


Fig. 3.8 Load cell and roller bearing at support location.

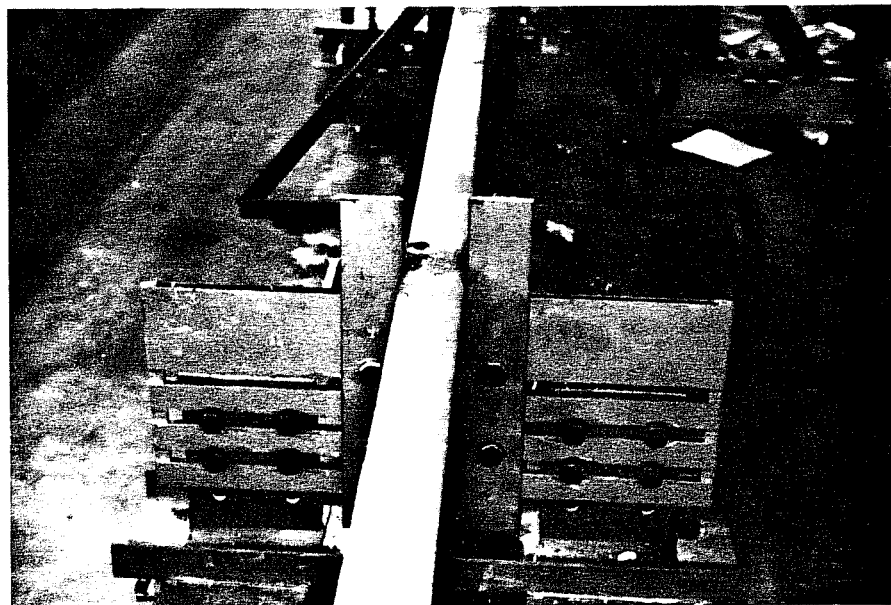


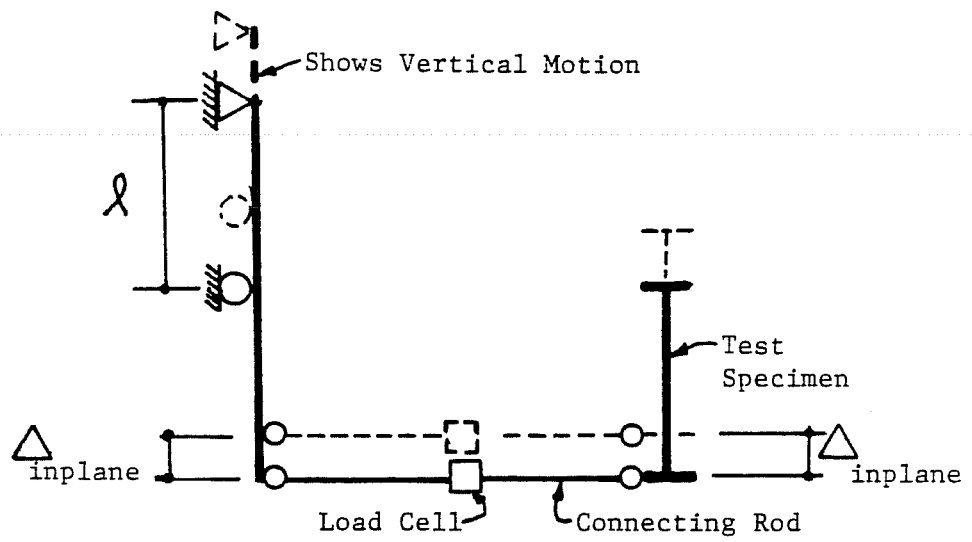
Fig. 3.9 Out-of-plane supports.

to provide lateral support for both flanges of the specimen and to accommodate the vertical deflection of the beam.

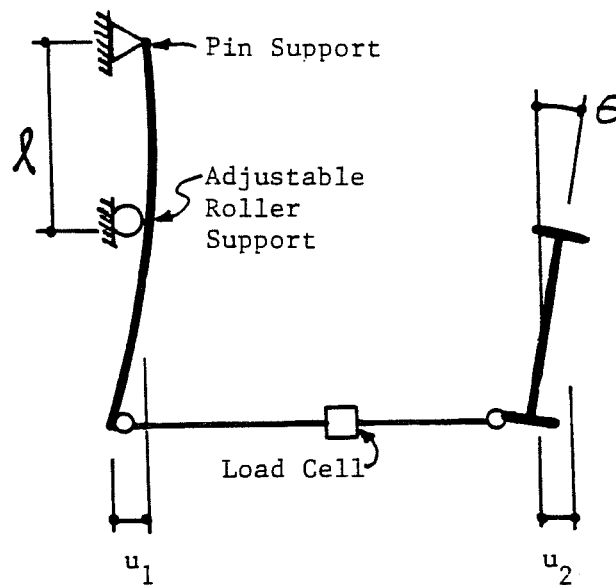
3.3 Brace Spring

A low brace stiffness was theoretically sufficient to buckle the test span into the second mode shape. A brace system utilizing flexure was chosen to supply the necessary flexibility. The overhanging cantilever arrangement, shown in Fig. 3.10(a), was mounted on a vertical track in order to compensate for the inplane deflection of the test specimen shown in the right side of the figure. A connecting rod with pinned ends was placed between the brace spring and the compression flange of the specimen to prevent any torque or a vertical component of force from being transmitted into the flange of the test specimen. A load cell was used at the center of this rod to measure the brace force. The brace mechanism involved flexing of the brace spring as buckling deflections occurred in the specimen, as shown in Fig. 3.10(b). Adjustment of the lower support of the brace spring enabled the stiffness to be varied. By reducing the length " l ", it was possible to decrease the brace stiffness.

The brace spring, shown in detail in Figs. 3.11(a) and 3.11(b), consisted of two $3/8 \times 2-1/2$ in. plates which were 2 ft long and had a yield stress of 100 ksi. The plates were connected by pairs of screws along the length of the brace bar as shown in Figs. 3.11(a) and (c). Although the screws were tight, they flexed elastically which permitted the plates to move relative to each other. This action was acceptable when the brace stiffness was low and the brace displacement, u_1 , in



(a) relative motion of brace spring and specimen



(b) flexing of bar resists buckling deflections

Fig. 3.10 Schematic of brace spring.

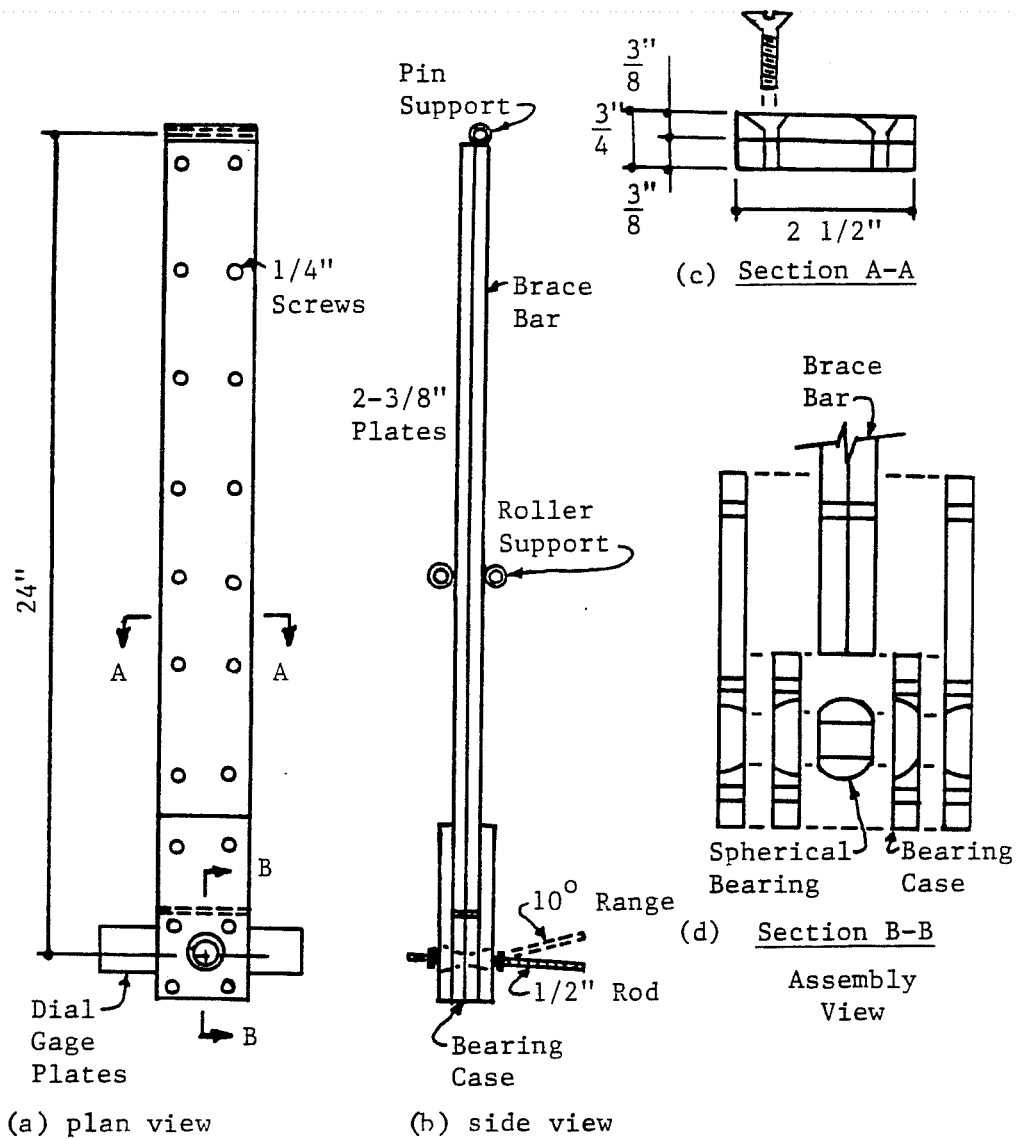
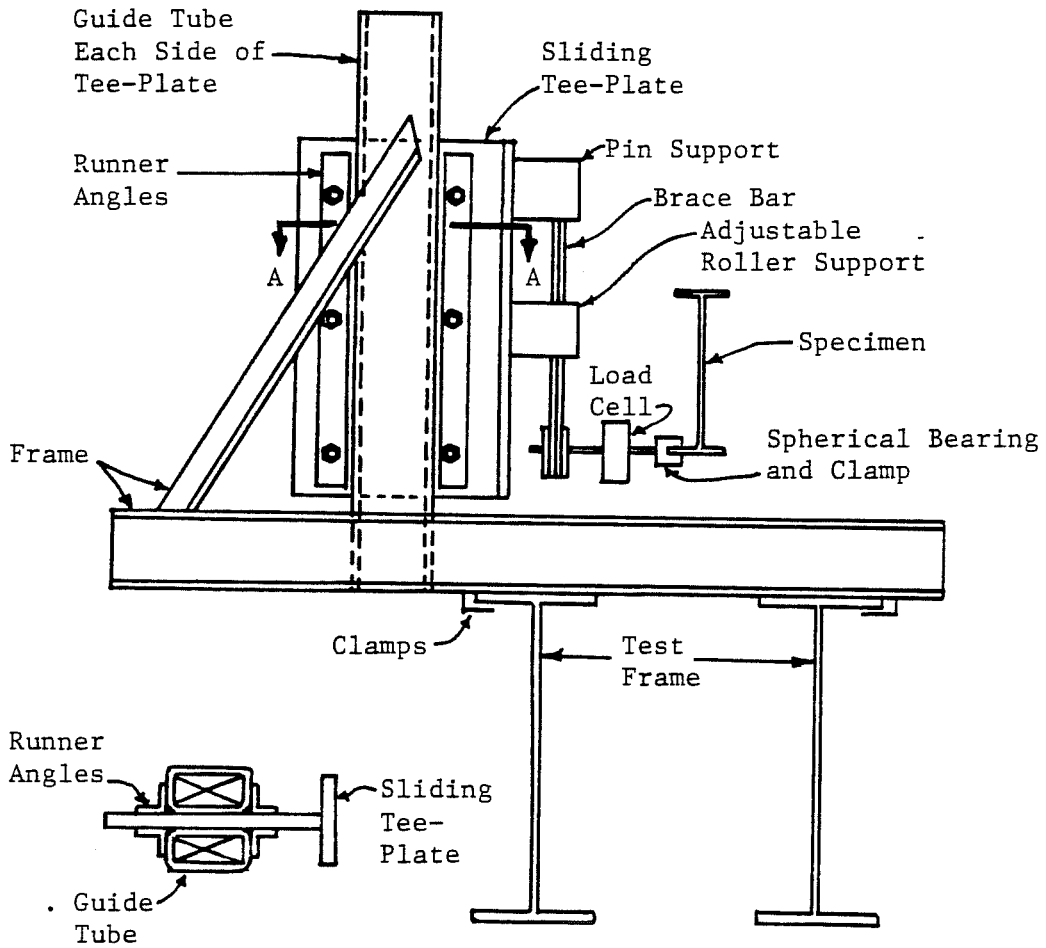


Fig. 3.11 Brace spring details.

Fig. 3.10(b), was large; however, problems with reproducibility were encountered when the brace was stiff and the brace displacements were small. The brace was subsequently improved by tack welding the two plates together for the tests involving high brace stiffnesses. In the future, a single plate is recommended for similar applications. The connecting rod was attached to the brace spring with a spherical bearing as shown in the assembly view in Fig. 3.11(d). This bearing was necessary to permit the vertical or horizontal inclination of the rod which was expected to occur during testing. A similar bearing was used at the other end of the rod where the brace was clamped to the flange at the specimen.

Because the test specimen deflected vertically during testing, it was necessary to adjust the connecting rod between the brace spring and the specimen to a level position so that the brace would develop the proper stiffness. A vertical track was devised to act as a support for the brace spring which allowed vertical movement of the entire assembly. The brace spring was mounted on a sliding tee-plate, as shown in Fig. 3.12, which had slotted holes so the upper and lower supports of the brace could be repositioned when a different brace stiffness was needed. Attached to this tee-plate was a pair of runner angles on each side which kept the tee-plate positioned between two vertical guide tubes. A frame on each side held each guide tube in place. These frames were interconnected so they worked together. The brace-spring frame was attached to the test frame. Using 0.001 in. dial gages, no perceptible deflections were observed at any point in this frame when force was



Section A-A

Plan View

Fig. 3.12 Brace spring mounted on sliding tee plate in frame.

placed in the brace spring. The brace spring and the brace spring frame are shown in Figs. 3.13 and 3.14.

The stiffness of the brace was determined in two ways. Prior to a series of tests where a specific brace stiffness was to be used, the brace was disconnected from the test specimen and connected to an auxiliary ram. The force imposed in the brace was measured with a load cell in the connecting rod and the deflections, u_1 and u_2 shown in Fig. 3.10(b), were recorded. The flexibility of the brace bar and load cell were determined and the inverse of the sum of these values was the stiffness of the brace at its connection to the flange of the specimen. The flexibility of the connecting screws, mentioned previously, was included in the flexibility of the brace bar and this flexibility was seen to be linearly elastic. During testing, the brace force was recorded as well as the deflection, u_1 , at the brace spring. The stiffness of the brace at the brace spring was obtained by measuring the slope of the brace force- u_1 plot shown in Fig. 3.15. The inverse of this stiffness, or the flexibility, was added to the flexibility of the load cell and the connecting rod which was determined during the pre-test calibration to get the flexibility of the brace at the flange of the specimen during a test.

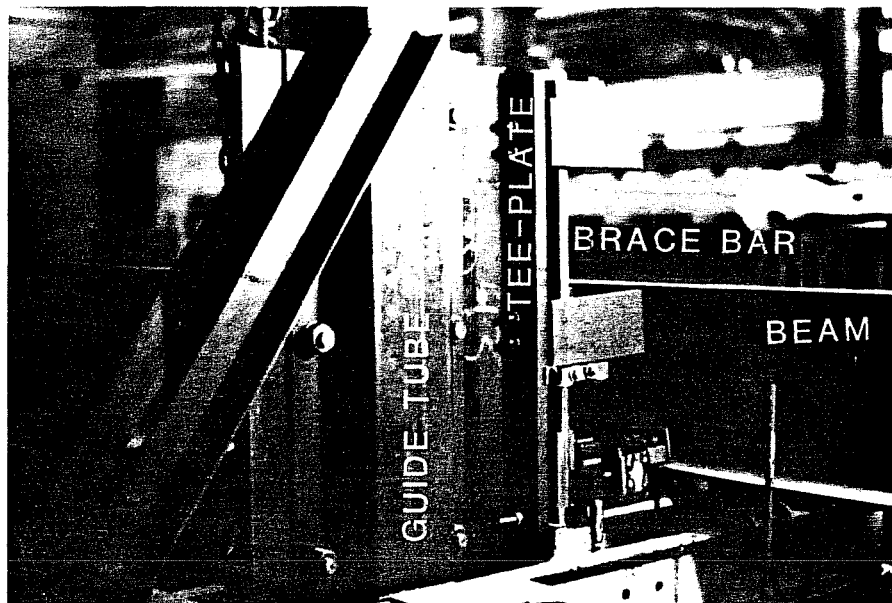
3.4 Forced Initial Imperfections

Forced imperfections or misalignments were imposed on the test specimen such that the section was displaced laterally but not twisted. The device producing the imperfection, shown in Fig. 3.16, prevented the beam from returning to its natural position but did not restrain motion



Fig. 3.13 Brace spring connected to brace bar.

Fig. 3.14 Vertical track for brace bar support which accommodates vertical motion.



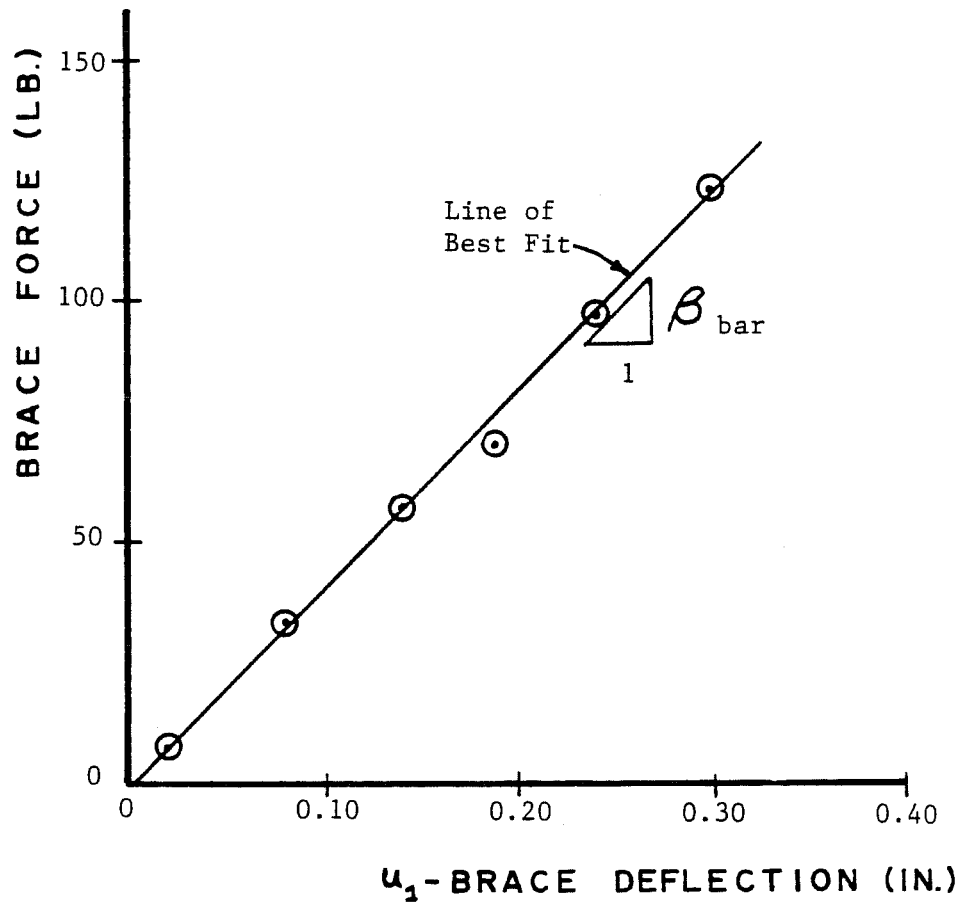


Fig. 3.15 Verification of brace spring stiffness during testing.

away from it. The device, termed the restraint angle, consisted of a series of angles welded together and was clamped to one of the frame girders. Threaded rods were passed through slots cut in the restraint angle, above and below the test specimen, and connected to a tube on the other side of the beam. Nuts were used to push the tube against the specimen in the direction of the restraint angle. The magnitude of the imperfection was set by temporarily placing 0.001 in. dial gages on the restraint angle to measure the initial deflection of the beam toward it. The specimen could be plumbed with a vertically held level by turning the nuts on the threaded rods. There was enough clearance between the upper and lower threaded rods to permit the vertical deflection of the beam throughout testing.

A pair of restraint angles were required to produce the various initial imperfection shapes. The restraint angles as shown in Fig. 3.17(a), were located at third points of the test span and oriented to produce the first mode shape. The second mode shape was formed by reversing one of the restraint angles as shown in Fig. 3.17(b). In both configurations, care was taken to tighten the nuts on the connecting rod from the brace spring to the specimen after all imperfections were imposed so that the initial force in the brace was zero.

The forcing of a misalignment into a beam is interesting since it occurs in actual structures and its effect on the brace force has not been determined experimentally. The behavior of a beam with a forced imperfection will not be the same as a beam with a natural or unforced imperfection of the same magnitude. When the imperfection is forced,

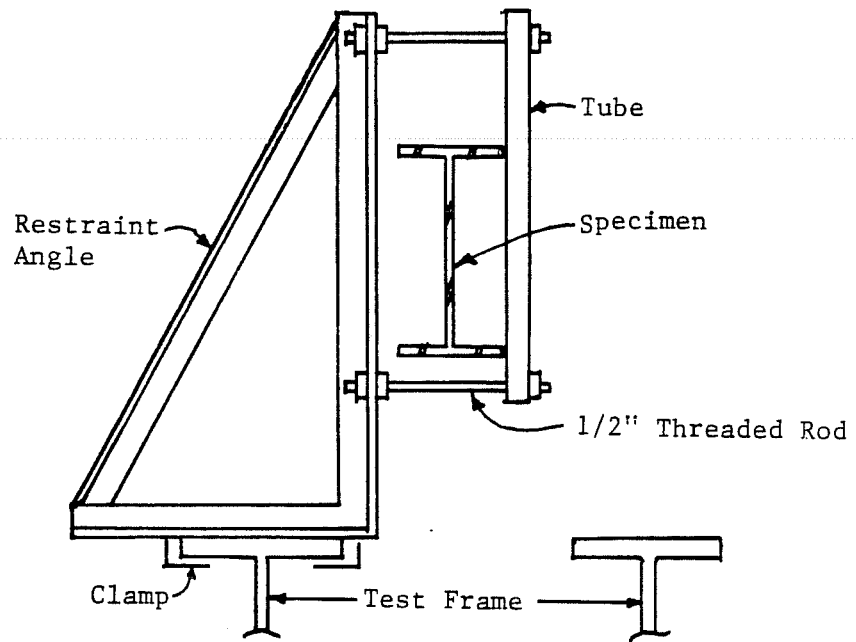


Fig. 3.16 Restraint angle for forced imperfections.

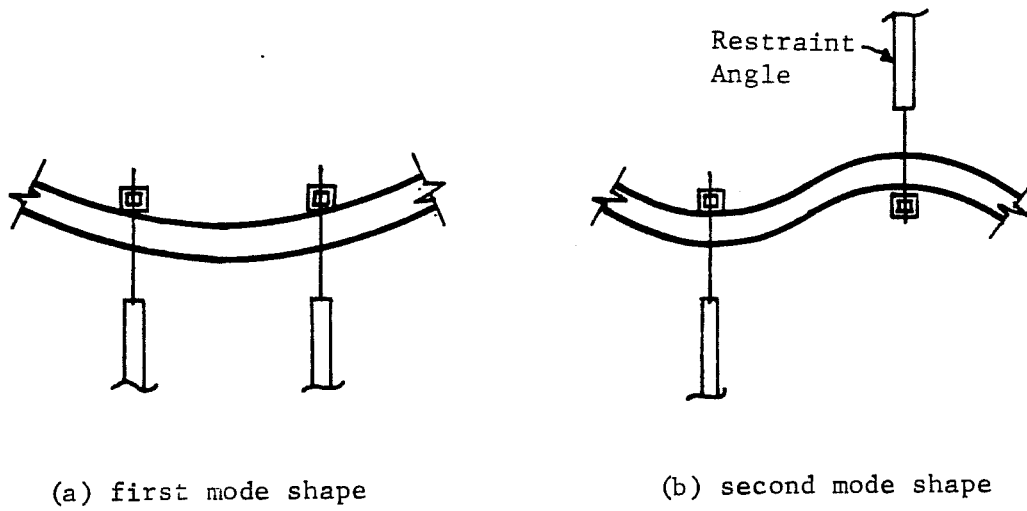


Fig. 3.17 Forced initial imperfections.

the tension flange is not allowed to straighten out as the beam moment increases as it would for the case of a natural imperfection. It may be speculated that the forcing of an imperfection alters the center of rotation from that of a beam with natural imperfections but this view has not been substantiated with a mathematical argument.

3.5 Load and Deflection Measurements

Inplane loads were measured at the hydraulic cylinders at pts. A, in Fig. 3.2, and at the load cells at pts. B. Pressure in the common hydraulic lines to the rams was sampled with a pressure transducer which was calibrated in a dead weight pressure tester. The ram was calibrated in a testing machine to determine its force-pressure relationship. The load cells were also calibrated.

Inplane deflections, at points B and D in Fig. 3.2, were observed using 0.001 in. dial gages. A datum was established as the line between the deflected positions of the supports at pts. B. The deflection at the midspan, pt. D, was added to the deflection of the datum line at this point, or average of the support readings, to get the midspan deflection of the beam relative to the supports.

The buckling or out-of-plane deflections were those of the brace point lateral displacement, and the lateral deflection and twist of the quarterpoint which is halfway between pts. C and D in Fig. 3.2. A 0.001 in. dial gage was used to measure the brace point displacement as discussed previously. The quarterpoint twist was measured using an inclinometer, as shown in Fig. 3.18, which was attached to the top flange of the specimen.

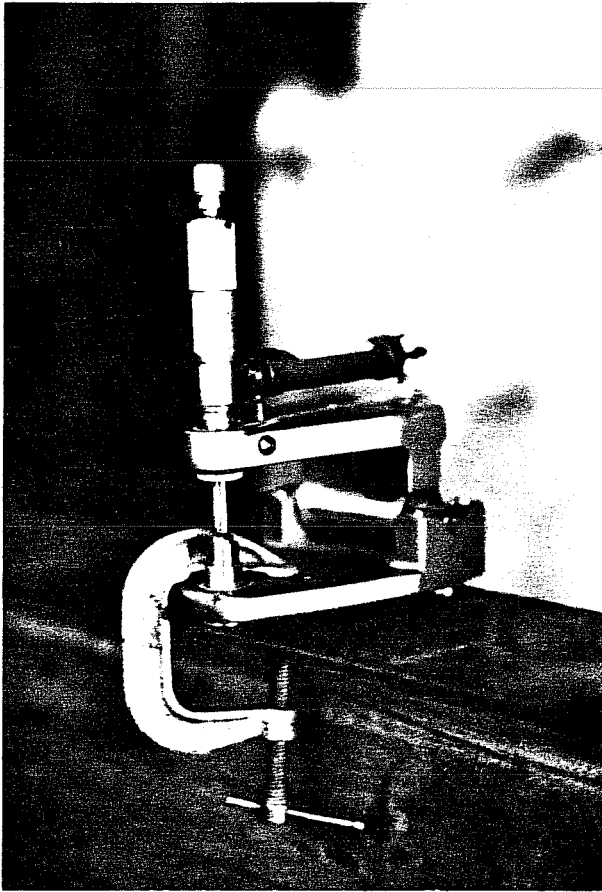
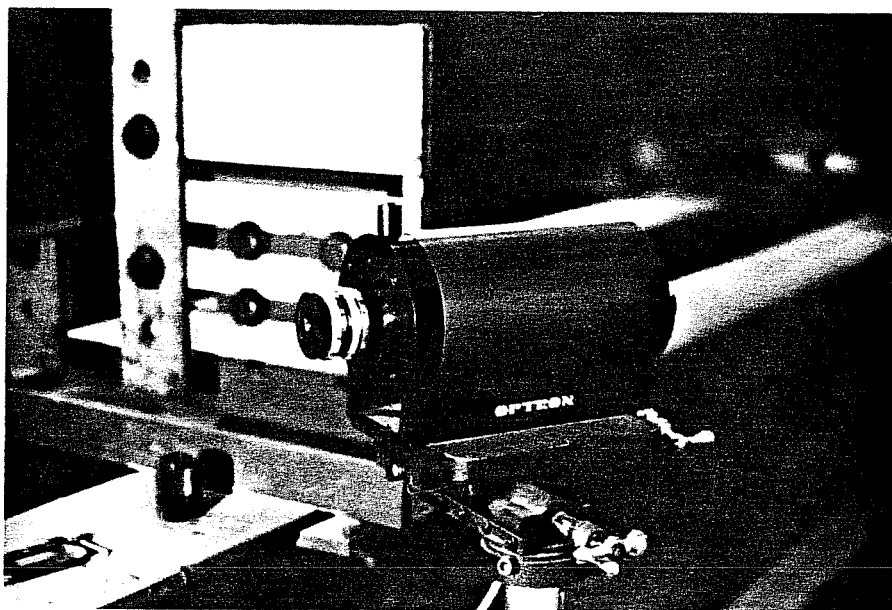


Fig. 3.18 Inclinometer.

Fig. 3.19 Optron--optical tracking device.



The quarterpoint was chosen for observation since the buckling deflections would be maximum at this location when the test span is buckled into the second mode shape. A biaxial tracking device, Optron, was used to follow the deflection of this point optically. The Optron, shown in Fig. 3.19, was able to detect the changing position of a target attached to the test specimen. The target was mounted on the bottom flange of the specimen and the horizontal motion was tracked. The device was calibrated for the specific distance to the target and with proper lighting resolved 0.005 in. displacements.

C H A P T E R I V

TEST PROCEDURE AND RESULTS

4.1 Test Procedure

Initially, the beam was bent under its self-weight in a direction opposite to that caused by the applied loading. Loading was performed by manually pumping oil to the hydraulic cylinders at each end of the test frame which were connected by a common line. A small amount of pressure was needed to overcome the moment due to self-weight and the midspan moment was then essentially zero. By increasing the hydraulic pressure, the midspan of the test beam continued to deflect vertically, as shown in Fig. 3.5, and the bottom flange was put into compression. The tendency of this flange to buckle laterally was restrained at the midspan by the bracing system. The connecting rod between the brace spring and the test beam was manually leveled by moving the sliding tee-plate for the brace spring, shown in Fig. 3.12, upward between the guide tubes of the brace spring frame. This procedure was done intermittently during loading and at the end of a particular load stage where loading was stopped and readings were taken. At the end of each increment of loading, frictions between the test specimen and the test frame were minimized at the lateral restraint points, A, B, and C, by vibrating the slotted bracing plates. Load and deflection readings were then taken. The load and deflection readings were observed to change slightly in a direction which was indicative of a reduction of frictional restraint.

Load was applied in 2000 lb increments until the buckling deflections started to increase rapidly. At this point, 500 to 1000 lb load stages were applied. Loading was stopped when the calculated value of the inplane and lateral bending stress reached the yield stress at the tips of the compression flange so that the specimen could be reused. The load vs. quarterpoint lateral deflection was plotted with an X-Y recorder during testing. The test specimen was at the limit of its load capacity when the slope of this plot was horizontal. The flange tip yielding interaction line was superimposed on this plot and the loading was terminated when the load vs. lateral deflection plot reached this line.

Other readings taken at each load stage were: inplane deflection at the support points and the midspan; the quarterpoint twist; and the brace lateral deflection and brace force. The inplane load-deflection plot was used to check for elastic behavior and frictional restraint by observing the shape of the plot. The brace force-deflection plot was also used to evaluate the reliability of the data and check for non-linearity or slippage which could occur in the brace or the connecting equipment. The buckling deflections, which were the quarterpoint lateral deflection and twist, and the brace point lateral deflection were used in plots, such as the Southwell plot, to extrapolate the critical moment for the test. These plots were also very helpful in detecting unwanted restraints to these buckling deflections. These plotting methods are discussed in more detail in Chapter V.

4.2 Determination of Midspan Moment

Forces were measured at the hydraulic cylinders and load cells which constitute the load and support points of the test beam, respectively. The measured hydraulic cylinder force is plotted along with the average force in the load cells as a function of inplane deflection as shown in Fig. 4.1. Superimposed on this figure is the plot of the theoretical load-deflection relationship which was calculated from the measured properties of the section and is shown as a dotted line. The variation of force with inplane deflection was expected to be linear when the load was in the elastic range. At any given load stage, the force in the hydraulic cylinders was between 3 and 5 percent greater than the average of the load cell forces. The two load cell forces differed by no more than 4% and often this difference was less than 2%. The average load cell force shows a much closer correlation to the values calculated from the measured section properties than does the hydraulic cylinder force. The difference between the load cell and hydraulic cylinder forces can be attributed to internal friction in the hydraulic cylinder. Therefore, the average load cell force was considered to be more representative of the actual load applied to the beam. The moment was calculated as the average load cell force times the distance between the load cell and the hydraulic cylinder at each end of the test frame.

4.3 Test Results

Thirty tests were performed of which the first ten were pilot tests and the last twenty, Tests 11 through 30, are reported here. Of

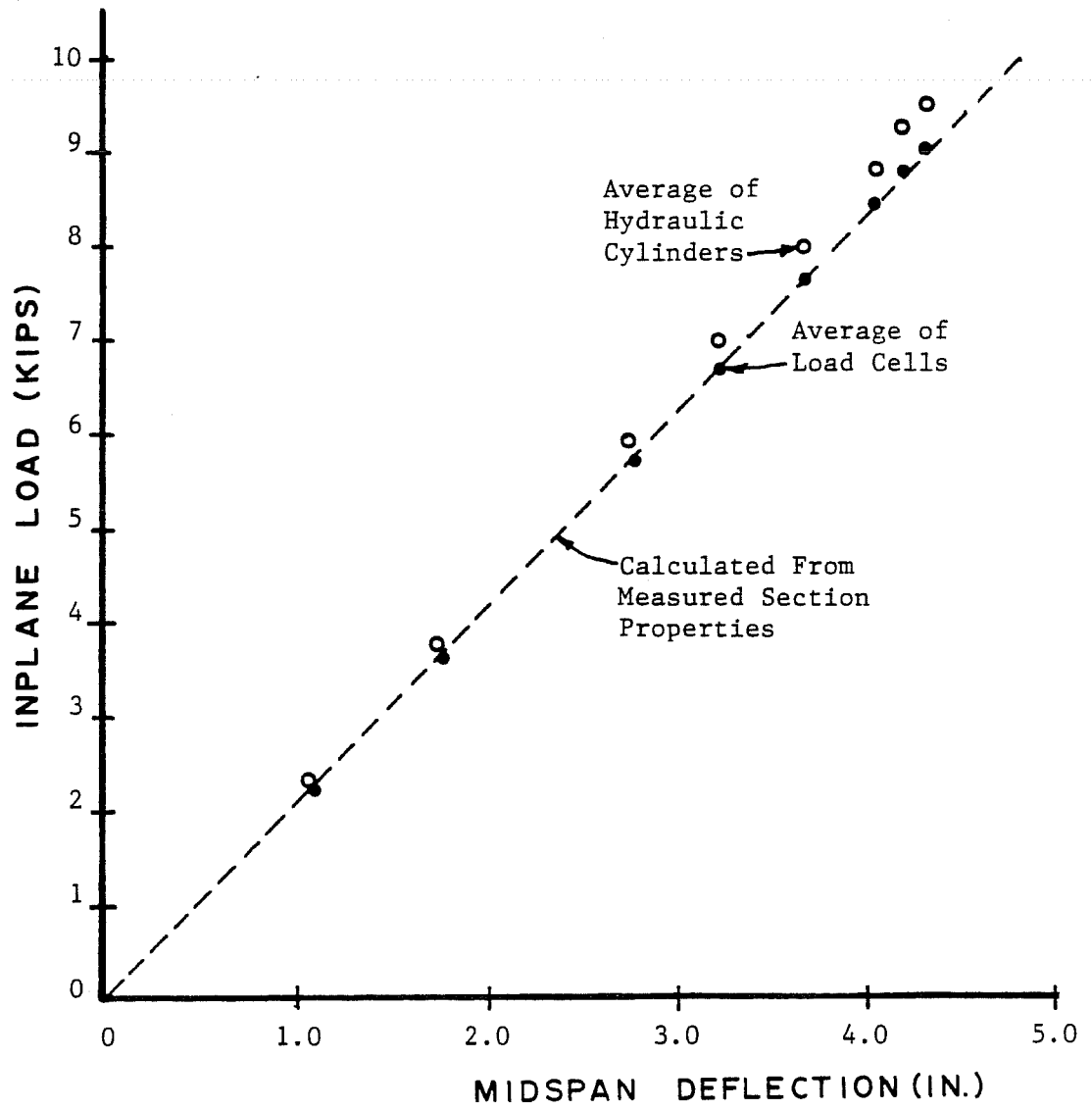
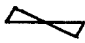
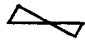
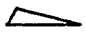

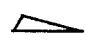


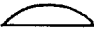
Fig. 4.1 Load vs. inplane deflection.

the last twenty tests, all were conducted in the elastic range except the last test, Test 30, which was taken to failure. The variables in the testing program were the stiffness of the brace and the magnitude and type of initial imperfection imposed on the specimen. The primary observations during testing were the force in the brace and the moment-displacement behavior at the brace point and quarterpoint. A theoretical ideal brace stiffness, calculated to be 0.70 kips per linear inch (kli) by using Eq. (2.7), was expected to be sufficient to force the test beam to buckle into the second mode shape. To establish the experimental value of the ideal brace stiffness, the stiffness of the brace used in Tests 11 through 21 was between 0 and 70 percent of the theoretical ideal value and the brace stiffness used in Tests 22 through 29 was between 1.3 and 5 times higher. In Test 30, the brace stiffness used was essentially that of a rigid brace since the stiffness was 26 times the theoretical value of the ideal brace stiffness.

In the first three columns of Table 4.1, the magnitudes of the brace stiffness and forced initial imperfection used for each test are presented. A test series consisted of group of tests having approximately the same brace stiffness and varying magnitudes of forced initial imperfections of 0, $L/2000$, and $L/1000$ of the 18 ft test span, or 0 in., 0.108 in., and 0.216 in, respectively. Tests 11 and 12 were a test series having no brace attached to the test specimen. Tests 13 through 18 had a brace stiffness of approximately 0.4 kli and were grouped into three pairs of tests each having a successively larger magnitude of initial imperfection. In Tests 19 through 21, a brace stiffness of

TABLE 4.1 BRACE FORCES

Test No.	Brace Stiffness (kli)	Forced Initial Imperf. (in.)	Highest Moment Reached (kips)	Max. Brace Force (lbs)	Compr. Region Force (k)	% of Compr. Force (%)
11	0.0	0.0 ¹	301.8 ²	---	30	---
12	0.0	0.205	280.5	---	28	---
13	0.350	0.000	426.2	116	43	0.27
14	0.400	0.000	424.8	128	43	0.30
15	0.380	0.105	381.7	123	38	0.32
16	0.380	0.105	401.8	146	40	0.37
17	0.390	0.216	384.1	139	39	0.36
18	0.420	0.195	386.6	145	39	0.37
19	0.530	0.000	439.8	94	44	0.21
20	0.510	0.113	409.4	123	41	0.30
21	0.490	0.214	374.5	123	38	0.32
22	1.250	0.000	492.1	88	49	0.18
23	1.90	0.000	531.5	89	53	0.17
24	1.60	0.000	545.8	32	55	0.06
25	1.13	0.220 	523.1	72	53	0.14
26	1.65	0.220 	530.0	77	53	0.15
27	0.880	0.220 	555.7	26	56	0.05
28	2.9	0.220 	581.3	46	58	0.08
29	3.2	0.218 	564.1	46	57	0.08
30	18. ₋ ⁺	0.000	610.5	97	61	0.16

¹ Shape is  unless otherwise noted.

² Includes 25.1 in.-k gravity moment.

$$M_g = 840 \text{ in.-k}$$

approximately 0.51 kli was used. In Tests 22 through 30, it became obvious that the test setup would not perform satisfactorily unless the magnitude of the forced initial imperfection was either zero or $L/1000$, because otherwise the test specimen would still be in contact with at least one of the restraint angles when other regions of the specimen were in danger of yielding due to the combination of inplane and out-of-plane bending stresses. Therefore, in Tests 22 to 30, the brace stiffness was varied but the magnitude and shape of the initial imperfection were chosen such that the specimen behaved properly.

As theoretically predicted, the test specimen buckled into the first mode shape when the brace stiffness was less than the ideal brace stiffness of 0.7 kli as was the case in Tests 11 through 21 and it buckled into the second mode shape when the brace stiffness was larger than this value as in Tests 22 through 30. The experimental value of the ideal brace stiffness was observed to be between the value of 0.53 kli and 0.88 kli used in Tests 19 and 27, respectively. In Table 4.1, the maximum brace force corresponding to the largest moment attained during each test is tabulated in column 5. The brace force is also given as a percentage of the force in the compression region of the specimen which is obtained by integrating the stresses over the compression area at the maximum moment. The largest brace forces were observed during the first mode tests where the forces were between 0.25 percent and 0.40 percent of the compression region force when the tests were stopped. If these tests were taken to failure, the brace force would have been expected to increase without bound. In the second mode

tests, Tests 22 to 30, the brace force reached a limiting value since the brace point developed into an inflection point. Of the tests which buckled into the second mode shape, the largest brace force was observed in Test 30 which was taken to failure. In this test, the brace force was 97 lbs, or 0.16 percent of the force in the compression region at the maximum moment.

In the following paragraphs, several representative tests are described in greater detail with emphasis on the moment-displacement behavior of the test specimen. Tests 11 and 12 were conducted with no brace attached at the midspan of the test span. Test 11 had no forced initial imperfection whereas the beam in Test 12 was displaced laterally a distance of $L/1000$, or 0.216 in., at the midspan of the test span as shown in Fig. 3.17(a). The lateral deflection at the quarter point was plotted as a function of inplane moment for both Tests 11 and 12 as shown in Fig. 4.2(a). Both curves have decreasing slopes with increasing moment which is characteristic of buckling deflections. The curve for Test 12 was flatter and did not have increasing deflections until the moment was about 125 in.-k. The compression flange of the beam did not deflect laterally until the out-of-plane P-delta moment was greater than the resisting out-of-plane moment which resulted from forcing the initial imperfection into the test span. Once the compression flange pulled away from the restraint angle, shown in Fig. 3.16, the deflection at a given load was greater than that for Test 11 where no imperfection was imposed. A plot of moment vs. the twist at the quarter point for both tests is shown in Fig. 4.2(b) and these displacements were similar

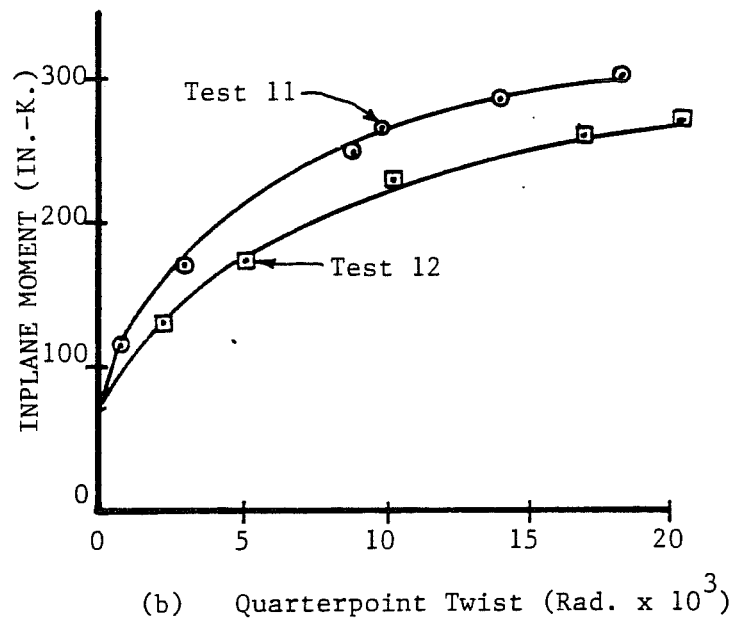
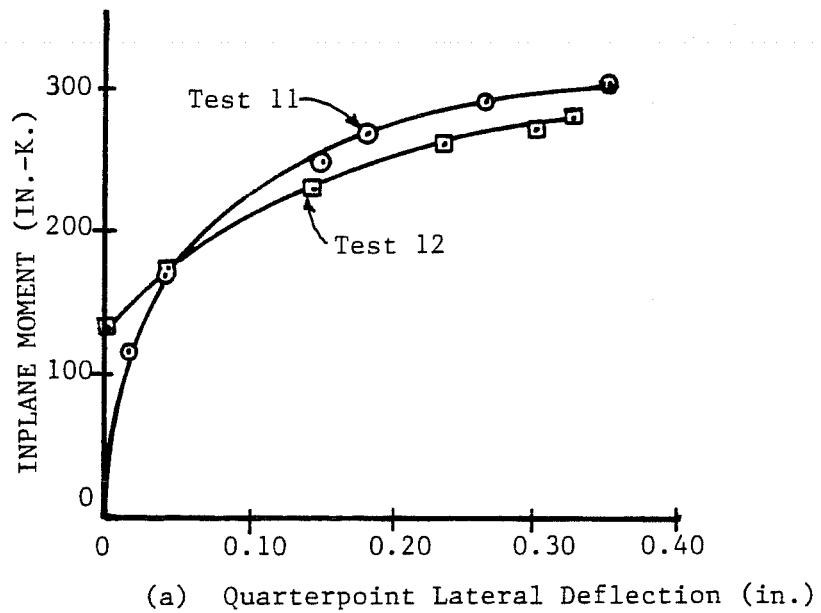
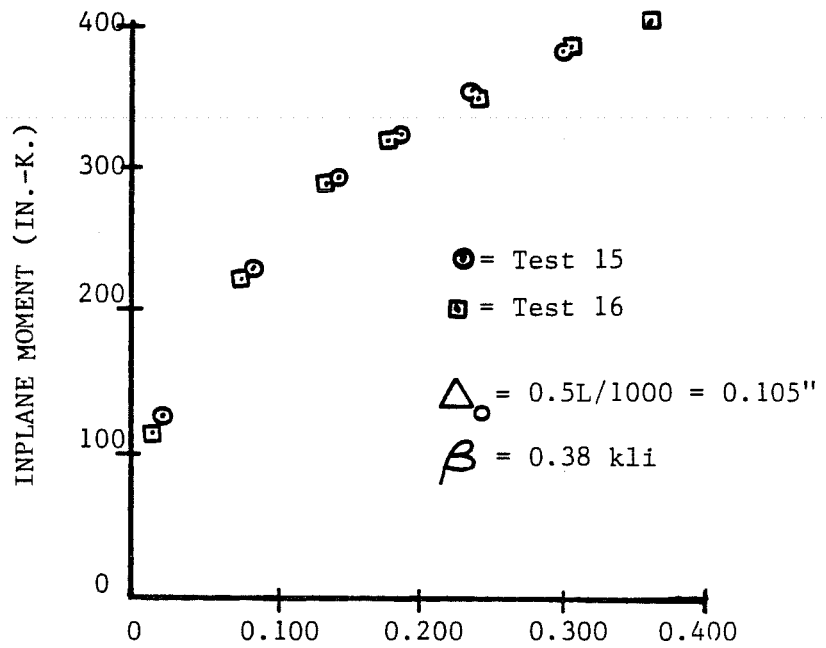


Fig. 4.2 Comparison of Tests 11 and 12.

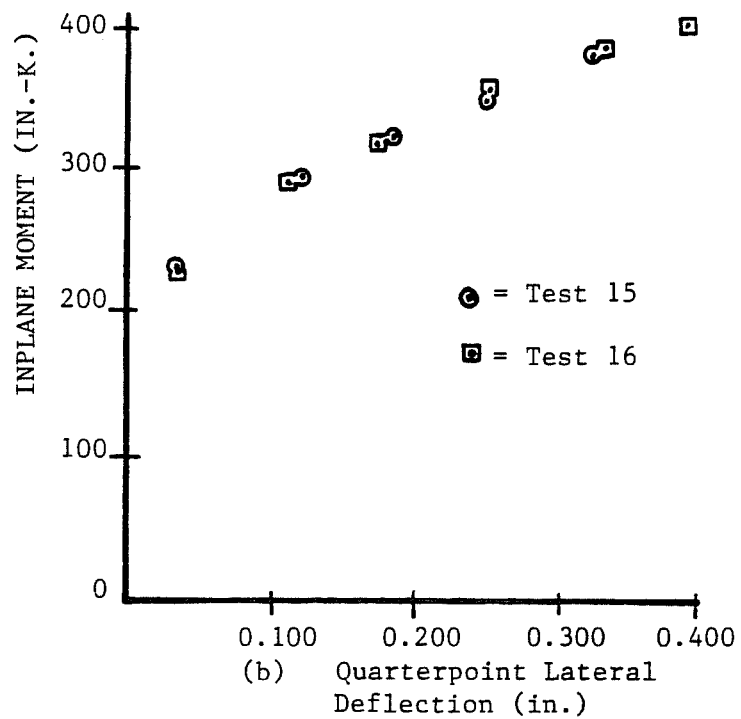
to those in Fig. 4.2(a). The maximum twist recorded was less than two degrees while the lateral deflection was approximately $3/8$ in.

In Tests 15 and 16, the stiffness of the brace at its connection to the test specimen was 0.38 kli or 55% of the ideal stiffness. The magnitude of the forced initial imperfection used was 0.105 in. or approximately $L/2000$. The test span deflected gradually into the first mode shape with increasing moment. A plot of the applied moment vs. brace deflection is shown in Fig. 4.3(a) and a plot of moment vs. deflection at the quarterpoint is shown in Fig. 4.3(b). The data points for Test 15 are shown in these plots with a circle, those for Test 16 are shown with a square, and the connecting curves are omitted for clarity. The data points for both tests follow almost exactly the same path for both types of deflection and demonstrate the reproducibility of these tests. In both cases, the moments are observed to be greater than those of the unbraced case for a given value of lateral deflection.

The brace stiffness in Test 25 was 1.13 kli, or 1.6 times the ideal stiffness, and this stiffness was sufficient to force the test span to buckle into the second mode shape. The deflection at the brace point was limited to approximately $1/16$ in. and the brace force was 72 lbs when the test was stopped due to excessive deflections at the quarterpoint. In Test 29, the brace stiffness was 3.2 kli, or 4.6 times the ideal stiffness. The span buckled into the second mode and when the test was stopped due to excessive quarterpoint deflections, the brace force was 46 lbs and the brace deflection was approximately 0.015 in. The effect of increasing the brace stiffness on the magnitude of the



(a) Brace Deflection (in.)



(b) Quarterpoint Lateral Deflection (in.)

Fig. 4.3 Comparison of Tests 15 and 16.

brace deflection and the moments is shown in Fig. 4.4. The brace deflection for Test 15, with the 0.38 kli brace stiffness, increased much more rapidly than those for Tests 25 and 29 which had brace stiffnesses that were able to force the specimen to buckle into the second mode. The brace deflections for Tests 25 and 29 appear to have increased to a finite limit rather than increasing without bound as in Test 15. The deflections at the quarterpoint, shown in Fig. 4.5, increase toward an infinite value for all tests. Also shown in Figure 4.5 is the plot for the unbraced case, Test 11. The increase in attainable moment for an increasing brace stiffness is clearly seen. The moments observed in Test 29, with the 3.2 kli brace, were almost double that of the unbraced span in Test 11.

The beam was tested to failure in Test 30 where the brace stiffness was approximately 18 kli, or 26 times the ideal stiffness. No forced imperfections were imposed on the specimen. The quarterpoint deflection of the compression flange, shown in Fig. 4.6, exceeded 0.75 in. when the section suddenly yielded at a moment of 611 in.-k. There was no appreciable increase in moment during the last 0.5 in. of this deflection and the force in the brace was 97 lbs.

The critical moment, defined as the moment when some or all of the test span has deflected an infinite distance, could not be observed directly from the moment-deflection plots. At high moments, however, the deflections which were increasing toward an infinite value could be mathematically extrapolated to the value of moment at which these deflections become infinite. This critical moment becomes the reference

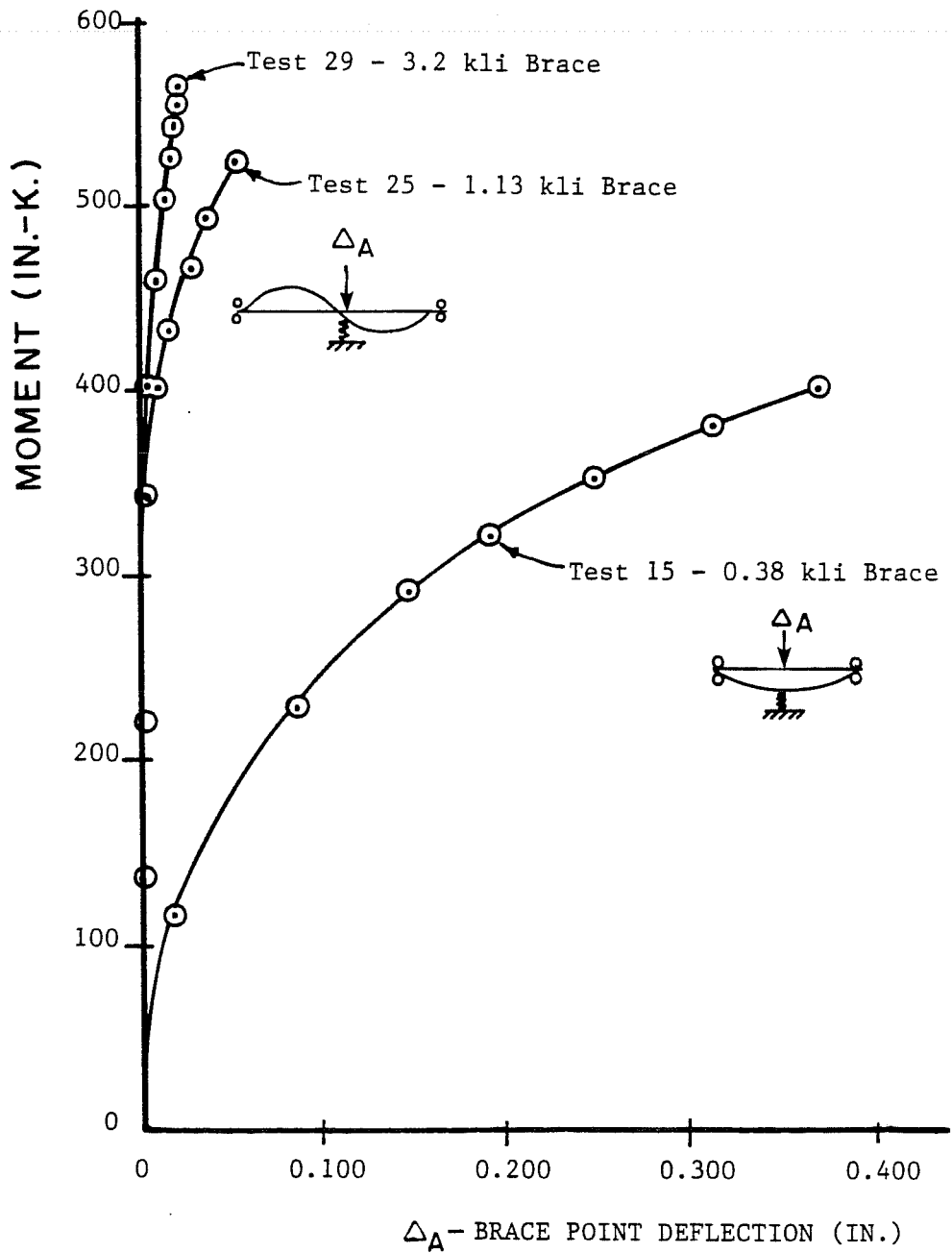


Fig. 4.4 Brace point deflection for various brace stiffnesses.

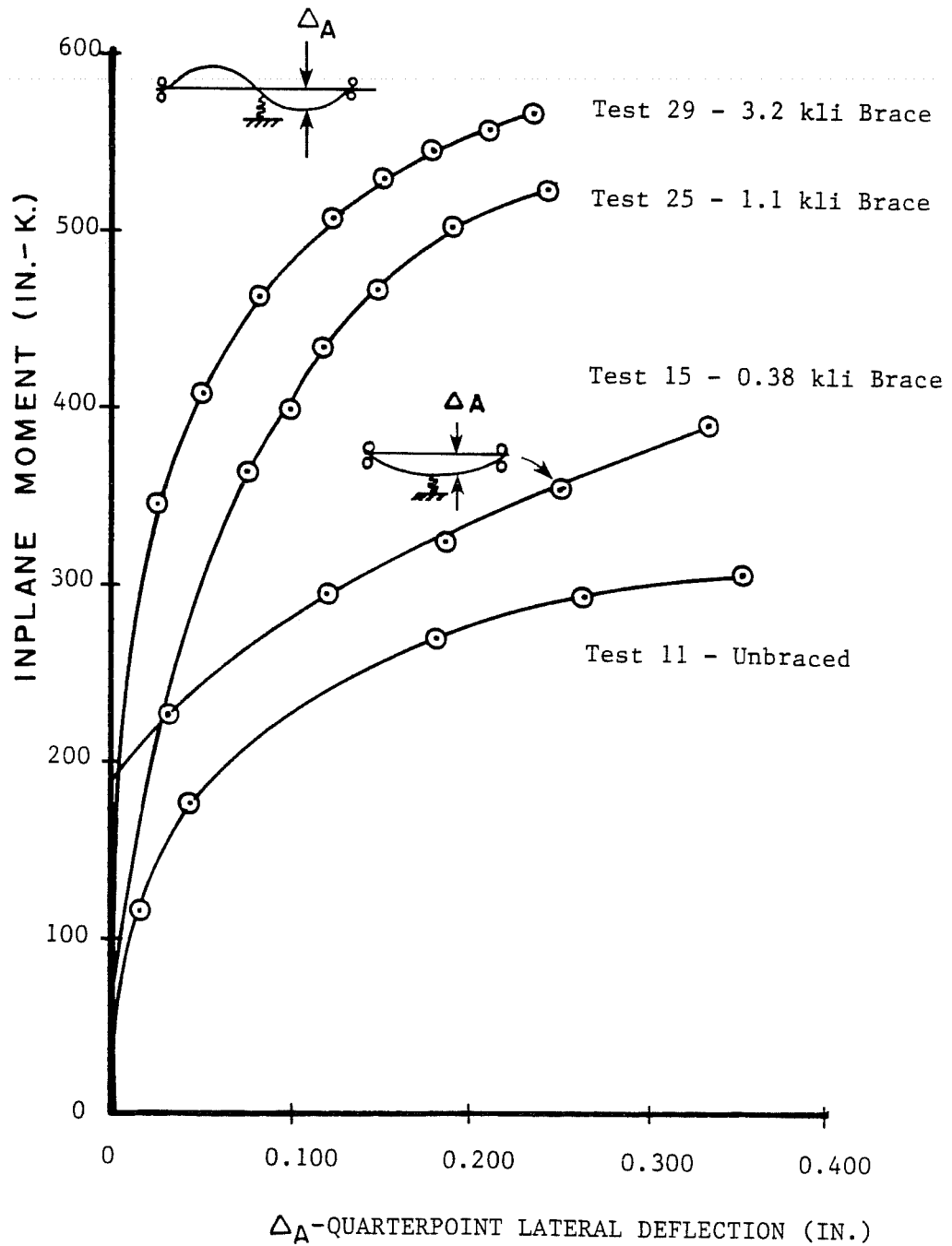


Fig. 4.5 Quarterpoint deflections for beam with various brace stiffnesses.

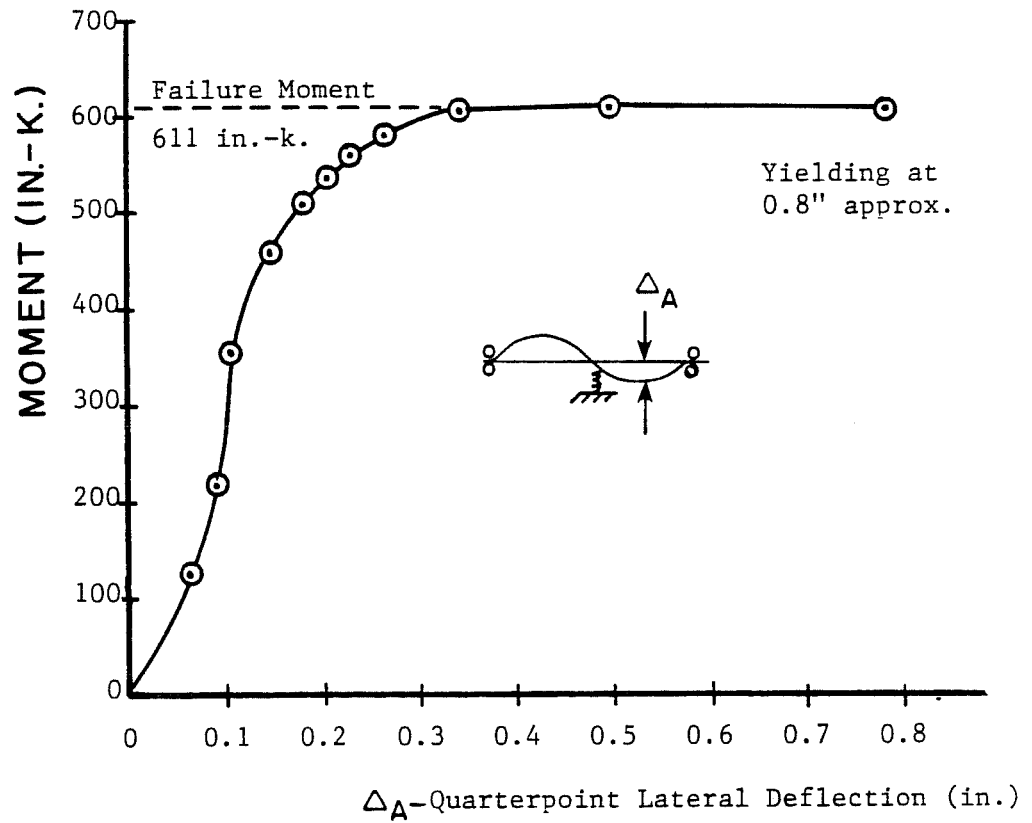


Fig. 4.6 Moment vs. quarterpoint lateral deflection for Test 30 taken to failure.

point to compare tests which were stopped prior to failure of the specimen to allow further testing in the elastic range with the same specimen. The critical moments are obtained and comparisons with analytical predictions are included in Chapter V.

C H A P T E R V

ANALYSIS OF TEST RESULTS

In this chapter the bifurcation moments of the test specimen with various brace stiffnesses are calculated using differential equations and finite element solutions. The analytical results are compared to the critical moments extrapolated from the test data. A plot of moment vs. brace stiffness is also presented and the observed brace forces are compared to analytical estimates.

5.1. Calculation of Bifurcation Moment

The critical moment for the beam can be obtained by treating the beam as a column to get an effective length factor and using Eqs. (2.3), (2.4), and (2.5). The critical moments were calculated using an alignment chart for a braced frame and assuming buckled shapes as shown in Fig. 3.3. The end restraint factors were modified for the presence of compression stress in the side spans and for deviations from the assumptions used in developing the charts. The calculated critical moments were 341 in.-k for the unbraced case and 594 in.-k for the second mode as shown in Fig. 3.3(b). These values include the 25 in.-k to overcome the gravity load moment in the specimen and correspond to values for a , in Eq. (2.2), of 0.66 and 0.47, respectively. Without the warping restraint produced by the continuity, these values of a would have been 1.0 and 0.5.

A finite element program, which could model the interaction between the buckling of the testspan and sidespans was used to check the results above and to calculate the critical moment at a particular brace stiffness. The program, BASP [7], which stands for Buckling Analysis of Stiffened Plate structures, was used to model the W12x16. A discussion of this program is given in Appendix C. Using the measured section properties, the first and second mode bifurcation moments, including the 25 in.-k gravity moment, are 339 and 598 in.-k. These values are within 1% of those calculated using Eq. (2.2). The results for brace stiffnesses between zero and ideal are given in section 5.4 where they are compared to the critical moments from the test results.

5.2 Techniques for Determining Critical Moments

Since the same beam was to be used for all tests, the beam load could not be taken to the critical value because second order stresses would cause yielding. Therefore, plotting techniques developed by Southwell, Lundquist and Meck, using the load-displacement data, were used to estimate the experimental elastic buckling load.

The deflections of an imperfect member increase without bound as the bifurcation load of an otherwise perfect member is approached. These deflections increase rapidly with increasing load or moment and are related, as is done in Ref. 6 by using Eq. (1.4), to the magnitude of the critical moment and the magnitude of the component of the initial shape which is similar to that of the bifurcation buckling mode shape. For example, if the imperfection shape is a half sine wave with a

midspan amplitude of Δ_o , the additional deflection, Δ_A , due to the applied load is given by Eq. (1.4). This equation can be rewritten as

$$\frac{\Delta_A}{P} = \frac{\Delta_A}{P_{cr}} + \frac{\Delta_o}{P_{cr}} \quad (5.1)$$

and when plotted as in Fig. 5.1, is the equation of the Southwell Plot [4]. For data points in the elastic range, the slope of the line of best fit through these points is the inverse of the critical load. The negative horizontal intercept is the magnitude of the initial imperfection. These two parameters are used in Eq. (1.4) to describe a hyperbola of best fit which passes through the origin of the load-deflection plot. In beam buckling tests, moment is used as the measure of load in Eqs. (1.4) and (5.1) since it is proportional to the inplane stress in the compression flange.

Lundquist [8] generalized the mathematics of a hyperbolic curve fit to pass the curve through a data point, called the reference point, which is held in higher confidence than the origin due to initial non-buckling related movements occurring when the load is first applied. The equation of the Lundquist plot is

$$\frac{\Delta_A - \Delta_R}{P - P_R} = \frac{\Delta_A - \Delta_R}{P_{cr} - P_R} + \frac{\Delta_o + \Delta_R}{P_{cr} - P_R} \quad (5.2)$$

where P_R and Δ_R are the load and deflection of the reference data point. The inverse of the slope of the Lundquist plot, shown in Fig. 5.2, is $P_{cr} - P_R$ or the difference between the critical load and the reference

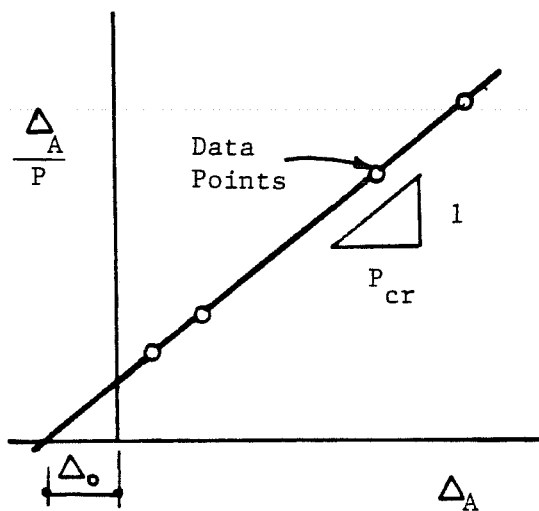


Fig. 5.1 Southwell plot.

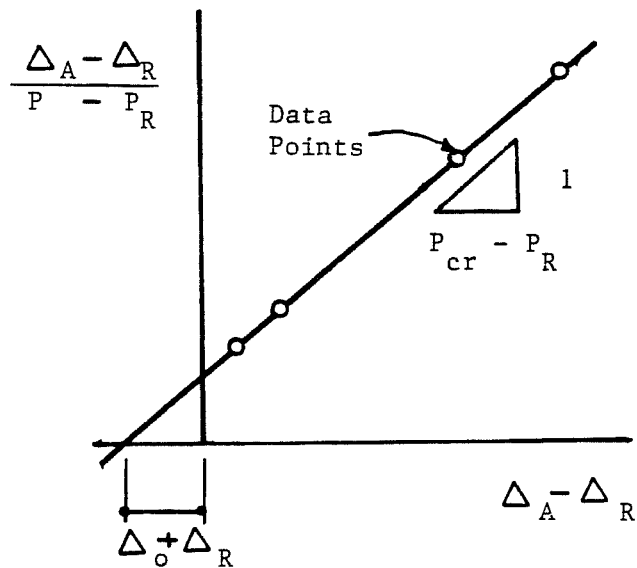


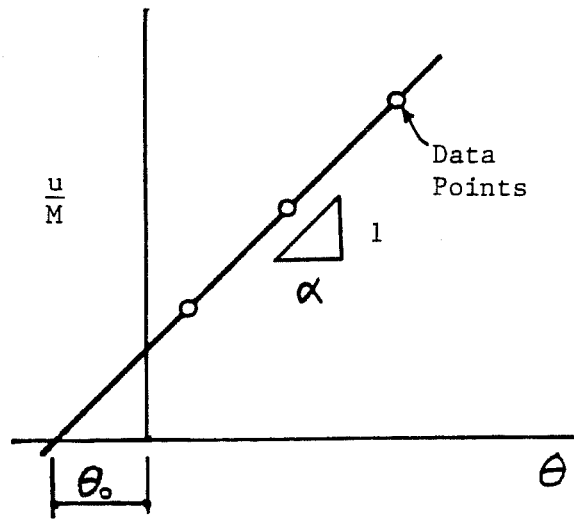
Fig. 5.2 Lundquist plot.

load. The negative horizontal intercept is the sum of the initial imperfection and the reference deflection. A Southwell plot is produced when P_R and Δ_R are equal to zero.

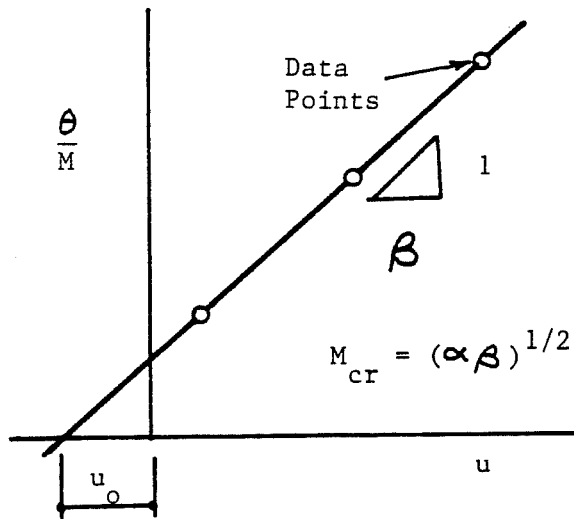
Meck [9] developed a plotting method specifically for beams. In the solution of the two simultaneous equations involving the lateral displacement and twist, one variable is usually solved in terms of the other. Plotting methods based on the resulting equation are complex and involve quadratic terms [3]. The slope of this equation does not become sufficiently linear until high moments are attained which limits their usefulness for plotting. Meck avoided this difficulty by not making the final substitution for an equation in one variable. Two equations are used which involve linear relations between functions of the lateral deflection and twist. A plot of the ratio of lateral deflection to moment as a function of twist is shown in Fig. 5.3(a) and a plot of the ratio of twist to moment as a function of lateral deflection is shown in Fig. 5.3(b). The slopes of the lines of best fit through the data points for these plots are defined as α and β , respectively. The critical moment is given by

$$M_{cr} = (\alpha\beta)^{1/2} \quad (5.3)$$

The initial lateral twist and deflection are found from the negative horizontal intercepts of Fig. 5.3(a) and 5.3(b), respectively. These plots are analogous to "Southwell" plots for beams [9].



(a) ratio of deflection to moment vs. twist



(b) ratio of twist to moment vs. deflection

Fig. 5.3 Meck plots for beam buckling.

5.3 Critical Moments from the Tests

Predictions of the critical moment for each test were made by applying the plotting techniques to the quarterpoint lateral deflection and twist and the brace point deflection. Figure 5.4 shows the Southwell and Lundquist plots for the quarterpoint twist in Test 11. The lower curve is the Southwell plot and the curves above it are Lundquist plots with the reference point taken at successively higher load stages. The curves having reference points at low load stages are more linear than those with reference points at high load stages. This occurs because the curve fitting process becomes more ill-conditioned, or susceptible to error, when the reference point is taken on the flatter region of the load-deflection curve. Focusing on the lower three curves, (a) the Southwell plot, (b) and (c) the Lundquist plots with reference points at the second and third load stages, the critical moments for these plots are 352, 351, and 350 in.-k, respectively. Meck plots for Test 11 are shown in Figs. 5.5 and 5.6 and the critical moment predicted by these plots is 350 in.-k. In this case, the critical moment for all three plotting techniques is about the same. The Southwell and Lundquist plots for the quarterpoint lateral deflection for this test also give similar results.

A complete summary of plotting results for all the tests is included in Appendix B. The results of the Meck and Southwell plots are extracted from this summary and given in Table 5.1. In this table, the test parameters are tabulated in the first three columns and the bifurcation moment predicted by the finite element program, BASP, is shown in

TEST NO. 11 - NO BRACING - NATURAL IMPERFECTIONS
 QUARTER POINT LATERAL DEFLECTION - IN.

THE BRACE STIFFNESS IS: 0.000
 THE INITIAL IMPERFECTION IS: 0.000

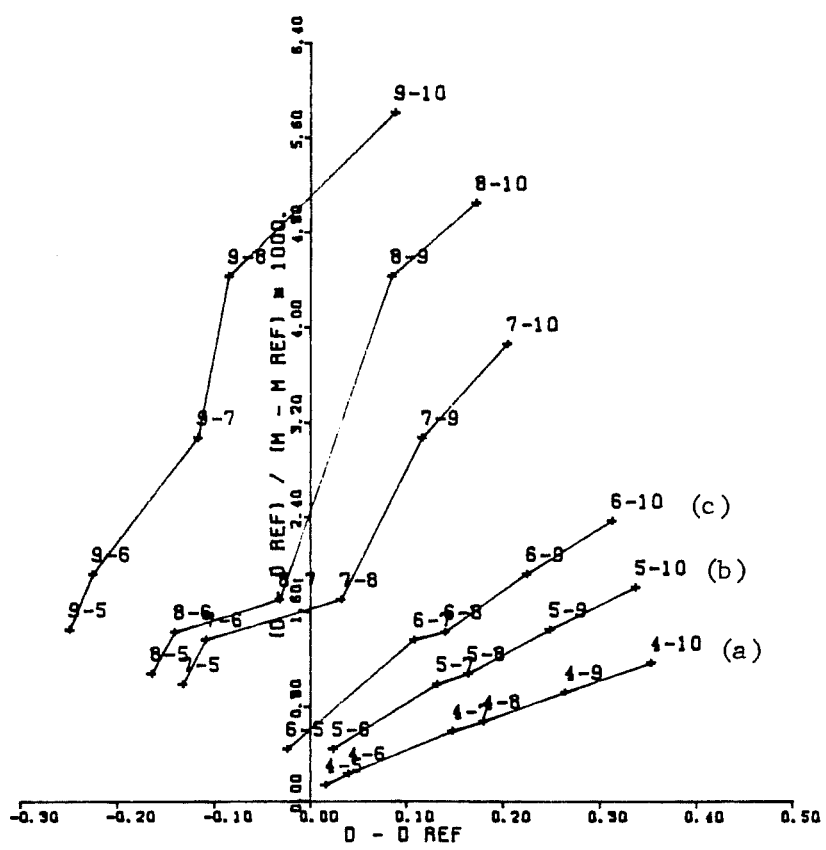


Fig. 5.4 Southwell (a) and Lundquist (b,c) plots for Test 11.

TEST NO. 11 - NO BRACING - NATURAL IMPERFECTIONS

MECK PLOT OF QUARTER POINT DISPLACEMENTS

THE BRACE STIFFNESS IS: 0.000
THE INITIAL IMPERFECTION IS: 0.000

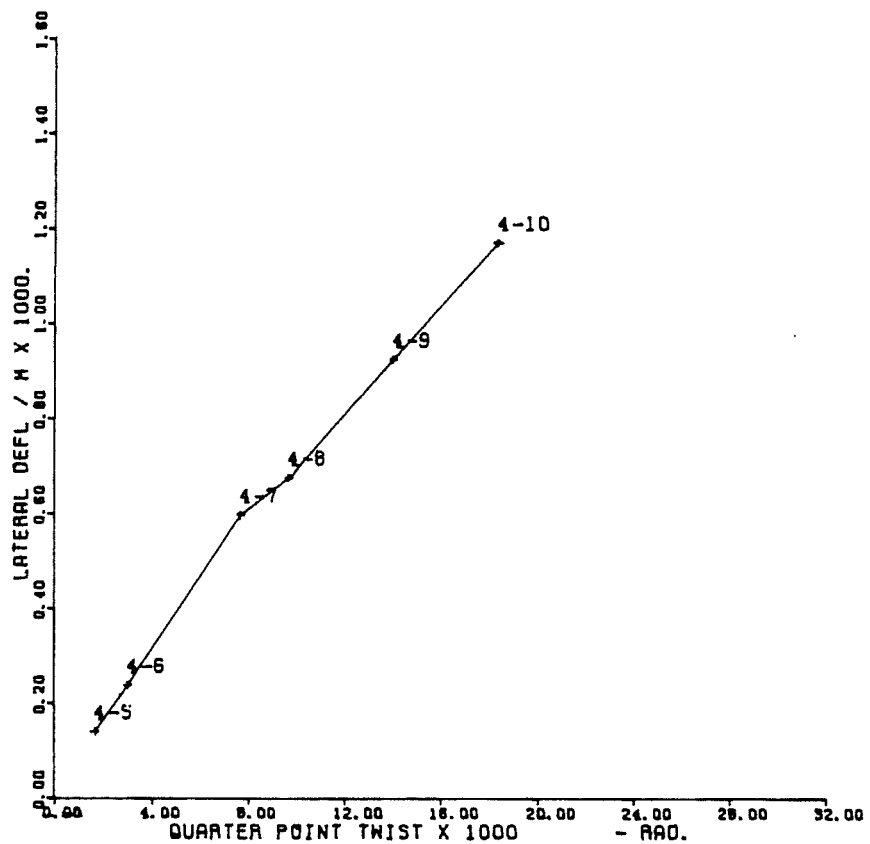


Fig. 5.5 Meck plot for Test 11-- u/M vs. θ .

TEST NO. 11 - NO BRACING - NATURAL IMPERFECTIONS

MECK PLOT OF QUARTER POINT DISPLACEMENTS

THE BRACE STIFFNESS IS: 0.000
THE INITIAL IMPERFECTION IS: 0.000

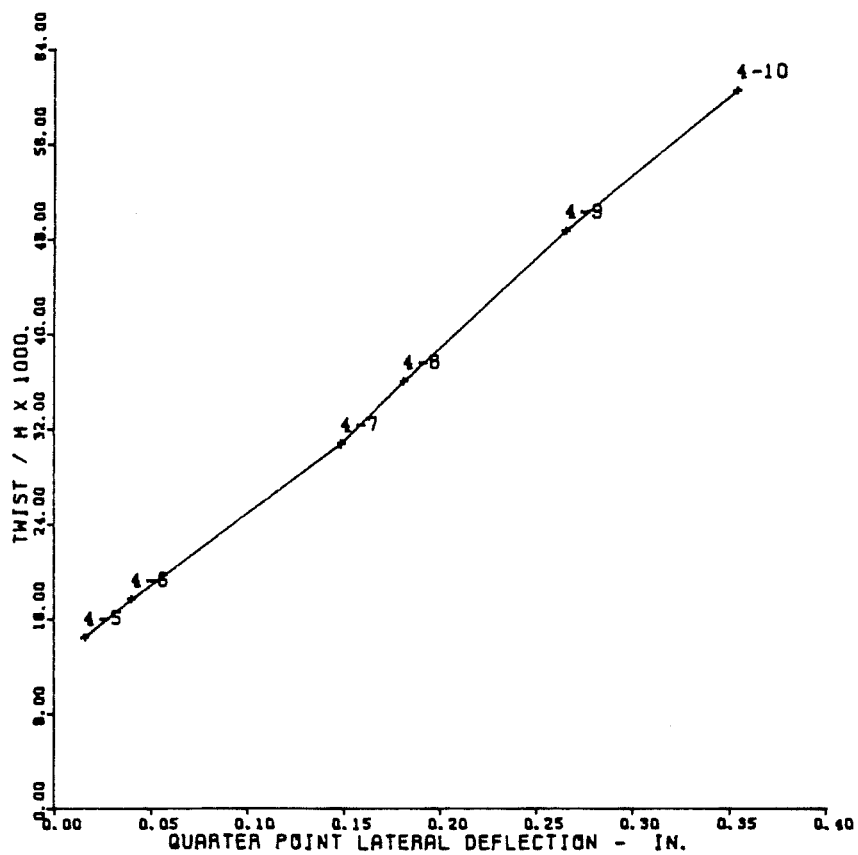



Fig. 5.6 Meck plot for Test 11-- θ/M vs. u .

TABLE 5.1 PLOTTING METHOD RESULTS

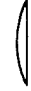
Test No.	Brace Stiffness (kli)	Forced Initial Imperf. (in.)	BASP Runs MBASP (in.-k)	Highest Moment Reached M/M _{BASP}	Meck Plot M _{cr} /M _{BASP}	Southwell Plot (ILS = 1)		
						1/4 pt. Defl. M _{cr} /M _{BASP}	1/4 pt. Twist M _{cr} /M _{BASP}	Br. Pt. Defl. M _{cr} /M _{BASP}
11	0.0	0.0 ¹	338.5 ²	0.89 ²	1.03	1.03	1.04	---
12	0.0	0.205	338.5	0.83	1.01	1.06	0.98	---
13	0.350	0.000	496.8	0.86	1.17	1.15	1.18	1.08
14	0.400	0.000	517.1	0.82	1.17	1.25	1.10	1.08
15	0.380	0.105	509.1	0.75	1.03	1.06	1.07	1.14
16	0.380	0.105	509.1	0.79	1.08	1.08	1.08	1.12
17	0.390	0.216	513.1	0.75	0.98	1.01	1.02	0.99
18	0.420	0.195	525.0	0.74	1.01	0.99	1.03	1.00
19	0.530	0.000	566.1	0.78	1.23	1.23	1.22	1.17
20	0.510	0.113	558.9	0.73	0.98	0.98	0.98	1.00
21	0.490	0.214	551.6	0.68	0.83	0.81	0.83	0.87
22	1.250	0.000	597.6	0.83	---	0.97	1.19	0.93
23	1.90	0.000	597.6	0.89	---	1.56	---	1.02
24	1.60	0.000	597.6	0.92	1.21	1.26	1.15	1.05
25	1.13	0.220	597.6	0.88	1.07	1.08	1.06	0.97
26	1.65	0.220	597.6	0.89	1.02	1.02	0.98	0.91
27	0.880	0.220	597.6	0.94	1.06	1.12	0.99	0.98

1 Shape is  unless otherwise noted.

2 All moments include 25.1 in.-k gravity moment.

TABLE 5.1 PLOTTING METHOD RESULTS (continued)

Test No.	Brace Stiffness (kli)	Forced Initial Imperf. (in.)	BASP Runs	Highest Moment Reached	Meck Plot	Southwell Plot (ILS = 1)			
						M_{cr}/M_{BASP}	Defl.	1/4 pt. Twist.	Br. Pt. Defl.
28	2.9	0.220 ¹	597.6 ²	0.98 ²	1.06	1.05	1.01	1.00	
29	3.2	0.218	597.6	0.95	1.05	1.07	1.03	0.95	
30	18.+	0.000	597.6	1.03	1.07	1.06	1.05	-----	

1 Shape is  unless otherwise noted.

2 All moments include 25.1 in-k gravity moment.

the fourth column. The highest moment attained during each test is normalized by the BASP bifurcation moment as in column 5 and as are the results of the plotting methods shown in the remaining columns. The results for the Meck plots are tabulated in column six and those for the Southwell plots are shown in the seventh through ninth columns. In some tests, scatter as high as 10% of the critical moment was observed between the results for the Southwell plots of the three buckling displacements measured. This scatter was most pronounced for the tests having forced initial imperfections and for tests having brace stiffnesses smaller than the ideal stiffness. The scatter was least where the beam buckled into the second mode shape. The Meck plots taken at the quarterpoint flange give results which are close to the average of the critical moments given by the Southwell plots. Typically, when one Meck plot had a significant decrease in slope, the other had an increase. The critical moment, from Eq. (5.3), was seen to be constant despite these changes in slope from one part of the plot to the next. For beam buckling tests, the Meck plots are more consistent than the Southwell and Lundquist plots since they tend to compensate for errors which distort the other plot types. The use of Meck plots is more appropriate for beam buckling tests where the lateral deflection and twist are recorded at a common location. The correlation between the critical load obtained from the Meck plots and the theoretical BASP prediction was fairly good; in most instances, the difference between the two loads was less than 10%.

No clear correlation was observed between the initial imperfection calculated from the plotting methods and the magnitude of the forced initial imperfection. This may be the result of the presence of initial moment as a consequence of forcing the section laterally. Also, the initial shape consists of a lateral deflection and twist which each may have components of mode shapes other than that of buckled shape and will affect the ability of the plotting methods to predict that initial shape.

Once the critical moment and initial imperfection are calculated from the plots, the resulting hyperbolic curve can be passed through the data points to assess the degree of fit. Figure 5.7 shows the hyperbola from a Southwell plot analysis superimposed on the quarterpoint twist data for Test 11. In this case, the moment-displacement curve was strongly hyperbolic throughout the entire range of moment. This was not true, in general, for the low moment range of tests having forced imperfections and was indicative of the inability of the plotting methods to provide a correlation between the calculated imperfection and the magnitude of the forced imperfection.

5.4 Moment vs. Brace Stiffness

The critical moments from the Meck plots are judged to be more reliable for beam buckling tests than those predicted by the Southwell and Lundquist plots. Figure 5.8 shows the critical moments from the Meck plots vs. the brace stiffness for that test superimposed on the BASP results from various brace stiffnesses. The critical moment for this unbraced case was within 3% of that predicted by BASP as seen

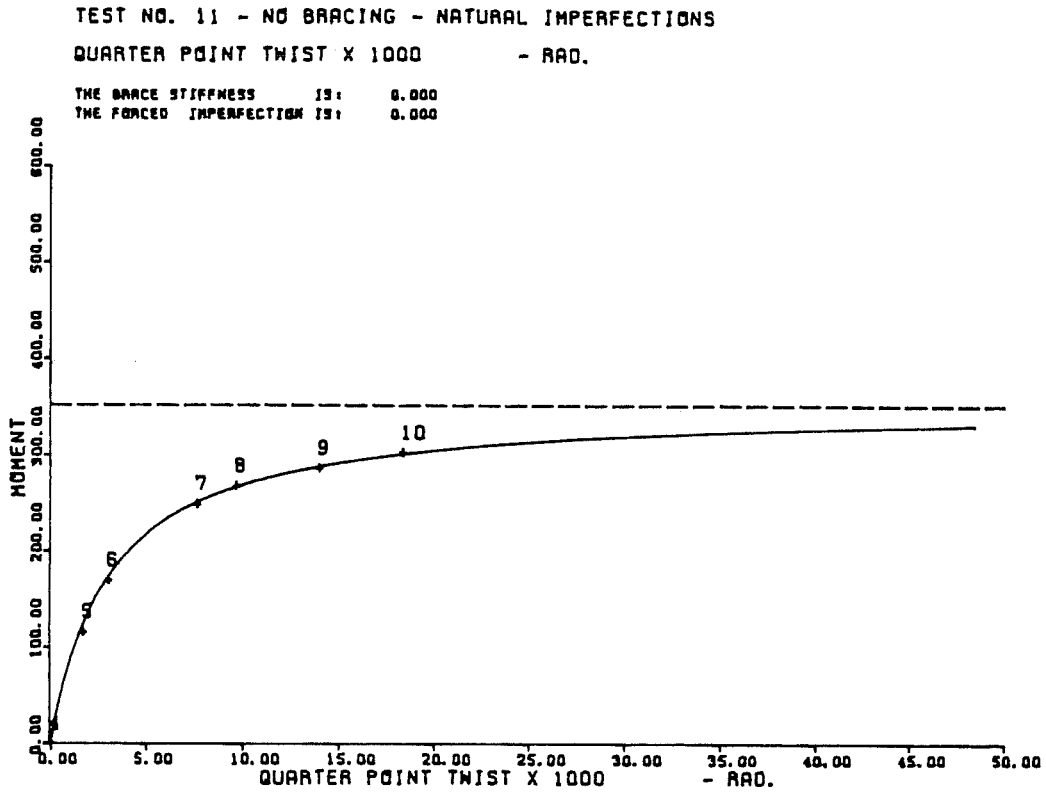


Fig. 5.7 Moment vs. deflection plot.

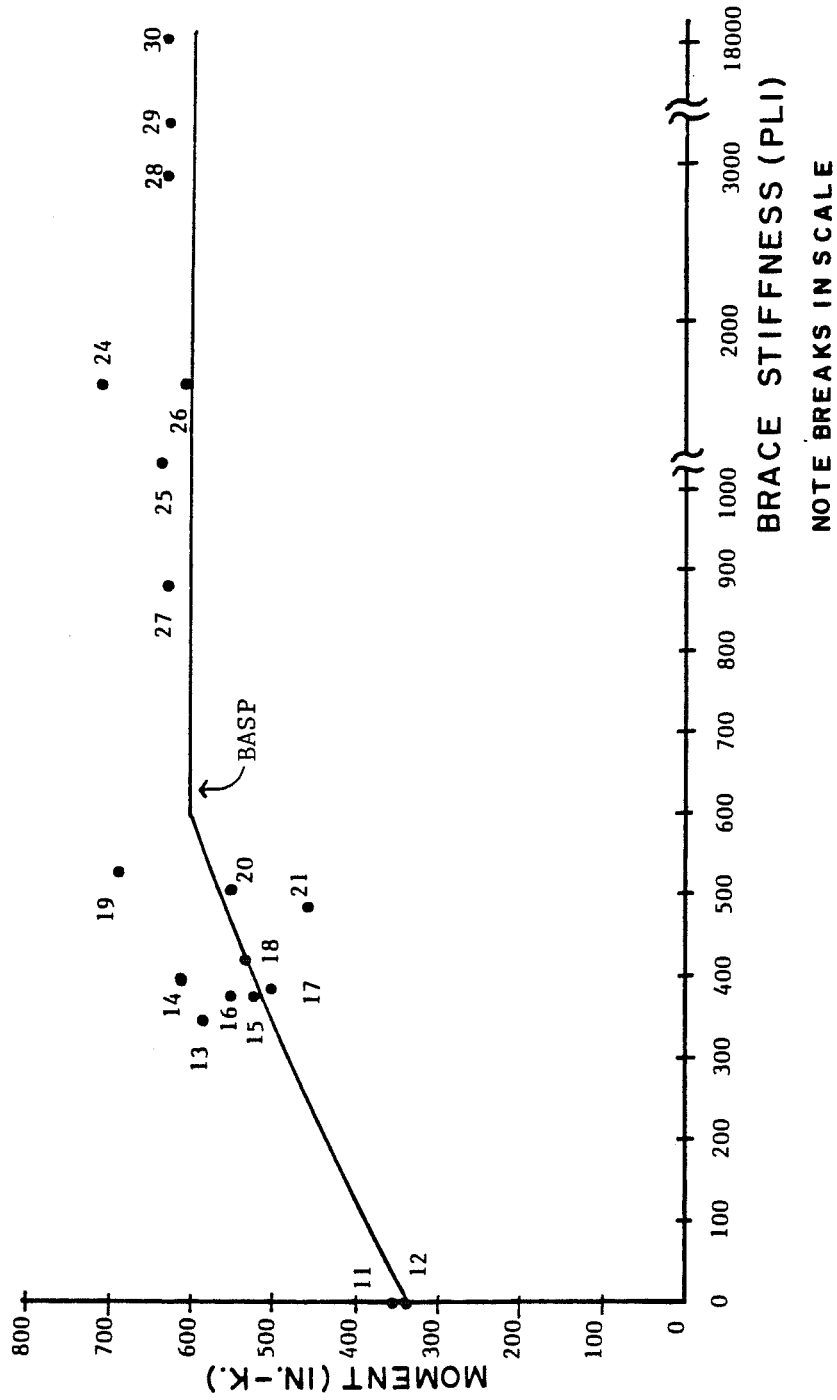


Fig. 5.8 Critical moment vs. brace stiffness; Meck plots (initial load stage = 1).

numerically in Table 5.1. The moments for the large number of tests which had a brace stiffness of approximately 400 pli ranged from 2% below to 17% above the BASP value. The increase in critical moment with increasing brace stiffness is apparent for Tests 11 through 21 which buckled into the first mode shape. The tests buckling into the second mode shape did not show a corresponding increase in moment. The critical moments from the Meck plots ranged from 2% to 7% above the BASP value for all but one of the second mode tests.

The theoretical value of the ideal brace stiffness is 0.70 kli using Eq. (2.7). Using BASP, the ideal stiffness for the test setup is 0.60 to 0.65 kli depending on the choice of starting mode shape for the BASP solution. The 15% difference is reasonable since BASP included the effect of the warping restraint at the ends of the test span. As seen in Fig. 5.8, the tests which buckled into the first mode fall to the left of the ideal stiffness and those buckling into the second mode are to the right. This confirms the assertion that a finite brace stiffness is sufficient to buckle the beam into the second mode shape. The precise value of the ideal stiffness could not be determined experimentally but its magnitude was between 0.53 and 0.88 kli which is consistent with the theoretical value of 0.70 kli.

After analysis of the plots of the 20 tests, Tests 22 and 23 were considered invalid due to unwanted restraint. In these tests, a restraint angle was discovered to be touching the test specimen at high moments which caused the section to twist only in a direction opposite to the buckling displacement. The extrapolated critical loads from

Tests 19, 20, and 21 were considered suspect. The critical moments for these tests varied by almost 50%, although the brace stiffness varied only 4%. Test 19 had no forced imperfections, whereas Tests 20 and 21 had forced imperfections of $L/2000$ and $L/1000$, respectively. The critical moment for Test 20 is very close to the value predicted by BASP but it should be rejected since the critical moments for its companion tests are erratic. Test 21 had a greater brace stiffness than that in Tests 17 and 18, and the initial imperfection was similar in all three cases, yet the experimental critical load is lower. The proximity of the brace stiffnesses used in these tests to the ideal stiffness causes the beam to buckle with a combination of the first and second mode shapes which skews the results of the plotting methods. In order to get reliable test results near the ideal brace stiffness, ultimate strength tests should be performed.

In Tests 13 through 21 which buckled into the first mode shape, the brace force was expected to increase toward an infinite value as the critical moment was approached. To avoid yielding of the specimen, the tests were stopped at moments between 75 and 90% of the critical moments. As seen in Table 4.1, the brace force never exceeded 0.4% of the compression region force, which varied between 30 and 60 kips, depending on the moment. These brace forces were larger than those of the tests buckling into the second mode shape where the brace force was expected to reach a limiting value. The largest brace force for the second mode tests was recorded in Test 30, which had an 18 ksi brace stiffness and was taken to failure. This force was 97 lbs, which was

0.16% of the compression region force. This brace force can be estimated analytically using Eq. (2.10):

$$F_{\text{brace}} = \beta \Delta_A = \frac{(4P_{\text{cr}}/L)}{(1 + b/b_o)} (\Delta_o + \Delta_A) \quad (2.10)$$

Although no forced imperfection was imposed on the specimen in Test 30, an initial imperfection of $L/1000$ is assumed to be present. P_{cr} equals 69.2 k for the second mode and the correction factor for the enhanced effectiveness of the brace at the top flange; $(1 + b/b_o)$ is 1.84. Assuming the 18 ksi brace to be rigid, so $\Delta_A = 0$, the brace force is calculated to be 150 lbs. This result is 50% greater than the 97-lb force observed, but is judged to be a reasonable estimate. The calculation might have been closer if the magnitude of the imperfection in the test specimen was accurately known.

Using Eq. (2.10), the total deflection divided by the length, $(\Delta_o + \Delta_A)/L$, can be related to the ratio of brace force to the critical load as

$$\frac{F_{\text{brace}}}{P_{\text{cr}}} = \frac{4}{(1 + b/b_o)} \left(\frac{\Delta_o + \Delta_A}{L} \right) \quad (5.4)$$

for the second mode tests. Since $F_{\text{brace}}/P_{\text{cr}}$ is less than 0.14% for these tests, the ratio $(\Delta_o + \Delta_A)/L$ is less than 0.07%, or 0.7/1000. Therefore, if the magnitude of this ratio is assumed to be larger than 0.7/1000 in Eq. (2.10), say 1/1000 or greater, the calculated brace force will be conservative.

C H A P T E R V I

EXAMPLE PROBLEMS

The purpose of these example problems is to demonstrate the use of the equations in Chapter II for the buckling of braced beams and to show that it is possible to apply the results of column bracing solutions to beams.

6.1 Beam Braced at Midspan

Consider a W12x16 beam, 216 in. long, loaded by uniform moment and braced at the midspan of the compression flange as in Fig. 2.3. The ideal brace stiffness is calculated using Eq. (2.7) as

$$\beta_{\text{ideal}} = \frac{4P_{e2}/L}{(1+b/b_0)} = \frac{4(69.2^k)/(216'')}{(1+5.99''/7.27'')} = 0.70^{\text{kl}} \quad (6.1)$$

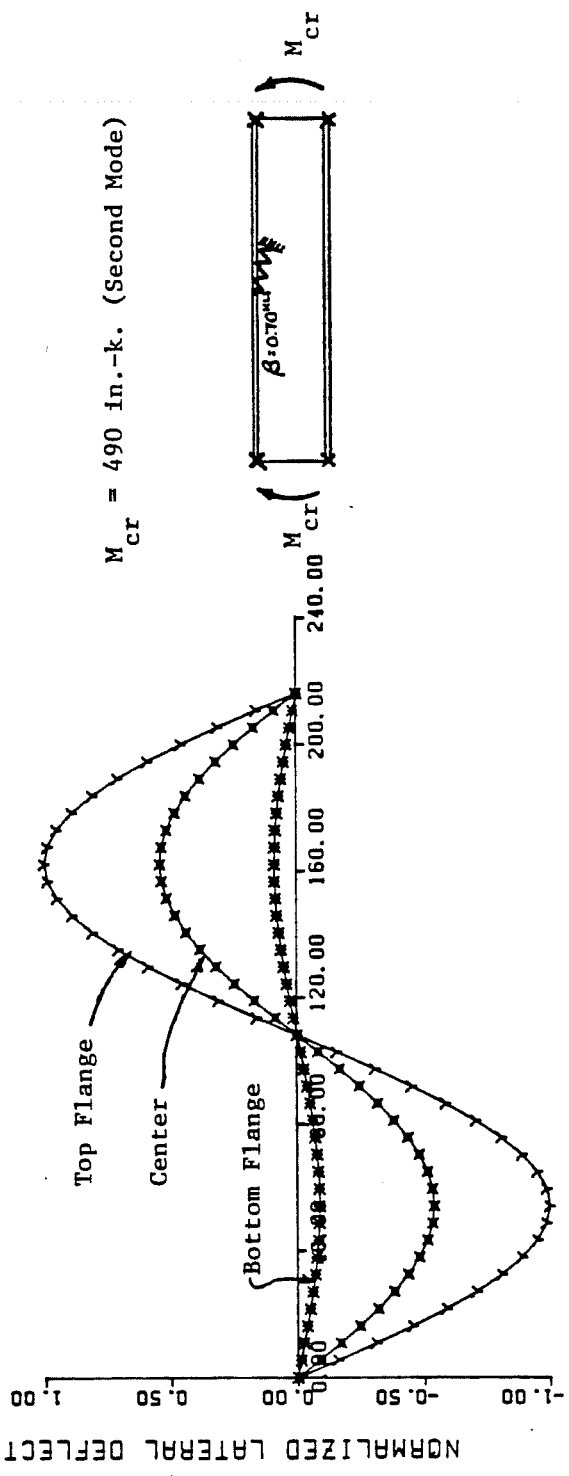
where b_0 is calculated using Eq. (2.4) with $\gamma = 157.4$ and $a = 0.5$. The critical moment for this case is 490 in.-k. These results have been confirmed using BASP and the buckled mode shape is shown in Fig. 6.1.

As discussed in section 2.2, the "beam flange as a column" analogy has been employed to calculate the required brace stiffness for beams. Using

$$\beta = 4 P/L \quad (1.3)$$

the proper "force," P , for this equation is

BASP-BUCKLING ANALYSIS OF STIFFENED PLATES
W12 X 16 18'-0 LONG PURE MOMENT



00.70 KLI BRACE AT MIDSPAN

Fig. 6.1 Beam braced at midspan at the compression flange.

$$P = \frac{P_{cr}}{(1+b/b_o)} = \frac{P_{cr} b_o}{b+b_o} = \frac{M_{cr}}{b+b_o} \quad (6.2)$$

Since $b + b_o$ will always be greater than the depth, d , the force P can be conservatively calculated as

$$P = M_{cr}/d \quad (6.3)$$

In the example above, $M_{cr}/d = 41$ k and the brace stiffness, calculated using Eq. (1.3), is 0.76 kli, which is 9% larger than the 0.70 kli calculated using Eq. (6.1). Since $(1 + b/b_o)$ is between 1.70 and 1.85 for most economy shapes with $aL/d = 10$, the brace stiffness calculated using M_{cr}/d as the force will be between 9 and 18% larger than the stiffness calculated using Eq. (6.1).

The compression region force has also been used, as P , in Eq. (1.3). In this case, the compression region force is calculated by integrating the stresses over the area above the neutral axis and is 48 k. The brace stiffness, using Eq. (1.3) is 0.89 kli, which is 27% larger than that given by Eq. (6.1).

In summary, the force in Eq. (1.3) can be taken as M_{cr}/d to obtain a reasonably accurate brace stiffness. However, the quantities P_{cr} and b_o are used directly in Eq. (2.5) and indirectly in Eq. (2.2) when M_{cr} is calculated and could easily be employed in Eq. (6.1) for the exact value of the ideal brace stiffness rather than resorting to approximations.

If a brace having the ideal stiffness is attached to an imperfect beam, the second mode moment can be attained only after the brace point has deflected an infinite distance, as given by Eq. (2.9). Assuming the beam has an imperfection at the midspan of $L/1000$, or 0.216 in., the stiffness necessary to limit the additional deflection to $L/1000$ also is calculated by rewriting Eq. (2.9) as

$$\begin{aligned} \beta_{\text{req'd}} &= \beta_{\text{ideal}} \left(1 + \frac{\Delta_o}{\Delta_A} \right) \\ &= 0.70^{\text{kli}} \left(1 + \frac{L/1000}{L/1000} \right) = 1.40^{\text{kli}} \end{aligned} \quad (6.4)$$

A stiffness of twice the ideal value of 0.70 kli, or 1.40 kli, is required to limit the additional deflection to the magnitude of the initial imperfection at the brace point. The brace force is given by Eq. (2.10) as

$$F_{\text{brace}} = \beta \Delta_A = (1.40^{\text{kli}})(0.216") = 0.3^{\text{k}} = 300 \text{ lb} \quad (6.5)$$

Safety factors should be applied to the results above before their use in design. The specification of safety factors is not within the scope of this study.

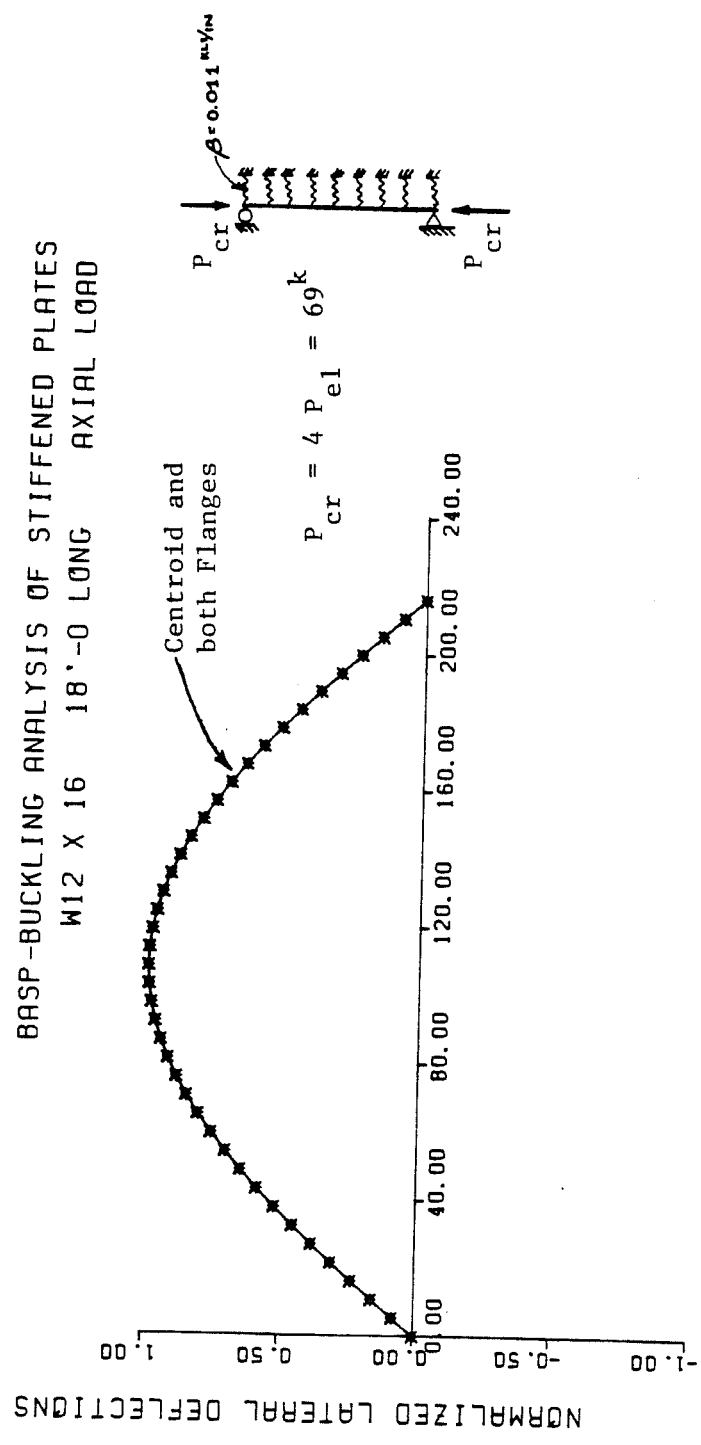
6.2 Distributed Brace Along the Compression Flange

The form of Eq. (2.5), $M_{cr} = P_{cr} b_0$, suggests that other solutions for braced columns can be applied to braced beams. For example, the stiffness of a brace distributed along the length of a column necessary to attain the second mode load, $a = 0.5$ in Eq. (2.3), is equal to the ideal brace stiffness for a brace at midspan divided by half the length of the column [10]. For a W12x16 column, 216 in. long, this stiffness is

$$\beta_{\text{distr}} = \frac{\beta_{\text{ideal}}}{0.5L} = \frac{4(69.2^k)/216''}{0.5(216'')} = 0.011 \text{ kli/in.} \quad (6.6)$$

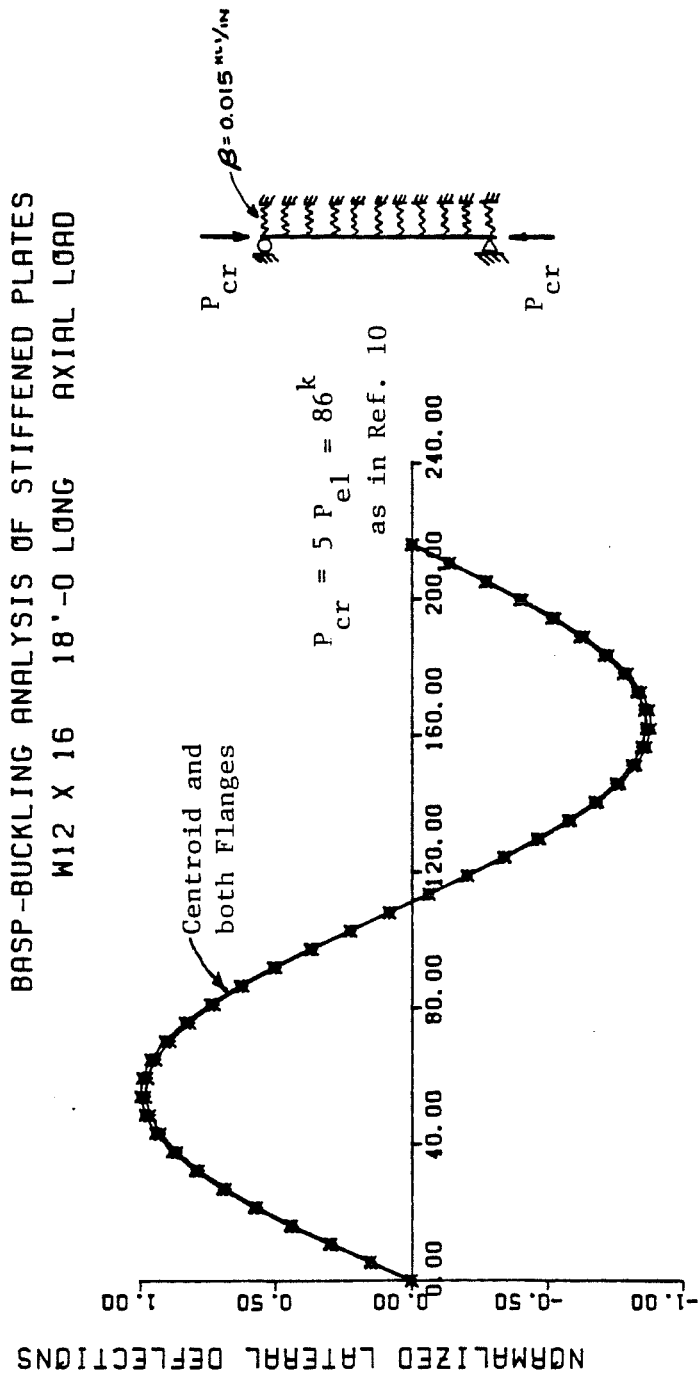
A column with a distributed brace of 0.011 kli/in. will carry the second mode load of 69.2 k. This result is confirmed by BASP and the buckled shape is shown in Fig. 6.2. When a brace stiffness of 0.015 kli is used the column buckles into the second mode shape, as shown in Fig. 6.3.

The results above can be used to find the distributed brace stiffness at the top flange of a beam loaded by uniform moment which will enable it to carry the second mode moment of 490 in.-k, as calculated in section 6.1. The brace stiffness for the column, Eq. (6.6), is divided by the correction factor for a brace at the top flange $(1 + b/b_0) = 1.84$, to get a distributed brace stiffness of 0.006 kli/in. Using BASP, the critical moment for this stiffness is 502 in.-k, which is within 2 percent of the second mode moment of 490 in.-k. At this moment, the beam is buckled into a shape similar to the first mode shape, as shown in Fig. 6.4.



0.011 KLI/IN. DISTR. BRACE

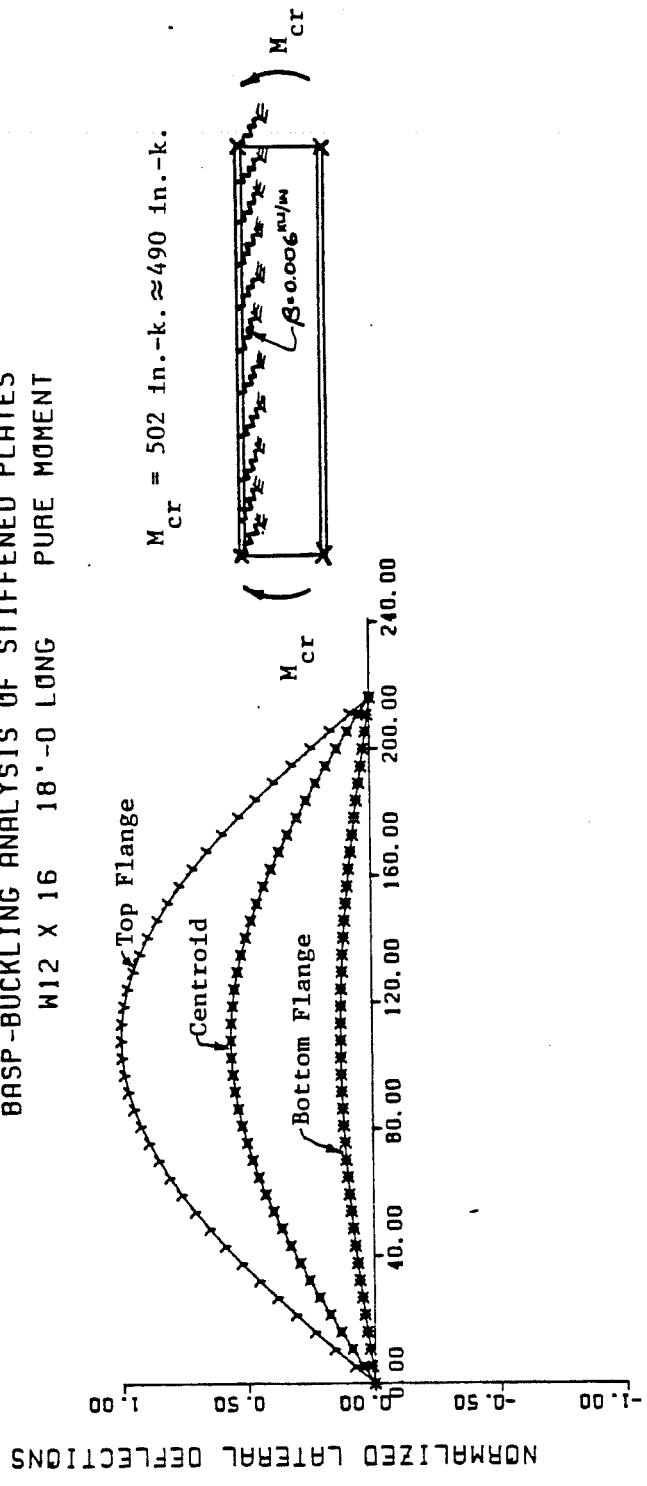
Fig. 6.2 Continuously braced column -- first mode shape.



0.015 KLI/IN. DISTR. BRACE

Fig. 6.3 Column with continuous brace---second mode shape.

BASP-BUCKLING ANALYSIS OF STIFFENED PLATES
W12 X 16 18'-0 LONG PURE MOMENT



0.006 KLI/I. DISTR. BRACE

Fig. 6.4 Beam with continuous brace at compression flange.

In summary, the buckling of braced beams loaded by uniform moment is similar to that of braced columns. Other solutions for braced columns may be found to be applicable to beams if analytical verification, such as by the program BASP, is made for these cases.

CHAPTER VII

CONCLUSIONS

The objectives of the testing program were to provide experimental data on the lateral-torsional buckling of braced beams. Of particular interest was the force in the brace, the magnitude of the brace stiffness necessary to develop a particular critical moment, and the effect of the type and magnitude of initial imperfection on the brace force and critical moment. To accomplish these objectives, a wide-flange beam was braced at midspan at the compression flange and loaded by uniform moment. Of the twenty tests reported in this study, all were conducted in the elastic range except for the last test which was taken to failure. The variables of the testing program were the stiffness of the brace and the magnitude and type of initial imperfection. The experimental findings were:

- 1) The beam buckled into the first mode shape when the brace stiffness was less than the theoretical ideal stiffness and the beam buckled into the second mode shape when the brace stiffness was larger than the ideal stiffness. The experimental value of the ideal brace stiffness was observed to be between 0.53 kips per linear inch (kli) and 0.88 kli in Tests 19 and 27, respectively. This experimental value is in agreement with the theoretical value of 0.70 kli.
- 2) Brace forces in the tests which buckled into the second mode shape were observed to approach a limiting value and were

smaller in magnitude than 0.2% of the force in the compression region of the beam. In the tests which buckled into the first mode shape, the brace forces were increasing rapidly when the tests were stopped in the elastic range.

In order to perform subsequent tests in the elastic range using the same specimen, the Southwell, Lundquist, and Meck plotting methods were utilized to predict the critical moments from the test data. The critical moments which were determined by the plotting methods are compared to the bifurcation moment obtained by using the finite element program, BASP. The analytical findings are:

- 1) The Meck plots are more appropriate for extrapolating the critical moment of the test beam than are the Southwell and Lundquist plots. This is due to the Meck plot's ability to compensate for errors which distort the other plotting methods.
- 2) Plots of the experimental relationships between the critical moment and brace stiffness indicate that the finite element program, BASP, accurately predicts the variation of bifurcation moment with brace stiffness.
- 3) No clear correlation was observed between the magnitude of the forced initial imperfection and the magnitude of the initial displacement predicted by the plotting methods.
- 4) The "beam flange as a column analogy" [6] was used to conservatively estimate the brace force in the tests which buckled into the second mode shape.

- 5) In the "beam flange as a column analogy," the correct force, P , to use in Eq. (1.3) to obtain the brace stiffness, is $P_{cr}/(1 + b/b_o)$; however, using a force calculated as M_{cr}/d will be 9% to 18% conservative for economy sections with $aL/d = 10$.
- 6) In calculating the critical moment for a beam under uniform moment, Eq. (2.7) from the SSRC Guide [1] may be rewritten in a more concise form as $M_{cr} = P_{cr} b_o$ [2] from which the similarities between the buckling of beams and columns can be observed.
- 7) In determining the required brace stiffness for a distributed brace at the compression flange of a beam under uniform moment, the solution for a continuously braced column [10] can be modified. The required brace stiffness is $\beta_{ideal}/0.5 L$ where β_{ideal} is shown in Eq. (2.7). Other solutions for braced columns may be applicable to beams under uniform moment if analytical verification, such as by the finite element program BASP, is obtained for these cases.

A P P E N D I X A

BRACED IMPERFECT COLUMN

Differential Equation for a Braced Imperfect Column

- Elastic brace at midspan, stiffness = β (for unbraced case, $\beta = 0$).
- Arbitrary initial imperfection shape, $\Delta_o = \sum_{n=1}^{\infty} \Delta_{on} \sin \frac{n\pi x}{L}$.

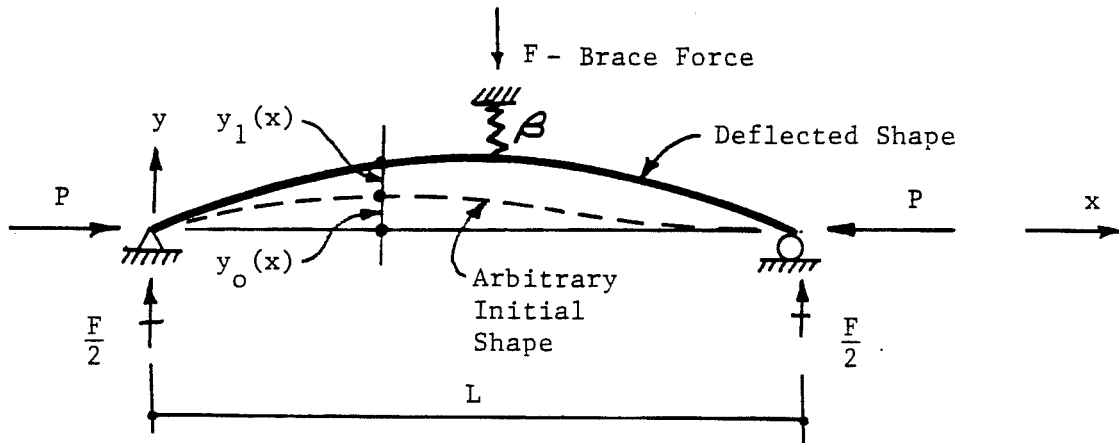


Fig. A.1 Deflections of a braced imperfect column.

Using symmetry, for $0 \leq x \leq L/2$

$$D^2 y_1 + k y_1 = \frac{Fx}{2EI} - k^2 \sum_{n=1}^{\infty} \Delta_{on} \sin \frac{n\pi x}{L} ;$$

$$k^2 = \frac{P}{EI}, \quad D = \frac{d}{dx}; \text{ the differential operator.}$$

The general and particular solution is

$$y_1(x) = c_1 \cos kx + c_2 \sin kx + \frac{Fx}{2P} \\ + \sum_{n=1}^{\infty} \left[\frac{P/n^2 P_{el}}{1-P/n^2 P_{el}} \right] \Delta_{on} \sin \frac{n\pi x}{L}$$

where

$$P_{el} = \frac{\pi^2 EI}{L^2}$$

For the right half of the column, use coordinate $x' = L - x$;

$$0 \leq x' \leq L/2$$

$$y_2(x') = c_3 \cos kx' + c_4 \sin kx' + \frac{Fx'}{2P} \\ + \sum_{n=1}^{\infty} \left[\frac{P/n^2 P_{el}}{1-P/n^2 P_{el}} \right] (-1)^{n-1} \Delta_{on} \sin \frac{n\pi x'}{L}$$

From pinned end boundary conditions

$$C_1 = C_3 = 0$$

From deflection compatibility at midspan

$$y_1(L/2) = y_2(L/2); C_2 = C_4$$

From slope compatibility at midspan

$$Dy_1(L/2) = -Dy_2(L/2) \text{ since } x = L - x' \text{ and } Dx = -Dx'$$

$$C_2 = C_4 = -(FL/4P)/((kL/2) \cos kL/2)$$

Substituting the coefficients and $F = \beta \Delta_A = \beta y_1(L/2)$ and $0 \leq x \leq L/2$

$$y_1(x) = \frac{\beta \Delta_A L}{4P} \left(\frac{2x}{L} - \frac{\sin kx}{\left(\frac{kL}{2}\right) \cos \frac{kL}{2}} \right) + \sum_{n=1,2,3,4,\dots}^{\infty} \left[\frac{P/n^2 P_{e1}}{1-P/n^2 P_{e1}} \right] \Delta_{on} \sin \frac{n\pi x}{L} \quad (\text{A.1})$$

where at midspan

$$\Delta_A = y_1\left(\frac{L}{2}\right) = \frac{\beta \Delta_A L}{4P} \left[1 - \frac{\tan kL/2}{kL/2} \right] + \dots \quad (\text{A.2})$$

$$+ \sum_{n=1,3,5,\dots}^{\infty} \left[\frac{P/n^2 P_{el}}{1-P/n^2 P_{el}} \right] \Delta_{on} (-1)^{(n-1)/2} \quad (\text{A.2, cont.})$$

Checking the unbraced case $\beta = 0$ and $0 \leq x \leq L/2$

$$\Delta_A = y \left(\frac{L}{2} \right) = \sum_{n=1,3,5,\dots}^{\infty} \left[\frac{P/n^2 P_{el}}{1-P/n^2 P_{el}} \right] \Delta_{on} (-1)^{(n-1)/2}$$

Which for a half wave imperfection with amplitude, Δ_{o1} , reduces to

$$\Delta_o = \Delta_{o1} \sin \frac{\pi x}{L}, \quad \Delta_A = \Delta_o \left[\frac{P/P_{el}}{1-P/P_{el}} \right]$$

When the brace stiffness, β , is finite,

$$\beta_{ideal} = 16 P_{el}/L = \frac{16\pi^2 EI}{L^3}$$

at $x = \frac{L}{2}$;

$$\Delta_A = \sum_{n=1,3,5,\dots}^{\infty} \frac{\left[\frac{P/n^2 P_{el}}{1-P/n^2 P_{el}} \right] \Delta_{on} (-1)^{(n-1)/2}}{\left(1 - \frac{\beta}{\beta_{ideal}} \left(1 - \frac{\tan kL/2}{kL/2} \right) \right)} \quad (\text{A.3})$$

which is derived from Eq. (A.2) by solving for Δ_A .

The deflection at any other location $y_1(x)$ is calculated by substituting Eq. (A.3) into Eq. (A.1) which is valid for $0 \leq x \leq L/2$. For the right half of the beam, multiply the imperfection Δ_{on} by $(-1)^{n-1}$ to get $y(x')$. Figure A.2 shows the brace point deflections of an imperfect column having a half wave imperfection shape and various brace stiffnesses. The horizontal axis is Δ_A/Δ_{O1} and the vertical axis is normalized to P/P_{e1} . The dotted curves are hyperbolas given by Eq. (A.4) where Δ_o and P_{cr} could be the parameters from a Southwell plot analysis.

$$\Delta_A = \Delta_o \frac{P/P_{cr}}{(1-P/P_{cr})} \quad (A.4)$$

Note that there is a singularity in Eq. (A.3) at $P=P_e$ but values in this vicinity can be calculated by taking P a very small distance away from P_{e1} on either side which will give the same magnitude for Δ_A .

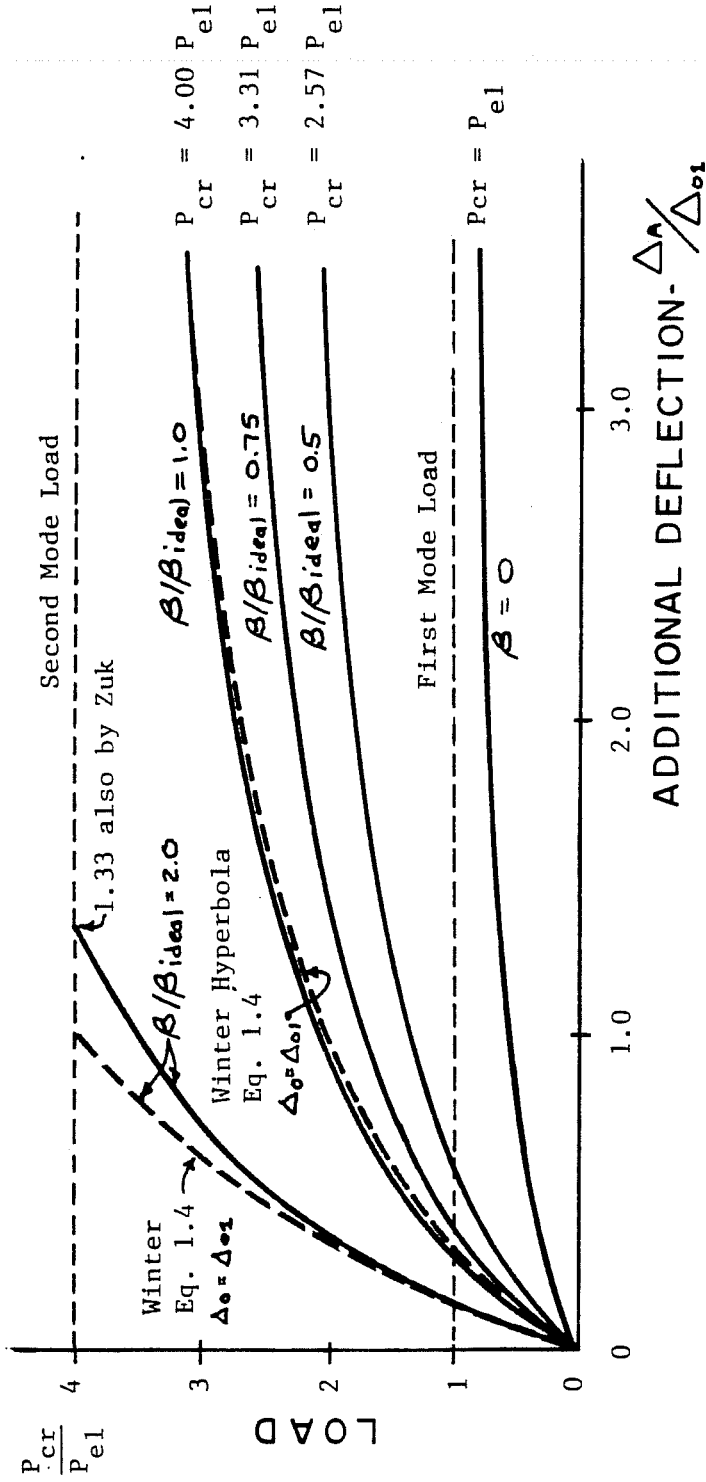






Fig. A.2 Deflections of imperfect column with various brace stiffnesses.

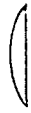
A P P E N D I X B

SUMMARY OF PLOTTING METHOD RESULTS

The following tables and plots represent the results of the Southwell, Lundquist and Meck plotting techniques. For the Southwell results, the critical moment and calculated initial imperfections are shown in Table B.1 for use in Eq. (1.4). Also tabulated are the results of the finite element program, BASP, and testing parameters such as brace stiffness, forced initial imperfection and the highest moment attained during the test. Following this table, a plot of critical moment vs. brace stiffness is given for the Southwell plots in Fig. B.1. The tabulation for the Lundquist results in Table B.2 follows the same format as the Southwell results except that the values of the moment and deflection at the reference load stage are given since they are required in Eq. (5.2). A plot of the Lundquist results is shown in Fig. B.2. The results from the Meck plots using quarterpoint displacements are shown in Table B.3. The results of Meck plots for the displacements at the centroid which were calculated from the flange deflection and twist were also tabulated; however, a greater scatter was observed for the centroid displacements than for those at the flange. Critical moment vs. brace stiffness plots for the Meck plots taken at the compression flange is shown in Fig. 5.8 and the plot for the results taken at the centroid is shown in Fig. B.3.

TABLE B.1 SOUTHWELL PLOTS (ILS = 1) RESULTS

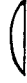
Test No.	Brace Stiffness (kli)	Forced Initial Imperf. (in.)	Highest Moment Reached (in.-k)	BASP Run M_{cr} (in.-k)	Quarterpoint		Quarterpoint		Brace Point Lat. Defl. M_{cr} (in.-k)	Brace Point Defl. Δ (in.)
					Lat. Defl. M_{cr} (in.-k)	Δ_0 (in.)	Twist $\theta \times 10^3$ (rads)	M_{cr} (in.-k)		
11	0.0	0.0 ¹	301.8 ²	338.5 ²	348.5	0.056	352.0	3.094		
12	0.0	0.205	280.5	338.5	359.1	0.094	331.5	4.665		
13	0.350	0.000	426.2	496.8	571.8	0.143	584.0	7.005	535.8	0.080
14	0.400	0.000	424.8	517.1	646.2	0.223	566.4	5.717	558.4	0.097
15	0.380	0.105	381.7	509.1	539.9	0.135	546.7	7.022	582.8	0.156
16	0.380	0.105	401.8	509.1	550.0	0.144	547.7	7.118	571.6	0.151
17	0.390	0.216	384.1	513.1	518.3	0.126	522.7	7.172	505.9	0.108
18	0.420	0.195	386.6	525.0	519.7	0.128	539.3	7.747	523.8	0.117
19	0.530	0.000	439.8	566.1	697.5	0.178	690.1	5.897	662.2	0.085
20	0.510	0.113	409.4	558.9	550.5	0.107	547.7	4.216	557.2	0.079
21	0.490	0.214	374.5	551.6	445.1	0.054	455.5	2.680	477.7	0.062
22	1.250	0.000	492.1	597.6	579.6	0.062	710.6	1.562	557.9	0.005
23	1.90	0.000	531.5	597.6	932.5	0.179	---	---	606.6	0.006
24	1.60	0.000	545.8	597.6	752.9	0.104	684.3	0.957	626.1	0.003
25	1.13	0.220 	523.1	597.6	647.1	0.061	631.7	2.311	581.3	0.005
26	1.65	0.220 	530.0	597.6	612.1	0.042	586.2	1.026	545.7	0.002
27	0.880	0.220 	555.7	597.6	671.7	0.062	594.2	0.555	586.1	0.001
28	2.9	0.220 	581.3	597.6	625.5	0.020	602.1	0.615	599.0	0.000+

1 Shape is  unless otherwise noted.

2 All moments include 25.1 in.-k gravity moment.

TABLE B.1 SOUTHWELL PLOTS (ILS = 1) RESULTS (continued)

Test No.	Brace Stiffness (kli)	Forced Initial Imperf. (in.)	Highest Moment Reached (in.-k)	BASP Run M_{cr} (in.-k)	Quarterpoint		Quarterpoint		Brace Point	
					Lat. Defl. M_{cr} (in.-k)	Δ^o (in.)	Twist $\theta_o \times 10^3$ (rads)	M_{cr} (in.-k)	Lat. Defl. M_{cr} (in.-k)	Δ^o (in.)
29	3.2	0.218 ¹	564.1 ²	597.6 ²	639.1	0.033	613.1	1.021	570.5	0.000+
30	18.+	0.000	610.5	597.6	643.6	0.026	627.6	0.673	-----	-----

1 Shape is  unless otherwise noted.

2 All moments include 25.1 in.-k gravity moment.

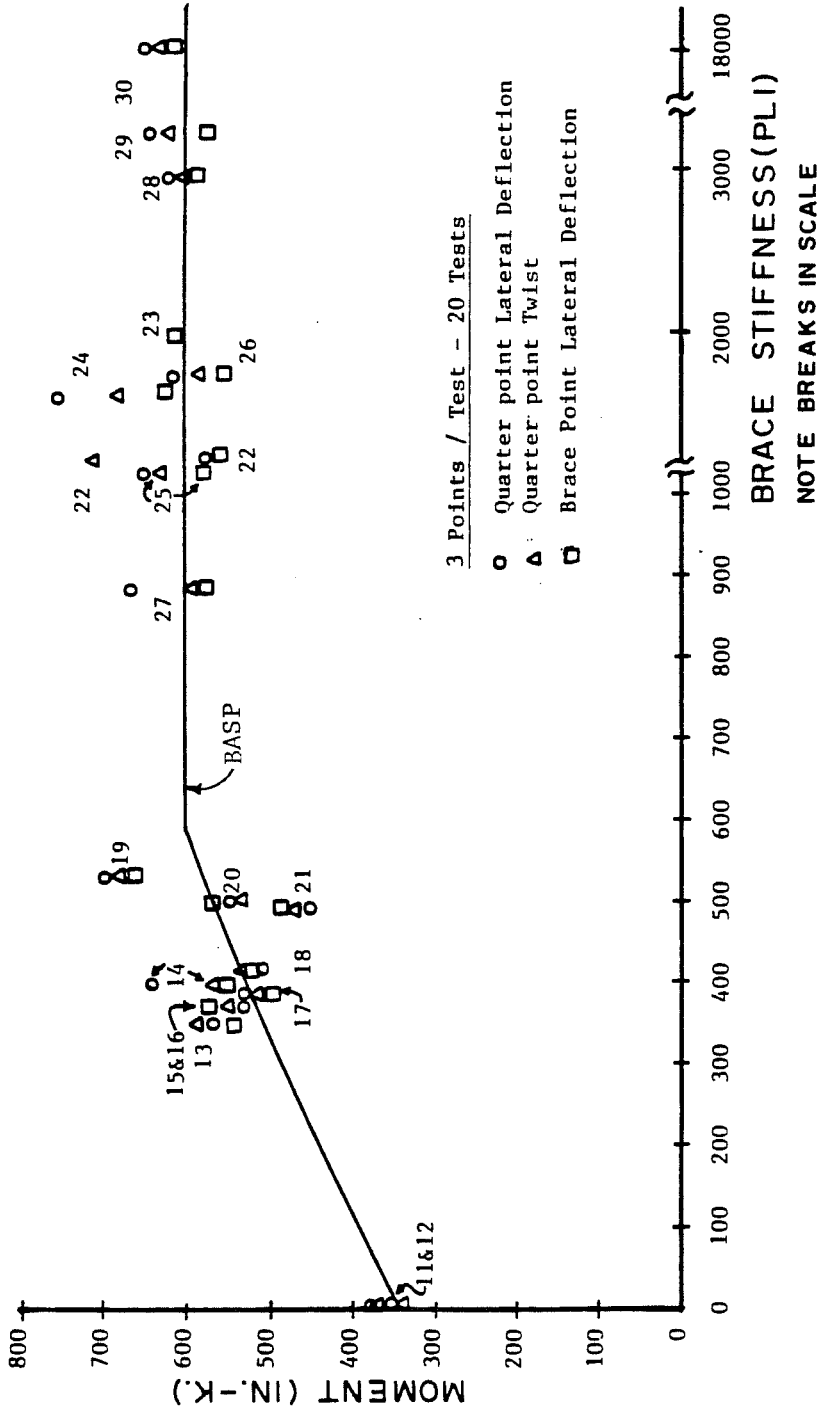
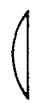


Fig. B.1 Critical moment vs. brace stiffness from Southwell plots.


TABLE B.2 LUNDQUIST PLOTS (ILS = 2) RESULTS

Test #	Brace Stiffness	Forced Initial Imperf. (in.)	Highest Moment Reached (in.-k)	BASP Run M_{cr} (in.-k)	Quarterpoint		Quarterpoint		Quarterpoint		Brace Point	
					Lat. Defl. M_{cr} M_{REF} (in.-k)	Δ_{REF}^o (in.)	Twist $\theta_o \times 10^3$ M_{cr} M_{REF} (in.-k)	$\theta_{REF}^o \times 10^3$ (rads)	Lat. Defl. M_{cr} M_{REF} (in.-k)	Δ_{REF}^o (in.)		
11	0.0	0.0 ¹	301.8 ²	338.5 ²	352.7	0.077	350.6	2.772				
12	0.0	0.205	280.5	338.5	115.3	0.016	115.3	1.67				
13	0.350	0.000	426.2	496.8	351.4	0.143	379.7	10.94				
14	0.400	0.000	424.8	517.1	70.8	-0.016	70.8	0.0				
15	0.380	0.105	381.7	509.1	618.5	0.254	539.4	2.310		539.4	0.087	
16	0.380	0.105	401.8	509.1	110.7	0.0	110.7	3.33		110.7	0.018	
17	0.390	0.216	384.1	513.1	718.6	0.404	562.0	5.180		556.4	0.092	
					114.3	0.000	114.3	1.67		114.3	0.027	
					636.6	0.372	578.3	10.702		633.6	0.256	
					125.6	-0.024	125.6	1.00		125.6	0.018	
					632.1	0.362	592.2	13.709		604.0	0.225	
					113.5	-0.028	113.5	-0.100		113.5	0.015	
					592.9	0.342	524.4	7.360		535.2	0.193	
					119.1	-0.032	119.1	2.07		119.1	0.001	

1 Shape is  unless otherwise noted.

2 All moments include 25.1 in.-k gravity moment.

TABLE B.2 LUNDQUIST PLOTS (ILS = 2) RESULTS (continued)


Test No.	Brace Stiffness (kli)	Forced Initial Imperf. (in.)	Highest Moment Reached (in.-k)	BASP Run M _{cr} (in.-k)	Quarterpoint		Quarterpoint		Brace Point	
					Lat. Defl. M _{cr} M _{REF} (in.-k)	Δ _{REF} (in.)	Twist θ _{cr} θ _{REF} (in.-k)	M _{cr} M _{REF} (in.-k)	Lat. Defl. Δ _{REF} (in.)	
18	0.420	0.195	386.6	525.0	579.8	0.307	544.8	8.551	558.9	0.208
					122.5	-0.02	122.5	1.93	122.5	0.004
19	0.530	0.000	439.8	566.1	867.9	0.439	709.5	6.942	688.5	0.108
					124.3	-0.012	124.3	1.03	124.3	0.013
20	0.510	0.113	409.4	558.9	653.8	0.318	594.6	8.144	600.4	0.141
					126.5	-0.028	126.5	0.00	126.5	0.004
21	0.490	0.214 ¹	374.5 ²	551.6 ²	488.7	0.173	474.3	4.812	497.6	0.098
					128.0	-0.028	128.0	0.13	128.0	0.009
22	1.250	0.000	492.1	597.6	593.5	0.112	640.0	0.058	556.4	0.005
					123.4	-0.012	123.4	0.97	123.4	0.002
23	1.90	0.000	531.5	597.6	---	---	---	---	---	---
24	1.60	0.000	545.8	597.6	687.3	0.010	660.3	0.756	582.9	-0.004
					145.8	0.064	145.8	1.13	145.8	0.006
25	1.13	0.220 	523.1	597.6	606.5	-0.010	586.5	2.007	591.2	0.010
					153.6	0.053	153.6	0.090	153.6	-0.001

¹ Shape is  unless otherwise noted.

² All moments include 25.1 in.-k gravity moment.

TABLE B.2 LUNDQUIST PLOTS (ILS = 2) RESULTS (continued)

Test No.	Brace Stiffness	Forced Initial Imperf.	(in.)	(in.-k)	BASP Run M _{CR}	Quarterpoint			Quarterpoint			Brace Point		
						Lat. Defl. M _{CR} M _{REF}	Lat. Defl. M _{CR} M _{REF}	Twist θ _o x 10 ³ θ _{REF} x 10 ³	Lat. Defl. M _{CR} M _{REF}	Lat. Defl. M _{CR} M _{REF}	Twist θ _o x 10 ³ θ _{REF} x 10 ³			
26	1.65	0.220	△ ¹	530.0	597.6	589.8	-0.010	628.0	1.058	544.8	0.001			
						128.1	0.042	128.1	0.267	128.1	0.000			
27	0.880	0.220	△	555.7	597.6	645.7	-0.004	593.5	0.468	612.0	0.005			
						135.8	0.053	135.8	0.233	135.8	0.003			
28	2.9	0.220	△	581.3	597.6	615.6	-0.027	601.3	0.158	597.1	-0.001			
						123.7	0.042	123.7	0.567	123.7	0.001			
29	3.2	0.218	△	564.1	597.6	624.0	-0.011	614.0	1.176	568.3	-0.002			
						134.0	0.038	134.0	0.167	134.0	0.002			
30	18.+	0.000		610.5	597.6	636.5	-0.038	626.4	-0.071	-----	-----			
						125.3	0.060	125.3	0.833	-----	-----			

1 Shape is  unless otherwise noted.

2 All moments include 25.1 in.-k gravity moment.

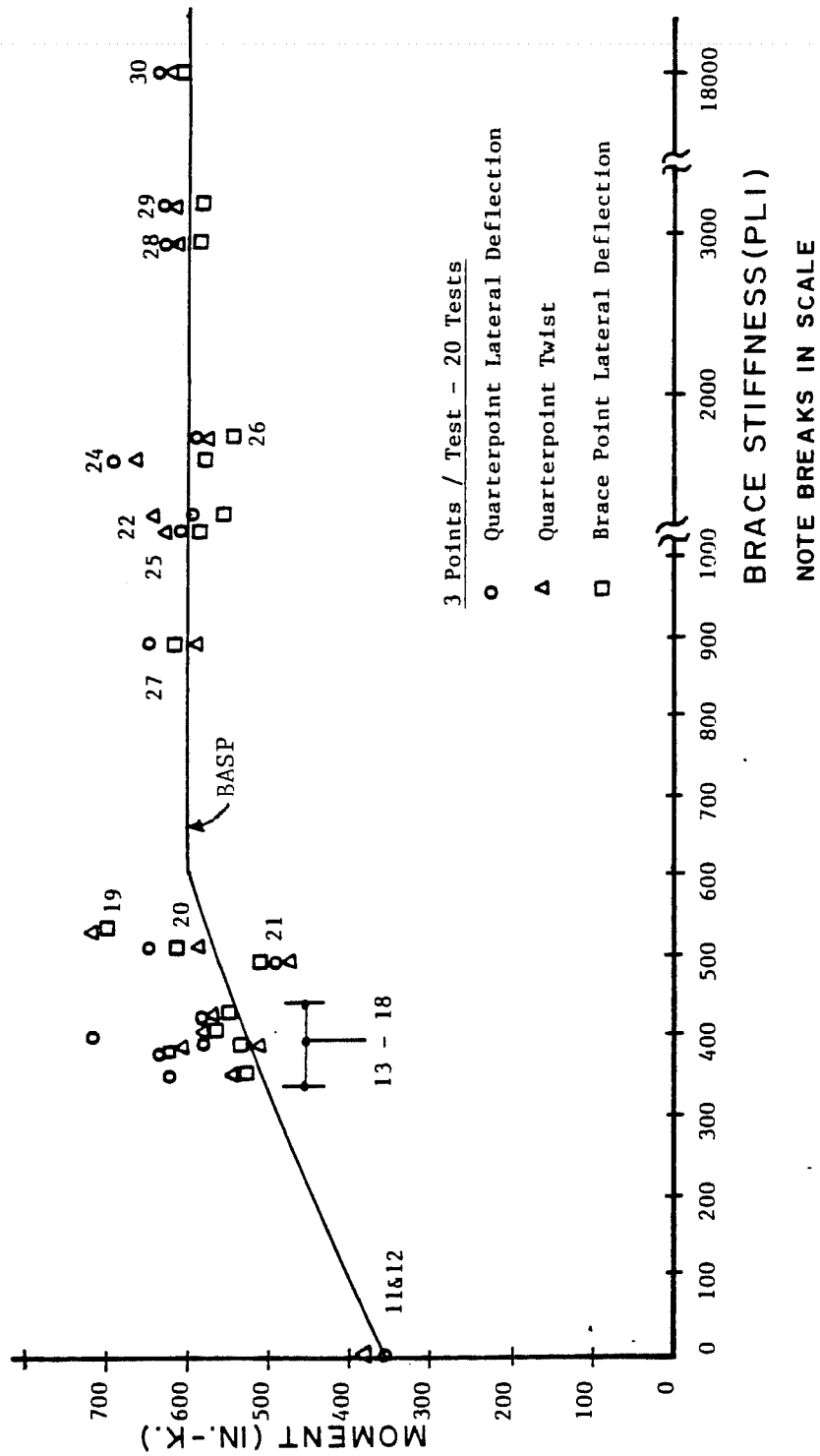



Fig. B.2 Critical moment vs. brace stiffness from Lundquist plots.

TABLE B.3 MECK PLOTS (ILS = 1) RESULTS (continued)

Test No.	Brace Stiffness (kli)	Forced Initial Imperf. (in.)	Highest Moment Reached (in.-k)	BASP Run M_{cr} (in.-k)	Quarterpoint Flange Displacements Δ_o M_{cr} (in.-k)	Quarterpoint Centroid Displacements Δ_o M_{cr} (in.-k)				
29	3.2	0.218 ¹	564.1 ²	596.7 ²	627.7	-0.026	4.505	636.3	-0.032	6.51
30	18.+	0.000	610.5	597.6	636.8	-0.119	10.43	644.5	-0.122	17.15

¹ Shape is  unless otherwise noted.

² All moments include 25.1 in.-k gravity moment.

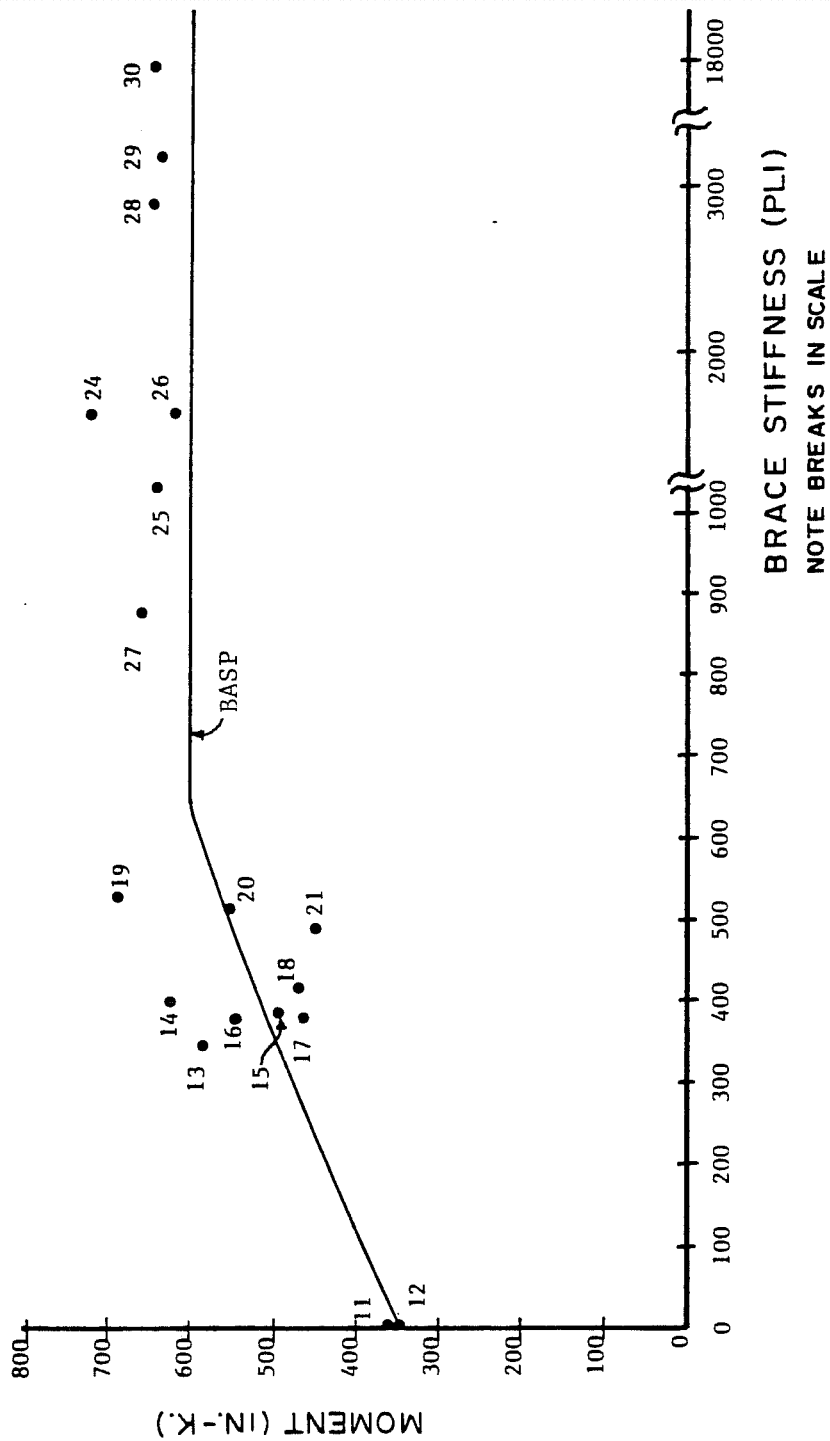


Fig. B.3 Critical moment vs. brace stiffness from Meck plots.

A P P E N D I X C

FINITE ELEMENT METHOD--BASP

A finite element program, BASP, which stands for Buckling Analysis of Stiffened Plate structures, was developed in 1974 at The University of Texas at Austin [7]. Structures to be analyzed by this program must have a plane of symmetry which acts as the mid-surface for plate elements in this plane. Stiffeners or beam elements can be oriented such that their strong direction neutral axis is in the symmetry plane. A beam or column having at least one axis of symmetry is easily modelled where the web is composed of plate elements and the flanges are beam elements.

The program analysis consists of two parts. An inplane analysis is performed to determine the normal stresses in the elements. These stresses correspond to a set of "unit" loads applied to the structure. Secondly, the geometric stiffness matrix is constructed to describe the out-of-plane behavior of the structure. Inverse iteration is used to find the eigenvalue of the mode to which the solution process converges. An assumption about the mode shape is required to start the solution process. This initial guess should be somewhat similar to that of the desired buckling mode shape. If the program converges on an undesired mode, the origin of the inverse iteration can be shifted, and the solution process will search for the mode nearest to this new origin. Once the eigenvalue is found, the buckling loads are found by multiplying the

unit loads by the eigenvalue. These loads are the bifurcation load for the particular mode shape to which the program converged.

The beam in Fig. 2.3 can be modeled as shown in Fig. C.1. In this figure, the web and flange elements correspond to the dimensions of a W12x16. The length is 216 in. and the depth is taken as the center to center spacing of the flanges. At least two elements are used for the depth of the web to model cross-sectional distortion. If the brace stiffness at midspan is taken as 0.70 kli , the eigenvalue will be 40.98 k and the critical moment will be 490 in.- k . A plot of the buckled shape can be seen in Fig. 6.1.

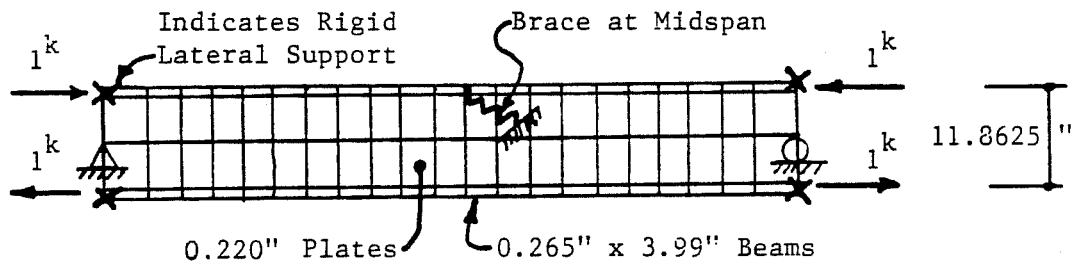


Fig. C.1 Model of W12x16.

N O T A T I O N

A	=	Area of cross-section
a	=	ratio of length associated with buckled mode shape to total length of beam
b	=	distance above shear center to brace attachment
b_o	=	distance below shear center to center of rotation of buckled shape
C_w	=	warping constant for torsion
d	=	depth of section
D	=	differential operator-- d/dx
E	=	elastic modulus
F_{brace}	=	force in brace
G	=	shear modulus
J	=	St. Venant torsional constant
k_{li}	=	kips per linear inch
I_x	=	strong axis moment of inertia
I_y	=	weak axis moment of inertia
L	=	total length of column or beam
M_{e1}	=	first mode moment
M_{e2}	=	second mode moment
M_{cr}	=	critical moment
M	=	moment at a given load stage or along length of beam
P	=	load at a given load stage
P_{cr}	=	critical load
P_{e1}	=	first mode or Euler load

P_{e2}	=	second mode moment
P_R	=	load at reference load stage
S_x	=	strong axis section moduli
S_y	=	weak axis section moduli
t_w	=	thickness of web
t_f	=	thickness of flange
u	=	lateral displacement of beam
X-X	=	strong axis of wide flange section
Y-Y	=	weak axis of wide flange section
z	=	distance along longitudinal axis of beam
α, β	=	inverse of slopes of Meck plots
β	=	brace stiffness
β_{distr}	=	stiffness of distributed brace along column or beam flange
β_{ideal}	=	ideal brace stiffness
Δ_o	=	magnitude of initial imperfection
Δ_A	=	additional deflection of brace
Δ_R	=	displacement at reference load stage
γ	=	torsion constant = $(\pi^2 E C_w / GJ)^{1/2}$
ϕ or θ	=	angle of twist about longitudinal axis of beam
π	=	pi or 3.14159...

REFERENCES

1. Johnston, B. G., ed., Structural Stability Research Council, Guide to Stability Design Criteria for Metal Structures, 3rd Edition. New York: John Wiley & Sons, Inc., 1976, Chapter 6.
2. Mutton, B. R., and Trahair, N. S., "Stiffness Requirements for Lateral Bracing," Journal of the Structural Division, ASCE, ST10, October 1973, pp. 2167-2181.
3. Trahair, N. S., "Deformations of Geometrically Imperfect Beams," Journal of the Structural Division, ASCE, ST7, July 1969, p. 1475.
4. Southwell, R. V., "On the Analysis of Experimental Observations in the Problems of Elastic Stability," Proceedings of the Royal Philosophical Society of London, Series A, Vol. 135, April 1932, p. 601.
5. Zuk, W., "Lateral Bracing Forces on Beams and Columns," Journal of the Engineering Mechanics Division, ASCE, EM3, July 1956.
6. Winter, G., "Lateral Bracing of Columns and Beams," Journal of the Structural Division, ASCE, ST2, March 1958, pp. 1561-1565.
7. Akay, H. U., Johnson, C. P., and Will, K. M., "Lateral and Local Buckling of Beams and Frames," Journal of the Structural Division, ASCE, ST9, September 1977, pp. 1821-1832.
8. Lundquist, E. E., "Generalized Analysis of Experimental Observations in Problems of Elastic Stability," National Advisory Committee for Aeronautics, NACA Technical Note No. 658, July 1958.
9. Meck, H. R., "Experimental Evaluation of Lateral Buckling Loads," Journal of the Engineering Mechanics Division, ASCE, EM2, April 1977, pp. 331-337.
10. Timoshenko, S. P., and Gere, J. M., Theory of Elastic Stability. New York: McGraw-Hill Book Company, Inc., 1961, pp. 94-98.

V I T A

Robert William Gedies was born in Boston, Massachusetts, on May 23, 1957, the son of Joan Helen Gedies and Robert Lawrence Gedies. Upon graduating from Arlington High School, Arlington, Massachusetts, he entered Northeastern University in Boston, Massachusetts, and participated in the Cooperative Education Program. He received the degree of Bachelor of Science from Northeastern University in June 1980. The following year he was employed as a design engineer by Simpson, Gumpertz and Heger, Inc., in Boston. In July 1981 he entered the Graduate School of The University of Texas at Austin.

Permanent address: 18 Cleveland Street
Arlington, Massachusetts 02174

This thesis was typed by Patricia Henderson.

